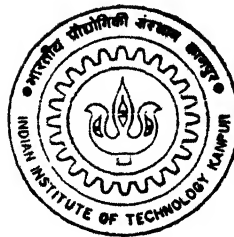


9610615

SINTERING OF T15 HIGH SPEED STEEL-ALUMINA PARTICULATE COMPOSITES

by

PALLAB MAJUMDAR



TH
MME 1998/M
m 4585
M

DEPARTMENT OF MATERIALS AND METALLURGICAL ENGINEERING

Indian Institute of Technology, Kanpur

MAY, 1998

MAJ
SIN

SINTERING OF T15 HIGH SPEED STEEL-ALUMINA PARTICULATE COMPOSITES

A Thesis Submitted
in Partial Fulfilment of the Requirements
for the Degree of

MASTER OF TECHNOLOGY

by

Pallab Majumdar

to the

DEPARTMENT OF MATERIALS AND METALLURGICAL
ENGINEERING

INDIAN INSTITUTE OF TECHNOLOGY
KANPUR

May 1998

3 JUL 1998

CENTRAL LIBRARY
I. I. T., KANPUR

No. A 125718

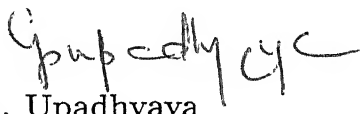
MME-1998-M-MAJ-SIN



A125718

CERTIFICATE

This is to certify that the present work, entitled Sintering of T15 High Speed Steel-Alumina Particulate Composites by Mr. Pallab Majumdar has been carried out under my supervision and to the best of my knowledge it has not been submitted elsewhere for a degree.


Dr. G.S. Upadhyaya

Professor

Department of Materials & Metallurgical Engineering

Indian Institute of Technology

Kanpur.

Date:

12-5-98

SYNOPSIS

The wear resistance in HSS is directly related to the volume fraction of hard phase present in the matrix. Although, the alloying elements present in the HSS, especially Vanadium, form hard carbide dispersoid, the addition of inert ceramic particles like alumina (Al_2O_3) with high hardness may further improve wear resistance. The HSS can be easily enriched by such ceramic particles through P/M route to produce full density metal-matrix composites with compositions and structures that would be difficult to produce by any other means.

In the present investigation, T15 HSS based particulate composites with different volume fraction of Al_2O_3 particles (0-8%) were prepared by blending their respective proportions, cold compacting at a pressure of 600 MPa to a green porosity level of 28-30% and sintering in a dynamic hydrogen atmosphere. The liquid phase sintering process was followed. To investigate the effect of copper on these composites, 5 wt.% of it was also added. The sintering temperatures selected were 1250, 1280 and 1300°C. Model experiment was also carried out at various sintering temperatures (500, 700, 900, 1100 and 1300°C) to assess the mode of sintering and effect of copper addition on it. During heat treatment optimum conditions were followed. Various mechanical properties like hardness, TRS, Sliding wear behaviour and study of magnetic properties i.e. Saturation magnetization and magnetic coercivity along with microstructural study were carried out for sintered as well as heat treated samples.

The result of the present investigation showed that enhanced densification occurred during super solidus sintering. Addition of copper also enhanced densification but in presence of sufficient amount of finer particles of T15 HSS, it decreased densification. Al_2O_3 particle addition to HSS led to decrease densification.

The Vicker macro hardness increased with the densification. Addition of copper also increased it. During heat treatment, the hardness of all compositions increased after quenching but during triple tempering no significant change was observed except composites containing copper where hardness dropped. During super solidus sintering, the micro hardness of ferrous matrix decreased. Coercivity variation is similar to that of microhardness. The saturation magnetization decreased with increasing copper and/or Al_2O_3 content. The wear resistance was maximum in the case of optimum sintering temperature. The addition of Al_2O_3 decreased the wear resistance except 2 vol.% composite, where it is comparable to that of T15 HSS. Copper addition has practically no effect on wear.

ACKNOWLEDGEMENT

It is with great pleasure that I express my deepest gratitude to my thesis supervisor prof. G.S. Upadhyaya for introducing me in the field of Powder Metallurgy and for his patience guidance, deep involvement and intuitive insight during the research work.

I would especially like to express my sincere thanks to Mr Soni for his invaluable support during my thesis.

I have indebted of Bikas and Santanu, without their kind assistance this work would have remained incomplete.

.I also thank to all my lab-mates for their kind help whenever needed.

My sincere thanks are due to all the staff of MME and ACMS Departments who helped in their respective ways for the completion of this thesis.

Contents

1	Literature Review	1
1.1	Introduction	1
1.2	Alloying Elements in HSS	1
1.3	Powder Production	2
1.3.1	Water Atomization	3
1.3.2	Gas Atomization	3
1.3.3	Reaction Spray Process from Salt Precursors	3
1.4	Consolidation Processes	4
1.4.1	Supersolidus Sintering	4
1.4.2	Hot Isostatic Pressing (HIP'ping)	5
1.4.3	Sinter-HIP	5
1.4.4	Other Hot Consolidation Processes	5
1.5	Sintering Variables	6
1.5.1	Powder Production Method	6
1.5.2	Particle Size, Shape and Distribution	7
1.5.3	Oxygen Content	7
1.5.4	Sintering Aids	8
1.5.5	Green Density	9
1.5.6	Sintering Atmosphere	9
1.5.7	Sintering Temperature and Time	10
1.5.8	Heating and Cooling Rate	11
1.6	Heat Treatment	12
1.7	Mechanical and Electrical Properties	13
1.7.1	Modulus of Elasticity	13
1.7.2	Hardness	13
1.7.3	Transverse Rupture Strength	14
1.7.4	Fracture Toughness	16
1.7.5	Fatigue	16

1.7.6	Superplasticity	17
1.7.7	Electrical Property	18
1.8	P/M Based Particulate Composites	18
1.9	Service Behavior	21
1.9.1	Grindability	21
1.9.2	Machinability	22
1.9.3	Cutting Performance	22
1.9.4	Wear Resistance	23
1.10	Applications	24
1.11	Scope of the Present Investigation	24
2	Experimental Procedure	26
2.1	Powders and Their Characteristics	26
2.2	Powder Mix Preparation	27
2.3	Room Temperature Compaction	27
2.4	Sintering	27
2.5	Sintered Density Measurement	28
2.6	Heat Treatment	28
2.6.1	Transformation Annealing	29
2.6.2	Hardening	29
2.6.3	Tempering	29
2.7	Hardness	29
2.8	Transverse Rupture Strength (TRS)	29
2.9	Sliding Wear Test	30
2.10	Magnetic Properties	31
2.10.1	Saturation Magnetization	31
2.10.2	Magnetic Coercivity	31
2.11	Microstructural Studies	32
2.11.1	Optical Metallography	32
2.12	SEM study	32
3	Experimental Results	33
3.1	Effect of sintering temperature and copper addition on T15 HSS and T15- 2vol%Al ₂ O ₃ composite.	33
3.1.1	Densification Behaviour	33
3.1.2	Vickers Macrohardness	34
3.1.3	Vickers Microhardness	34

3.1.4	Magnetic Properties	35
3.1.5	Microstructural Analysis	36
3.2	Effect of Al_2O_3 content and 5wt% Copper Addition on T15- Al_2O_3 composites	37
3.2.1	Densification Behaviour	37
3.2.2	Vickers Hardness	37
3.2.3	Transverse Rupture Strength (TRS)	38
3.2.4	Sliding Wear Behaviour	38
3.2.5	Magnetic Properties	41
3.2.6	Microstructural Analysis	42
4	Discussion	44
4.1	T15 HSS (with or without copper/ Al_2O_3 : Model Study)	44
4.2	T15- Al_2O_3 composites	47
4.3	Role of Copper on T15- Al_2O_3 composites	48
5	Conclusion	50
6	References	52

List of Figures

Fig 1.1 Mechanism of supersolidus liquid phase sintering of high speed steels [15].

Fig 1.2 Schematic flow sheet for (a) ASEA-STORA and (b) Crucible steel methods for production of high speed steels [5].

Fig 1.3 Schematic of microstructure of as-sintered P/M HSS [14].

Fig 1.4 Relation between oxygen content of powder and carbon loss during sintering and between oxygen content before and after sintering: ○ Okayama et al. [27] and □ Wahling et al. [2].

Fig 1.5 Phase diagram of Fe-W-Cr-C system at W=18%, Cr=4%, showing the region with liquid phase and the supersolidus sintering temperature range [15].

Fig 1.6 Effect of Porosity on elastic modulus of R12M3K8F2 ("T, grade) high speed steel [38].

Fig 1.7 Effect of sintering temperature on hardness for T1 high speed steel by addition of carbon [29].

Fig 1.8 Effect of process variables on apparent hardness of M3/2 high speed steel (a) compaction pressure, 1120°C, 30 min; (b) cooling rate, 1120°C, 30 min; (c) number of temperings, 60 min. tempering at 560°C, sintering temperature 1120°C, sintering time 30 min; (d) Cu content, 1120°C, 60 min vacuum, □ =admixed, ◇ =infiltrated; [39].

Fig 1.9 Effect of process variables on TRS of M3/2 high speed steel (a) compaction pressure, 1120°C, 30 min. cooling rate 40 K min⁻¹, 90N₂-10H₂; (b) sintering time, 1120°C, cooling rate 2.5 K min⁻¹, 80N₂-20H₂, compaction pressure 620 MPa; (c) sintering temperature, 1120°C, 15 min, cooling rate 2.5 K min⁻¹, 80N₂-20H₂, compaction pressure 620 MPa. (d) Cu content, 1120°C, 60 min, vacuum, compaction pressure 620 MPa, □ =admixed, ◇ =infiltrated; [39].

Fig 1.10 Dependence of fracture toughness on hardness of T6 and T15 P/M high speed steels [44].

Fig 1.11 Dependence of fracture toughness on the amount of retained austenite of T6 and T15 P/M high speed steels. Chain lines represent the 95% confidence limits [44].

Fig 1.12 Fatigue life as a function of effective tension stress of different grades of P/M high speed steels. Effective compressive stress 3100 MPa (dotted lines) and 0 MPa (solid

Lines) $\pm 5^\circ$.

Fig 1.13 The effect of TiC additions on the sintering behaviour of M3/2 high speed steel [50].

Fig 1.14 Comparative results of grindability tests of various P/M and I/M HSS grades [5].

Fig 1.15 Cut-off machinability of P/M and conventional M2 in the annealed condition (R_b 100): [63].

Fig 1.16 Continuous cutting test response of sintered and wrought BT6 high speed steels [65].

Fig 1.17 Intermittent cutting behaviour of wrought (transverse/longitudinal) and sintered BT6 high speed steel. Cutting speed 30 m min^{-1} , slotted ENB workpiece. (Feed 0.254 mm/rev , Depth of cut 2.54 mm): [65].

Fig 1.18 Cutting performance of sintered M3/2 (S6-5-3) high speed steel during spade drilling [2].

Fig 1.19 Cutting performance of sintered high speed steels during turning in single point turning test [2].

Fig 1.20 Cutting performance of sintered high speed steels during milling of M35 (S6-5-3-5) work piece [2].

Fig 1.21 Abrasive wear rate versus hardness for high speed steels [70].

Fig 1.22 Wear scar volume plotted as a function of hardness [70].

Fig. 3.1 Effect of sintering temperature on (a) Densification parameter (b) Sintered density and (c) sintered porosity of T15 HSS with or without the addition of 5 wt% copper.

Fig. 3.2 Effect of sintering temperature on (a) Densification parameter and (b) Sintered density of T15 HSS and T15-2 vol% Al_2O_3 compositions with or without the addition of 5 wt% copper.

Fig. 3.3 Effect of sintering temperature on the porosity of T15 HSS and T15-2 vol% Al_2O_3 compositions with or without the addition of 5 wt% copper.

Fig. 3.4 effect of repressing and resintering on T15 HSS and T15-2 vol% Al_2O_3 compositions (sintered at 1300°C) with or without the addition of copper.

Fig. 3.5 Effect of sintering temperature on Vickers hardness of T15 HSS and T15-2 vol% Al_2O_3 compositions with or without the addition of 5 wt% copper.

Fig. 3.6 Effect of sintering temperature on matrix microhardness of T15 HSS and T15-2 vol% Al_2O_3 compositions with or without the addition of 5 wt% copper.

Fig. 3.7 Effect of sintering temperature on saturation magnetization of T15 HSS and T15-2 vol% Al_2O_3 compositions with or without the addition of 5 wt% copper.

Fig. 3.8 Effect of sintering temperature on magnetic coercivity of T15 HSS and T15-2

vol% Al_2O_3 compositions with or without the addition of 5 wt% copper

Fig. 3.9 The optical microstructures of T15 HSS with or without the addition of copper sintered at (a) 500 (b) 700 (c) 900 (d) 1100 and (e) 1300°C respectively

Fig. 3.10 The optical microstructures of T15-2 vol% Al_2O_3 composite with or without the addition of 5 wt% copper sintered at (a) 1100 and (b) 1300°C respectively.

Fig. 3.11 The optical microstructures of T15 HSS and T15-2 vol% Al_2O_3 compositions with or without the addition of 5 wt% copper (sintered at 1300°C) after repressing/resintering; (a) T15 HSS (b) T15+2 vol% Al_2O_3 (c) T15+5 wt% 5 Cu (d) T15+2 vol% Al_2O_3 +5 wt% Cu.

Fig. 3.12 Effect of sintering and repressing/resintering on av. grain size of T15 HSS and T15-2 vol% Al_2O_3 compositions with or without the addition of 5 wt% copper (all sintered at 1300°C).

Fig. 3.13 Effect of Al_2O_3 addition on densification behaviour of T15 HSS with or without the addition of 5 wt% copper sintered at various temperatures.

Fig. 3.14 Vickers hardness variation of sintered (1250°C) and heat treated T15 HSS and its Al_2O_3 containing composites with or without 5 wt% copper addition.

Fig. 3.15 Vickers hardness variation of sintered (1280°C) and heat treated T15 HSS and its Al_2O_3 containing composites with or without 5 wt% copper addition.

Fig. 3.16 Vickers hardness variation of sintered (1300°C) and heat treated T15 HSS and its Al_2O_3 containing composites with or without 5 wt% copper addition.

Fig. 3.17 Effect of Al_2O_3 addition on TRS of sintered T15 HSS with or without 5 wt% copper addition.

Fig. 3.18 Effect of Al_2O_3 content on sliding wear behaviour of T15 HSS sintered at 1250°C temperature and tested at 1.5 and 2.5 kg loads.

Fig. 3.19 Effect of Al_2O_3 content on sliding wear behaviour of T15 HSS with 5 wt% copper sintered at 1250°C temperature and tested at 1.5 and 2.5 kg loads.

Fig. 3.20 Effect of Al_2O_3 content on frictional force of T15 HSS sintered at 1250°C temperature and tested at 1.5 and 2.5 kg loads.

Fig. 3.21 Effect of Al_2O_3 content on frictional force of T15 HSS with 5 wt% copper sintered at 1250°C temperature and tested at 1.5 and 2.5 kg loads.

Fig. 3.22 Effect of Al_2O_3 content on sliding wear behaviour of T15 HSS sintered at 1280°C temperature and tested at 1.5 and 2.5 kg loads.

Fig. 3.23 Effect of Al_2O_3 content on sliding wear behaviour of T15 HSS with 5 wt% copper sintered at 1280°C temperature and tested at 1.5 and 2.5 kg loads.

Fig. 3.24 Effect of Al_2O_3 content on frictional force of T15 HSS sintered at 1280°C temperature and tested at 1.5 and 2.5 kg loads.

Fig. 3.25 Effect of Al_2O_3 content on frictional force of T15 HSS with 5 wt% copper

sintered at 1280°C temperature and tested at 1.5 and 2.5 kg loads.

Fig. 3.26 Effect of Al_2O_3 content on sliding wear behaviour of T15 HSS sintered at 1300°C temperature and tested at 1.5 and 2.5 kg loads.

Fig. 3.27 Effect of Al_2O_3 content on sliding wear behaviour of T15 HSS with 5 wt% copper sintered at 1300°C temperature and tested at 1.5 and 2.5 kg loads.

Fig. 3.28 Effect of Al_2O_3 content on frictional force of T15 HSS sintered at 1300°C temperature and tested at 1.5 and 2.5 kg loads.

Fig. 3.29 Effect of Al_2O_3 content on frictional force of T15 HSS with 5 wt% copper sintered at 1300°C temperature and tested at 1.5 and 2.5 kg loads.

Fig. 3.30 Variation of saturation magnetization with respect to Al_2O_3 content in sintered and heat treated T15 HSS with or without 5 wt% copper addition.

Fig. 3.31 Variation of magnetic coercivity with respect to Al_2O_3 content in sintered and heat treated T15 HSS with or without 5 wt% copper addition.

Fig. 3.32 The optical microstructures of T15 HSS and its containing Al_2O_3 composites with or without 5 wt% copper sintered at 1300°C temperature, (a) T15 HSS (b) T15+5 wt% Cu (c) T15+2 vol% Al_2O_3 (d) T15+2 vol% Al_2O_3 +5 wt% Cu (e) T15+4 vol% Al_2O_3 (f) T15+4 vol% Al_2O_3 +5 wt% Cu (g) T15+6 vol% Al_2O_3 (h) T15+6 vol% Al_2O_3 +5 wt% Cu (i) T15+8 vol% Al_2O_3 (j) T15+8 vol% Al_2O_3 +5 wt% Cu.

Fig. 3.33 Effect of Al_2O_3 content on average grain size of sintered T15 HSS with or without 5 wt% copper addition.

Fig. 3.34 The optical microstructures of T15 HSS and its containing Al_2O_3 composites with or without 5 wt% copper (sintered at 1300°C) after quenching; (a) T15 HSS (b) T15+5 wt% Cu (c) T15+2 vol% Al_2O_3 (d) T15+2 vol% Al_2O_3 +5 wt% Cu (e) T15+4 vol% Al_2O_3 (f) T15+4 vol% Al_2O_3 +5 wt% Cu (g) T15+6 vol% Al_2O_3 (h) T15+6 vol% Al_2O_3 +5 wt% Cu (i) T15+8 vol% Al_2O_3 (j) T15+8 vol% Al_2O_3 +5 wt% Cu.

Fig. 3.35 The optical microstructures of T15 HSS and its containing Al_2O_3 composites with or without 5 wt% copper (sintered at 1300°C) after triple tempering; (a) T15 HSS (b) T15+5 wt% Cu (c) T15+2 vol% Al_2O_3 (d) T15+2 vol% Al_2O_3 +5 wt% Cu (e) T15+4 vol% Al_2O_3 (f) T15+4 vol% Al_2O_3 +5 wt% Cu (g) T15+6 vol% Al_2O_3 (h) T15+6 vol% Al_2O_3 +5 wt% Cu (i) T15+8 vol% Al_2O_3 (j) T15+8 vol% Al_2O_3 +5 wt% Cu.

Fig. 3.36 The SEM micrographs of the worn pin surfaces of sintered (at 1300°C) T15 HSS and its containing Al_2O_3 composites with or without 5 wt% copper (sintered at 1300°C) after triple tempering; (a) T15 HSS (b) T15+5 wt% Cu (c) T15+2 vol% Al_2O_3 (d) T15+2 vol% Al_2O_3 +5 wt% Cu (e) T15+4 vol% Al_2O_3 (f) T15+4 vol% Al_2O_3 +5 wt% Cu (g) T15+6 vol% Al_2O_3 (h) T15+6 vol% Al_2O_3 +5 wt% Cu

List of Tables

Table 1.1 Composition limits of principal types of HSS [6].

Table 1.2 Fracture toughness of sintered and wrought high speed steels [3].

Table 1.3 Properties (average values) of (P/M) HSS and HSS + TiC composites in various states of heat treatment [49].

Table 1.4 Wear behaviour of sintered R6M5F3 ('M' grade) and R12MF5 ('T' grade) high speed steels during cutting [30].

Chapter 1

Literature Review

1.1 Introduction

High Speed Steels (HSS) are basically a group of iron base alloys containing some 20-30% of mainly carbide forming alloying elements and can be hardened to a level of up to 65-70 HR_c, and that no appreciable softening takes place until temperatures in the region of 600°C are reached. The microstructure consists of tough tempered martensite matrix with a dispersion of wear resistance, high hardness alloy carbides [1-3]

HSS have a sufficient temperature gap that exists between liquidus and solidus temperatures. In case of conventional steel making, this makes it prone to carbide segregation during solidification, which gives embrittling effect. To avoid these problems, measures like electroslag remelting, inoculation of the melt, casting relatively small ingot etc. have been attempted with partial success [4,5].

Powder metallurgy (P/M) processes are attractive in solving these problems. The main idea, behind adopting P/M processing route, is that the segregation is limited within individual powder particle (maximum 250 μm dia.). Due to relatively high cooling rates achieved during atomization processes, segregation within every powder particle is minimized. Additionally, P/M HSS practice can contain a large quantity of small size carbide particles distributed homogeneously in the matrix, which is not possible by conventional route. Other advantages of P/M HSS are increased alloying flexibility, improved toughness, superior grindability, less distortion during heat treatment, isotropic mechanical properties, near net shape processing, good machinability, and improved tool life [6-8].

1.2 Alloying Elements in HSS

The basic alloying elements of HSS include: carbon, chromium, tungsten, molybdenum, vanadium, and sometimes, cobalt. Besides, the other alloying elements, which can be

added, are niobium, tantalum, titanium, silicon, nitrogen, and nickel [1]

Carbon can effect the carbide as well as matrix. It produces the required amount and type of carbide, and also has an important role in regard to hardening operation. With increasing carbon content, the amount of retained austenite also increases, which results the decrease in as-quenched hardness and coarser grain size. Chromium increases the fraction of retained austenite and leads to secondary hardening, after tempering. It also prevents scaling. Tungsten and molybdenum perform similar functions and are more or less interchangeable on an atomic basis. 1 mass % molybdenum is equivalent to ~ 1.6 -2 mass % tungsten. Both the elements promote resistance to tempering. The austenite in molybdenum HSS is reported to be less stable than that of tungsten steels, giving some practical advantage during heat treatment. Vanadium acts as a grain refiner as it provides a very stable carbide which prevents grain growth during heat treatment. Cobalt enters into matrix and raises the solidus temperature and thus provides an opportunity to raise the hardening temperature. This results in enhanced carbide dissolution, which in turn increases the amount of retained austenite on hardening. Niobium has a similar effect to that of vanadium, but has a higher affinity for carbon. Tantalum, when present above 6 % leads to the formation of stable carbides. Titanium is a strong carbide former and its addition causes reduction in ledeburite content as a result of TiC precipitation. Presence of 1 % titanium eliminates the eutectic completely. Silicon raises the solubility of carbon in the matrix and hence the as-quenched hardness. It also leads to reduce the solubility of M_2C type carbides, accelerating their transformation to the round-shaped M_6C type carbides. Nitrogen lowers the as-quenched hardness and raises the tempered hardness. It suppresses the M_2C type carbides formation, stabilizes austenite, and increases the retention on quenching. Nickel is a non-carbide former and is usually regarded as undesirable in HSS as its addition can increase the amount of retained austenite up to 80 % during cooling.

There are two major classes of HSS: molybdenum high speed steels, also called group 'M', and tungsten high speed steels, also called group 'T'. The main advantage of group 'M' steels is lower initial cost due to lower atomic weight of molybdenum than tungsten. Table 1.1 shows the composition limits of various HSS.

1.3 Powder Production

HSS powders are produced by induction melting of virgin raw materials and/or scrap followed by gas or water atomization. Besides, reaction spray process is also a novel method for preparing HSS powders with remarkable properties.

Designation		Composition								
AISI	UNS	C	Mn	Si	Cr	Ni	Mo	W	V	Co
Molybdenum HSS										
M1	T11301	0.78-0.88	0.15-0.40	0.20-0.50	3.50-4.00	0.30 max	8.20-9.20	1.40-2.10	1.00-1.35	4.50-5.50
M2	T11302	0.78-0.88; 0.95-1.05	0.15-0.40	0.20-0.45	3.75-4.50	0.30 max	4.50-5.50	5.50-6.75	1.75-2.20	...
M3/1	T11313	1.00-1.10	0.15-0.40	0.20-0.45	3.75-4.50	0.30 max	4.75-6.50	5.00-6.75	2.25-2.75	...
M3/2	T11323	1.15-1.25	0.15-0.40	0.20-0.45	3.75-4.50	0.30 max	4.75-6.50	5.00-6.75	2.75-3.75	...
M4	T11304	1.25-1.40	0.15-0.40	0.20-0.45	3.75-4.75	0.30 max	4.25-5.50	5.25 -6.50	3.75-4.50	...
M7	T11307	0.97-1.05	0.15-0.40	0.20-0.55	3.50-4.00	0.30 max	8.20-9.20	1.40-2.10	1.75-2.25	...
M10	T11310	0.84-0.94; 0.95-1.05	0.10-0.40	0.20-0.45	3.75-4.50	0.30 max	7.75-8.50	...	1.80-2.20	...
M30	T11330	0.75-0.85	0.15-0.40	0.20-0.45	3.50-4.25	0.30 max	7.75-9.00	1.30-2.30	1.00-1.40	4.50-5.50
M33	T11333	0.85-0.92	0.15-0.40	0.15-0.50	3.50-4.00	0.30 max	9.00 10.00	1.30-2.30	1.00-1.40	4.50-5.50
M34	T11334	0.85-0.92	0.15-0.40	0.20-0.45	3.50-4.00	0.30 max	7.75-9.20	1.40-2.10	1.90-2.30	7.75-8.75
M35	T11335	0.82-0.88	0.15-0.40	0.20-0.45	3.75-4.50	0.30 max	4.50-5.50	5.50-6.75	1.75-2.25	4.50-5.50
M36	T11336	0.80-0.90	0.15-0.40	0.20-0.45	3.75-4.50	0.30 max	4.50-5.50	5.50-6.50	1.75-2.25	7.75-8.75
M41	T11341	1.05-1.15	0.20-0.60	0.15-0.50	3.75-4.50	0.30 max	3.25-4.25	6.25-7.00	1.75-2.25	4.75-5.75
M42	T11342	1.05-1.15	0.15-0.40	0.15-0.65	3.50-4.25	0.30 max	9.00-10.00	1.15-1.85	0.95-1.35	7.75-8.75
M43	T11343	1.15-1.25	0.20-0.40	0.15-0.65	3.50-4.25	0.30 max	7.50-8.50	2.25-3.00	1.50-1.75	7.75-8.75
M44	T11344	1.10-1.20	0.20-0.40	0.30-0.55	4.00-4.75	0.30 max	6.00-7.00	5.00-5.75	1.85-2.20	11.00-12.25
M46	T11346	1.22-1.30	0.20-0.40	0.40-0.65	3.70-4.20	0.30 max	8.00-8.50	1.90-2.20	3.00-3.30	7.80-8.80
M47	T11347	1.05-1.15	0.15-0.40	0.20-0.45	3.50-4.00	0.30 max	9.25-10.00	1.30-1.80	1.15-1.35	4.75-5.25
M48	T11348	1.42-1.52	0.15-0.40	0.15-0.40	3.50-4.00	0.30 max	4.75-5.50	9.50-10.50	2.75-3.25	8.00-10.00
M62	T11362	1.25-1.35	0.15-0.40	0.15-0.40	3.50-4.00	0.30 max	10.00-11.00	5.75-6.50	1.80-2.10

Contd....

Designation		Composition								
AISI	UNS	C	Mn	Si	Cr	Ni	Mo	W	V	Co
Tungsten HSS										
T1	T12001	0.65-0.80	0.10-0.40	0.20-0.40	3.75-4.50	0.30 max	17.25-18.75	0.90-1.30
T2	T12002	0.80-0.90	0.20-0.40	0.20-0.40	3.75-4.50	0.30 max	1.0 max	17.50-19.00	1.80-2.40
T4	T12004	0.70-0.80	0.10-0.40	0.20-0.40	3.75-4.50	0.30 max	0.40-1.00	17.50-19.00	0.80-1.20	4.25-5.75
T5	T12005	0.75-0.85	0.20-0.40	0.20-0.40	3.75-5.00	0.30 max	0.50-1.25	17.50-19.00	1.80-2.40	7.00-9.50
T6	T12006	0.75-0.85	0.20-0.40	0.20-0.40	4.00-4.75	0.30 max	0.40-1.00	18.50-21.00	1.50-2.10	11.00-13.00
T8	T12008	0.75-0.85	0.20-0.40	0.20-0.40	3.75-4.50	0.30 max	0.40-1.00	13.25-14.75	1.80-2.40	4.25-5.75
T15	T12015	1.50-1.60	0.15-0.40	0.15-0.40	3.75-5.00	0.30 max	1.00 max	11.75-13.00	4.50-5.25	4.75-5.25
Intermediate HSS										
M50	T11350	0.78-0.88	0.15-0.45	0.20-0.60	3.75-4.50	0.30 max	3.90-4.75	0.80-1.25
M52	T11352	0.85-0.95	0.15-0.45	0.20-0.60	3.50-4.30	0.30 max	4.00-4.90	0.75-1.50	1.65-2.25

Table 1.1 Composition limits of principal types of HSS [6].

1.3.1 Water Atomization

In water atomization high pressure water jets are directed against the melt stream, forcing disintegration and rapid solidification. Water atomized powders have irregularly shaped particles coated with a thin oxide film and lower tap densities. The improvements are going in the direction of new nozzle construction where very small powder particles are exposed for a very short time to oxidative influence of water or steam at high cooling rate [9].

The major problem of water atomized powder is the presence of considerable amount of oxygen in the form of difficult to reduce oxide inclusions, which are formed as a result of oxidation of alloying elements during the reaction of melt drops with water. This inhibits diffusion during sintering and has a marked deleterious effect on the ductility and impact strength. Oxide inclusions are almost completely reduced by annealing either in vacuum or hydrogen atmosphere. During such heat treatment, martensite and retained austenite are transformed into a matrix of ferrite and spheroidal carbide. This renders the powder softer and more ductile and suitable for compaction [6,10].

1.3.2 Gas Atomization

In gas atomization, a stream of liquid metal is broken up by means of a high pressure gas stream. The resulting liquid droplets spheroidize in free fall before solidification, due to surface tension. Nitrogen or argon can be used as atomizing gas. The powders have oxygen content less than 200 ppm [6] and can be characterized by good flowability and high apparent density. Addition of a plasticizing binder (paraffin wax) in the range of 1-3 wt. % markedly improves the compactability of the powders. The prior melt history before atomization improves the properties of the powders. This treatment has also a favourable effect on microstructure of the steels and facilitates a uniform distribution of the alloying elements in them [11,12].

1.3.3 Reaction Spray Process from Salt Precursors

In reaction spray process (Reaktion-Spruh-Verfahren or RSV), the improvements are expected not only for powder processing but also for properties of sintered parts, such as homogeneous distribution of carbide phases in the metallic binder phase, fine grained microstructure, and high purity [13].

In this process an aqueous solution of metal salts, according to the desired alloy composition, is atomized by the spraying system in a reactor. The solvent evaporates in the tube of the reactor ($T > 800^{\circ}\text{C}$) leaving fine salt particles, which mainly react to metal oxides. Solid and gaseous products are subsequently separated. The mixed oxide powder

is carburized with graphite or carburizing gases in a fluidized bed reactor at temperatures below 1100°C in order to obtain fine grained powder with primary particles being in the sub-micron range. The agglomerates can be disintegrated by gentle milling.

1.4 Consolidation Processes

1.4.1 Supersolidus Sintering

Supersolidus sintering involves densification by melt formation in a pre-alloyed powder compact by heating it above the solidus temperature. In this type of liquid phase sintering solid and liquid phases have much closer compositions. It was found [14], that a very limited amount of densification occurs through solid state diffusion till the temperature is within a few degree of the optimum sintering temperature range. In the optimum temperature range, fine particle melt preferentially to form a small quantity of viscous liquid phase. Melting also occurs over the surfaces of large particles and to some extent at the grain boundaries within particles. The densification very likely occurs through rearrangement with substantial contribution by particle deformation as the matrix is very low in strength at this temperature. Solution-reprecipitation stage does not play any significant role in the densification due to high viscosity of the liquid phase. Takajo et al. [15] proposed that powder particles are sintered in solid phase to form a skeleton before the formation of liquid phase. When liquid phase appears, it disintegrates the skeleton into almost individual solid grains. The grains rearrange their configuration and a rapid densification follows. The solid grains grow by a solution-reprecipitation process, in which the material transport occurs through the liquid phase. Fig. 1.1 schematically represents the mechanism.

The acceptable microstructures and properties are obtained over only a narrow sintering range, which is called 'sintering window'. This 'sintering window' is located within the austenite + carbide + liquid region of the equilibrium diagram. Sintering below this range yields excessive porosity, while sintering at higher temperatures results in coarse eutectic and grain boundary carbides, which can damage mechanical properties. The sintering time should be adequate for achieving full density. However, excessive duration should be avoided as carbides and grains grow rapidly at higher temperatures [3,14]. According to Takajo et al. [15], after 10 min. of sintering at the optimum sintering temperature, pores are practically eliminated and solid grains grow to some extent. The grain growth continues with sintering time. During cooling the liquid phase decomposes into austenite and carbide phases, which are mainly found along boundaries. Additional carbide precipitation from the austenite is characterized by finer carbides inside the grains.

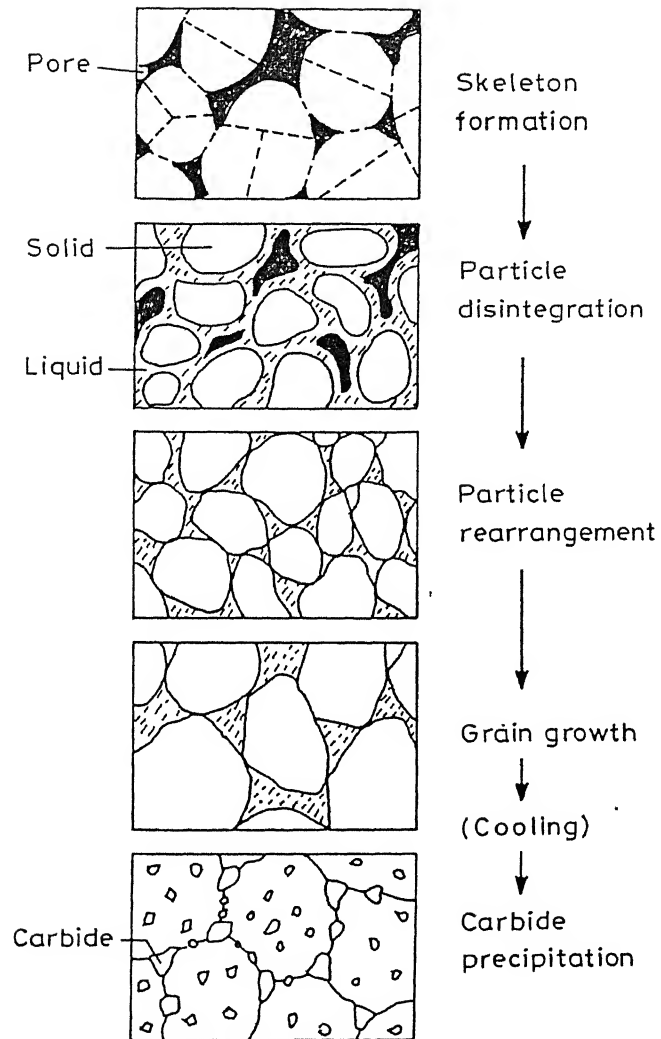


Fig 1.1 Mechanism of supersolidus liquid phase sintering of high speed steels [15].

1.4.2 Hot Isostatic Pressing (HIP'ping)

In this method, the powder is poured into a steel capsule, which is vacuum sealed and heated to specific temperature. It is then isostatically compacted to achieve a full density product. Consolidation is typically done at 1100°C at 100 MPa. for 1 hour [6]. The compacts are further processed to the desired billet and bar sizes by conventional hot rolling and forging. This route is best suited to the production of the large sections, where conventional product costs are highest [16]. This process was developed to the production stage by ASEA-STORA (now Uddeholm) in Sweden and crucible steel in USA. The principal steps of both the processes are shown in Fig. 1.2(a) and Fig. 1.2(b) respectively.

1.4.3 Sinter-HIP

This process is more economical for the production of P/M HSS. At first, sintering of the material is done at just sufficiently high temperature to remove interconnecting porosity. Any remaining closed porosity is subsequently removed by containerless-HIP'ping to full density with a microstructure intermediate between the 'direct sintering' and the fully HIP'ped material. By varying sintering conditions prior to HIP'ping it is possible to control the microstructures, particularly, grain and carbide sizes [3,17]. Martin et al. [18], using water atomized T15 HSS powder, observed the effect of HIP'ping on the microstructure of sintered materials. The as sintered microstructure consisted of vanadium rich MC-type carbides and tungsten rich M_6C -type carbides in a bainite matrix with retained austenite. After HIP'ping, the fully sintered microstructure shows a fine distribution of the tungsten carbides, while the vanadium rich carbides do not undergo any significant alternations. Sintering followed by HIP'ping improves the fracture strength of the P/M HSS.

1.4.4 Other Hot Consolidation Processes

Hot extrusion was first applied by Davy-Loewy in UK [19] for consolidation of HSS powders. Water atomized prealloyed powder was isostatically compacted at pressure of 200-240 MPa within closely supported shaped moulds to produce extrusion billets ranging from 5 to 40 kgs. in weight. The billets were sintered ($T \sim 1150^\circ\text{C}$) in vacuum to reduce its oxygen content from around 1500-2000 ppm to a level of 50-150 ppm and subsequently hot extruded ($T \sim 1200^\circ\text{C}$) to bars [20]. Extrusion is possible over a range of ratios from 10 to 75:1. A new production process of sintered hollow HSS bar blanks by binder assisted powder extrusion method has been developed by Hitachi Metals Limited [21].

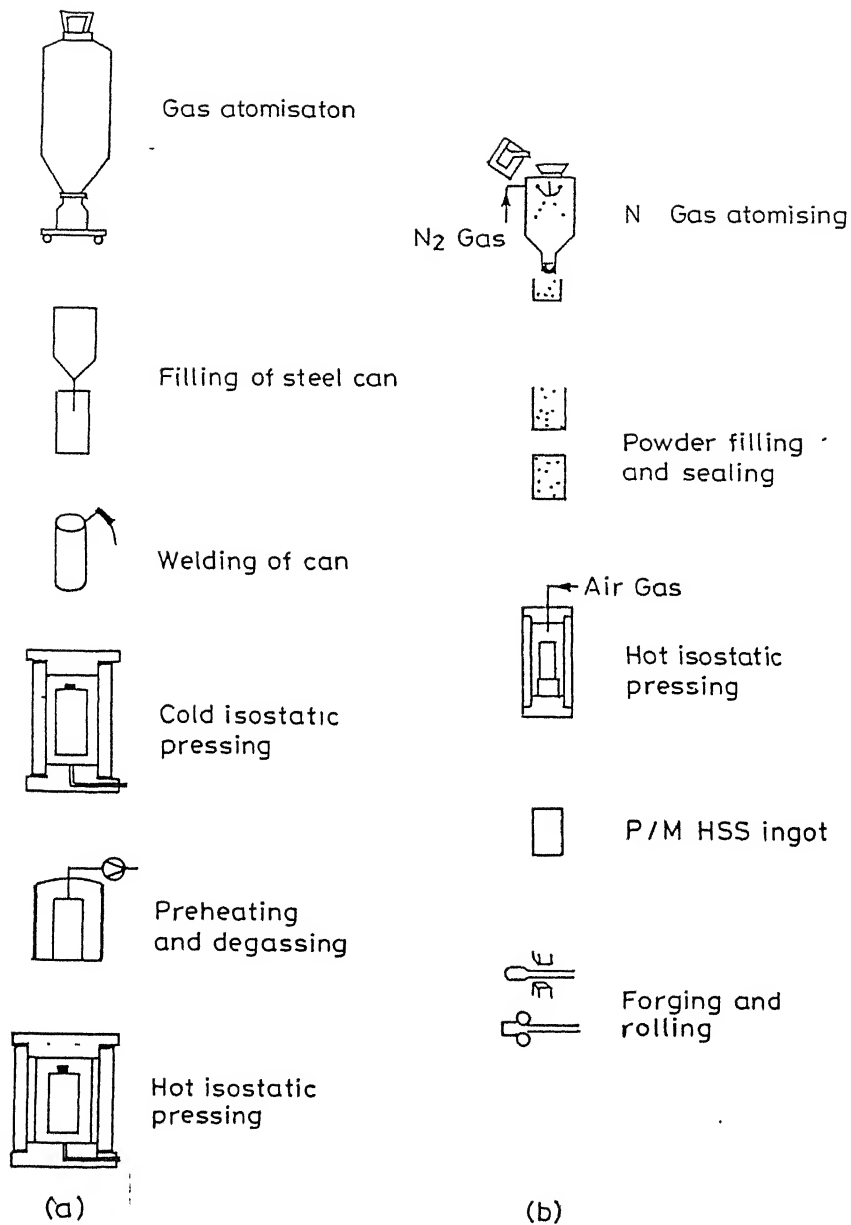


Fig 1.2 Schematic flow sheet for (a) ASEA-STORA and (b) Crucible steel methods for production of high speed steels [5].

In powder forging process, gas atomized HSS powders are forged to semifinished products, blanks or slugs. However, the process becomes economical only for parts above 10 kgs. in weight because of the need to can and to vacuum degas prior to forging [3].

In addition, pseudo-HIP process has been developed in which high temperature isostatic pressing conditions similar to HIP have been imparted. Examples of such processes are STAMP process, CAP (consolidation by atmospheric pressure) process, rotary forging process, etc. [5].

In STAMP process, gas atomized powder is encapsulated. After degasing and subsequently preheating, the capsule is inserted into a pressure chamber of a hydraulic press at temperature 1100-1200°C. The pressure vessel is filled with an easily deformable and thermally stable powdered material of low thermal conductivity. These granulates are pressed and the pressure is transmitted to the capsule leading to full density within a small interval of time and subsequently, the capsule is hot forged.

In CAP process, gas atomized powder is chemically treated and dried. The powder with a thin and uniform chemical coating is filled in a borosilicate glass mould. The mould is sealed after evacuation and is placed in a graphite crucible and subsequently, heated in standard atmospheric conditions. At high temperature, the mould softens and powder gets sintered to 95-99 % of theoretical density. The sintered billet is subjected to hot working operation.

In rotary forging process, gas atomized powder is encapsulated in low carbon steel container. After evacuation and sealing, the capsule is placed to rotary hearth furnace for sintering and subsequently, subjected to rotary forging operation where it is subjected to hot forging by simultaneous application of four hammers arranged in one plane.

1.5 Sintering Variables

Sintering variables have a significant role in determining the properties of the sintered products.

1.5.1 Powder Production Method

For liquid phase sintering of HSS, a powder compact having high green density, high green strength, and low oxygen content produces excellent sintered properties [16]. Gas atomized powders have less oxygen content but result is very poor strength owing to their round shape. The irregular particle shape from water atomization is preferred for compaction, since this gives a higher green strength. But the oxygen content of water atomized powder is higher. Additions of inoculations accelerate the rate of quench of

the molten steel, thereby an irregular particle shape and low surface oxide levels can be achieved [22]. However, microstructural coarsening during super solidus liquid phase sintering (SLPS) eliminates the initial powder fabrication effects [23].

1.5.2 Particle Size, Shape and Distribution

The HSS family is unique in allowing even relatively coarse fractions to be compacted and sintered to full density. It is because of the stability of the carbides of molybdenum, tungsten and vanadium that it is possible to satisfactorily sinter such coarse powders [14]. Kulkarni [24], using water atomized M2 and T15 HSS, found that the green density for the finest fraction is somewhat higher than the coarser fraction. At temperatures less than the optimum, the finest fraction achieves higher sintered densities than the coarser fractions. The differences in sintering rate are much larger for T15 than for M2. At lower sintering temperature, the coarser fractions show many large pores. At higher sintering temperature, the large residual pores seen in the coarser fractions are difficult to eliminate by longer sintering time without adversely affecting the microstructure. Larger the pores more difficult in filling them completely. Thus, to have full density and satisfactorily microstructure, it is important to have a reasonable amount of particles of fine size ($<45\mu\text{m}$). But there is no upper limit provided the oxygen content is low and the powder lot as a whole has adequate green strength. Fig. 1.3 shows that the location of the porosity is primarily at the grain boundaries. Baglyuk et al. [25], using gas atomized R6M5K5 HSS ('M' grade), reported that a reduction in average particle size increases shrinkage after sintering.

The sintering temperatures and conditions for very fine milled powders which are equiaxed in shape and water atomized powders which are irregular in shape are remarkably similar. Any difference in sintering of fine milled or pulverized powders seems more because of their higher oxygen content and effect on carbon content [16]. According to Kulkarni [24], for the similar conditions of surface chemistry and green density, particle shape is likely to have less influence than particle size.

A broad particle size distribution increases the packing density and co-ordination, and thereby, speeding densification while reducing the net dimensional change [23].

1.5.3 Oxygen Content

One of the main factors which adversely affects the quality of HSS powders is their high oxygen content. Surface oxide on metallic particles are detrimental since they alter the liquid wetting and spreading characteristics. Higher oxygen content also reduces the carbon content during sintering and this depletion raises the temperature for optimal

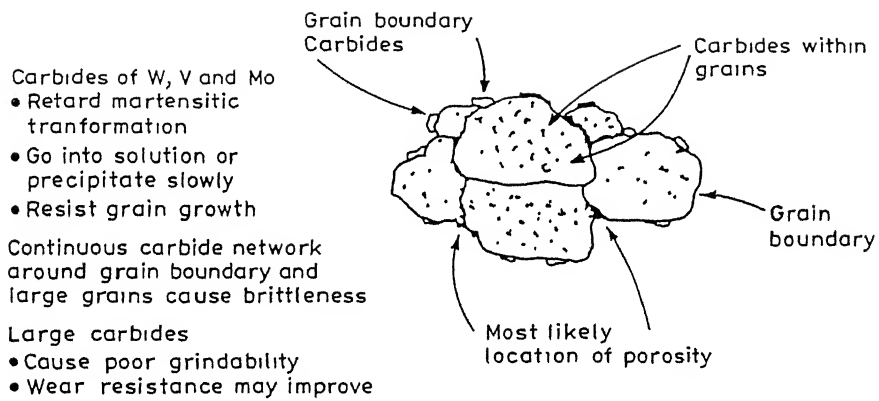


Fig 1.3 Schematic of microstructure of as-sintered P/M HSS [14].

sintering. Oxygen from the annealed powder reacts with the carbon during sintering to form CO. About 0.01% carbon is lost for every 0.01% oxygen present in the annealed powder. There are two main processes of reduction of HSS powders, reduction in a vacuum and reduction in a very dry hydrogen atmosphere with a dew point between -40°C to -70°C . It was found that vacuum annealing resulting in powder with better sinterability than hydrogen annealing. Application of vacuum is likely to shift the equilibrium of the CO formation reaction, which is the decisive factor for reducing the oxygen content, to the forward direction. However, decreasing the amount of oxygen has its drawbacks as well, since it lowers the sintering activity of the powders. So, the presence of a sufficient amount of residual oxygen is essential for the activation of the sintering process. The effect of oxygen content on HSS powders during sintering is schematically present in Fig. 1.4 [14,16,26].

Sumitomo Metal Industries Limited (Japan) has developed a novel powder production process in which melt of the HSS is atomized with oil. The aim is to reduce the oxygen content. Here the rate of particle cooling is less than water atomization process [28].

1.5.4 Sintering Aids

The carbon content of the HSS is one of the most decisive factors in affecting sintering temperature. Addition of graphite before sintering can play a very important role, since it can alter the optimal sintering temperature for the system through the change of solidus line and can balance the carbon loss caused by the reduction of oxides. In the range of technical interest the solidus temperature is lower by 9°C as the carbon content increases by 0.1%. Besides, carbon addition can eliminate porosity, extend the sintering range and improve the microstructure [2,29,30].

Activated sintering of HSS (namely: M3/2, M35, T15 and T42 grades) to full density at temperatures in the range of $1120-1150^{\circ}\text{C}$ can be achieved by the addition of eutectic or Cu_3P alloys or copper-phosphorus system [3]. Phosphorus (in the form of Cu-P), added by blending, allows full density to be achieved by a form of activated liquid phase sintering at $\sim 1130^{\circ}\text{C}$ with M3/2 HSS [17]. The mechanisms leading to densification are complex. Studies have shown that densification occurs in several stages due to a successive series of liquid phases formed at different temperatures. Within the temperature range of $1050-1150^{\circ}\text{C}$, these liquid phase reactions can occur, including iron-iron phosphide eutectic, melting of copper and an austenite plus M_6C carbide eutectic.

Dudrová et al. [31] reported that addition of 6% copper and 0.35% graphite in the M2 grade HSS increases densification during sintering in vacuum. The addition

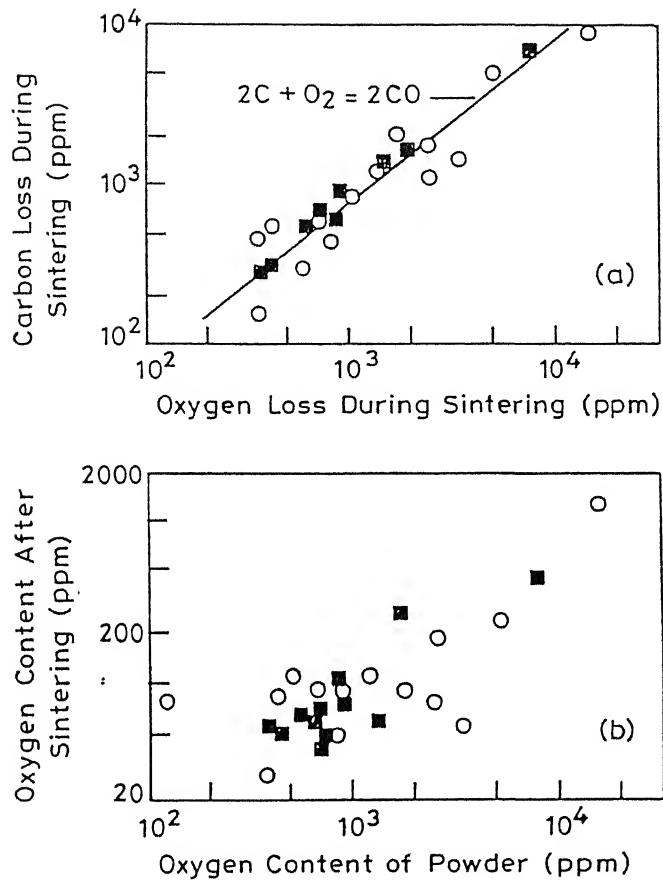


Fig 1.4 Relation between oxygen content of powder and carbon loss during sintering and between oxygen content before and after sintering: ○ Okayama et al. [27] and ■ Wahling et al. [2].

of graphite causes a pronounced increase in density. This is related to acceleration of reduction processes before the development of a higher portion of closed porosity. Additionally, carbon slows down penetration and diffusion saturation of the matrix and thereby, increases the proportion of free copper and promotes the process of secondary rearrangement. Although, the addition of graphite to HSS powders without copper gives high densification, it also results in degradation of microstructure due to the development of continuous eutectic phase, coarse carbide, and considerable coarsening of grains.

Igharo et al. [32] proposed that mixed HSS (Fe-0.63C-4.1Cr-5.0Mo-3.0V-6.2W) and iron powders containing phosphorus could be sintered with good dimensional control and adequate mechanical properties. The sintering characteristics of mixed HSS plus Fe-P powder compacts are strongly dependent on the phosphorus content. In general, good dimensional control is achieved except at large concentration of phosphorus where excessive shrinkage is found. However, good dimensional control can be restored by adding excess carbon.

Elemental boron is found to be a very potent aid to densification, since they lower the densification temperatures. Boron is more potent than graphite, but the necessary small addition of it makes process control more difficult. Moreover, boron is not normally included in the standard composition of HSS [33].

1.5.5 Green Density

The green density increases with increasing compaction pressure. All other conditions being equal a higher density compact requires a lower temperature for full densification during sintering. If the density is too low it may not be possible to eliminate some large residual pores. Green densities in excess of 85% (approx.) can trap gas in the pores. Also, higher green densities have an adverse effect on capillary flow of the liquid and hinder final densification. In practice, a green density of about 70% results in effective densification. Density gradient in the green compact is a source of distortion during sintering [14,16,23].

1.5.6 Sintering Atmosphere

Vacuum sintering is usually the best choice for SLPS. In this atmosphere the as sintered density is close to the theoretical density and the microstructure is very fine. The use of vacuum during the final densification stage avoids the trapping of gas in the pores. However, the specimen still contains some large pores, up to about 100 μm in diameter. The structure of these pores is similar to those in the argon or hydrogen sintered samples and thus, it is probable that the pores formed by a similar mechanism [23,34].

Hydrogen sintered HSS requires a lower sintering temperature to achieve high density than vacuum sintered HSS. This is because of the good thermal conductivity and also during sintering, a fresh oxide surface of the metal powder is immediately reduced by hydrogen. It has been investigated that the samples sintered in argon or hydrogen atmosphere contain relatively large amounts of pores. The pore size decreases with increase in the compaction pressure, but the pore volume is virtually unaffected by the compaction pressure. The pores are rounded and evenly distributed which leads to the assumption that they are trapped gas pores [7.34].

Sintering in nitrogen rich atmosphere results in full density and near net shape at temperatures 30-50°C lower than in vacuum and also widening of 'sintering gate'. The degree of oversintering possible, without the formation of a continuous deleterious layer of eutectic carbide, is increased by sintering in nitrogen atmosphere. This atmosphere also offers additional benefits associated with microstructural control which gives finer grain size, finer carbonitrides instead of massive carbides and improved mechanical properties. During sintering some carbon in MC is substituted by nitrogen, giving carbonitrides. The carbonitrides are smaller in size than original MC carbides which indicates that a process of dissolution of MC carbides and reprecipitation of carbonitrides takes place during sintering. The carbon which is rejected as a result of this process lowers the solidus and therefore, the sintering temperatures. It also stabilizes the austenite and increases the amount of retained austenite. When a substantial amount of carbonitrides is present after nitrogen sintering, oversintering has only a minor effect on grain growth since carbonitrides do not dissolve and/or grow during oversintering [35].

1.5.7 Sintering Temperature and Time

Sintering temperature is the most important process variable in SLPS of HSS. The optimum temperature for sintering a specific lot of HSS powder is slightly above the solidus and depends on its actual chemistry and some process variables. The sintering temperatures generally lie between 1150°C and 1350°C. At temperatures below the solidus, the controlling mechanism is solid state diffusion and even at prolonged durations at these temperatures pores are not eliminated. The microstructure of undersintered specimen consists of very fine carbides and grains in addition to porosity. At correct sintering temperatures, full density is achieved within a few minutes. The microstructure has little or no porosity or no eutectic or evidence of melting in addition to uniformly dispersed carbides, and uniform grain size. With further increase in temperature, though full density is achieved, there is a tendency for grain coarsening, formation of a continuous network of massive carbides at the grain boundaries and porosities with sharp ends usually at

triple points. If the sintering temperature is extremely high incipient melting may occur in local zones and may result in eutectic formation during cooling. Presence of excessive amount of liquid phase due to oversintering may cause slumping of the specimen. Fig 1.5 indicates the sintering range for T1 grade HSS [6,14,33,34].

Moon et al [28], using T1 grade HSS, proposed that slight decrease in sintered density with increasing temperature might be related to homogenization of elementary powders during sintering. The change of mole volume and formation of Kirkendall pores can accompany homogenization resulting in a swelling effect. However, several investigators have reported that this slight reduction in density is due to either microstructural changes or loss of some volatile components [14,36].

In conclusion, the control of temperature is essential for proper sintering. The solidus of HSS, in principle, also depends on the local composition which may be difficult from the average bulk chemistry. Furthermore, the temperature range required for sintering to full density is extremely narrow, so uniform temperature distribution in the furnace is necessary [14,37].

In addition to sintering temperature, the sintering time is also another variable. However, the densification process is less sensitive to sintering time than to sintering temperature. At the optimal sintering temperature, full density is obtained within a reasonable sintering period. But at lower sintering temperatures, density level does not reach 90% even after a long period of holding. Increasing the sintering temperature decreases the amount of time required to achieve full density. High temperatures also reduce the time between reaching full density and oversintering. The sintered density increases slowly with increasing time, being logarithmic of the sintering time. Prolonged holds give relatively minor benefits and often cause property and density decrements [6,14,16,34].

1.5.8 Heating and Cooling Rate

The heating rate is dictated by furnace capabilities and a need to reduce surface oxides prior to significant densification. Faster heating gives faster densification in SLPS, since less homogenization occurs. With slow heating, the compositional gradients in the powder are reduced, giving less densification at temperatures below the optimal sintering temperature. When the powder is slowly heated or annealed prior to SLPS, the volume of liquid becomes invariant with sintering time. Typical heating rates in practice are between 0.5 and 10°C/min [23].

The microstructure and properties observed after SLPS depend on the cooling rate [15,23]. Phase transformations can also take place during cooling which affect the end

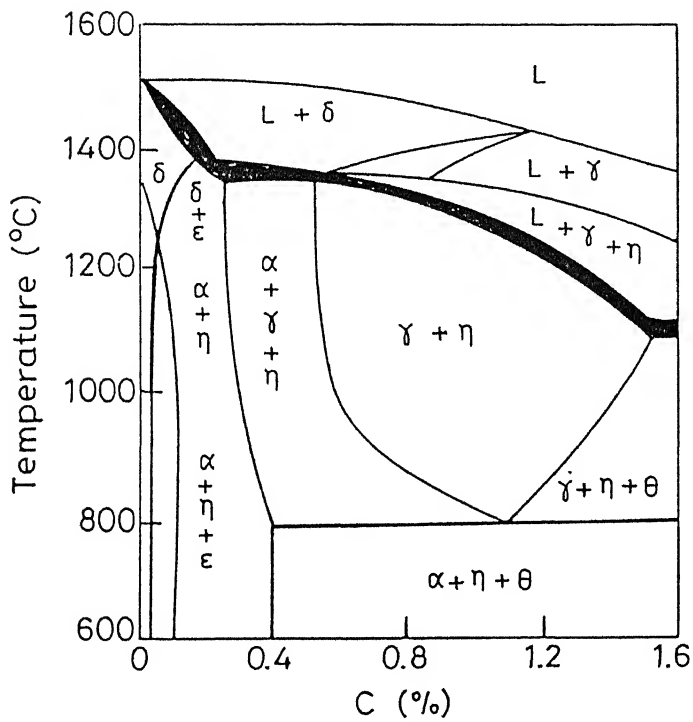


Fig 1.5 Phase diagram of Fe-W-Cr-C system at W=18%, Cr=4%, showing the region with liquid phase and the supersolidus sintering temperature range [15].

properties. Very rapid cooling leads to solidification pores which are detrimental for properties. Holds at temperatures just above the solidus during cooling increase the final density by minimizing solidification porosity. Slow cooling decomposes the grain boundary film that is liquid at the sintering temperature. This can be beneficial to the mechanical properties but adds expense to the sintering cycle.

1.6 Heat Treatment

Proper heat treatment of sintered HSS is essential for developing their properties. P/M HSS are subjected to same basic heat treatment as their conventional counterparts, but they tend to respond more rapidly and with better predictability because of their more uniform microstructure and finer carbide size. The basic heat treatment used include preheating, austenitizing, quenching and tempering. The basic heat treatment steps are [1,6]:-

- Annealing- Heat to 850 to 900°C, then slow cool (10°C/h) to 700°C. This step is needed to relieve the internal stresses developed during sintering and to provide optimum austenite grain size in the hardened samples.
- Stress relieving (before hardening):- Hold for (approx.) 2 hr. at 600 to 700°C, then slow cool to 500°C in furnace. It helps in minimizing distortion on hardening.
- Hardening- Preheat in two steps, first at 450 to 500°C and then at 850 to 900°C. Austenitize at 1050 to 1180°C and quench, preferably in neutral salt bath. Cool to hand warmth. The austenitizing temperatures of 'T' grade HSS are in the range of 1204 - 1310°C and those of 'M' grade HSS are in the range of 1093 - 1246°C [1].
- Tempering;- Raise temperature to 560°C or higher. Repeat two or three times for at least 1hr. at full temperature. Cool to room temperature between tempers. The purpose of it is to soften the martensite in the usual way, to provide secondary hardening by precipitation hardening, and to 'condition' the retained austenite by precipitation of carbide so that it can transform into martensite on cooling to room temperature.

The extent of distortion during heat treatment depends on the type and degree of segregation. But in case of HSS, as these are segregation free, variations in dimensional change are smaller and more uniform in all directions. The dimensional change can, therefore, be predicted more accurately. Moreover, in contrast to defective sintering, if a product achieves inferior final properties due to defective heat treatment, a corrective

heat treatment can be done without spoiling the part. A poorly sintered part can never achieve the best of properties. in spite of best heat treatment offered to it [34].

1.7 Mechanical and Electrical Properties

The mechanical properties are dependent on the residual porosity and sintered microstructure [16]. Sintered HSS can suffer from three major strength reducing microstructural defects, namely. (i) metallic/non-metallic inclusions. caused by contamination during powder processing, (ii) porosity, if the sintering temperature and time are chosen too low, (iii) carbide/grain coarsening, if the sintering temperature and time are too high.

1.7.1 Modulus of Elasticity

Presence of residual porosity of the sintered HSS reduces its elastic property. Andrievskii et al. [38] proposed that in the porosity range $\sim 20\%$ the effect of porosity on the modulus of elasticity is almost linear. This is in agreement with a large number of the well known dependences $E=f(P)$, where E is modulus of elasticity and P is porosity. It was found that R6M5F3 HSS ('M' grade) with a porosity of 2.5% has an elasticity modulus of 225 GPa and R12MF5 HSS ('T' grade) with a porosity of 5%, has an elasticity modulus of 218 GPa. The effect of porosity on the elastic property of HSS is shown in Fig. 1.6.

1.7.2 Hardness

Apparent hardness is a bulk property and in P/M HSS it is a complex measure of the combined effect of some factors, which include grain size, matrix strength, type, volume fraction and size distribution of carbides, the extent of carbide coarsening and porosity [39,41].

The sintered hardness of the HSS depends on the sintering temperature and cooling rate after sintering and the hardness after heat treatment depends on the composition and heat treatment conditions [3,29,39]. Generally, specimens sintered at optimal sintering temperature give higher hardness than the specimens sintered at other temperatures, which may be attributed to residual pores for the specimens sintered at lower temperature, and to the oversintered structure of the specimen sintered at higher temperature. Addition of carbon also improves the hardness. Fig. 1.7. shows the effect of sintering temperature on hardness for HSS by addition of carbon.

The most important factor affecting the apparent hardness is the cooling rate after sintering. which depends on the type of furnace used for sintering. The cooling rates

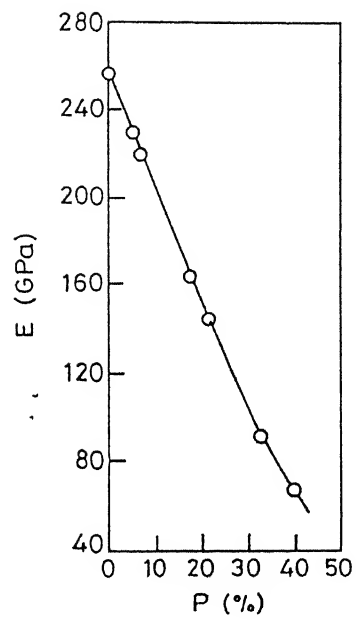


Fig 1.6 Effect of Porosity on elastic modulus of R12M3K8F2 ("T", grade) high speed steel [38].

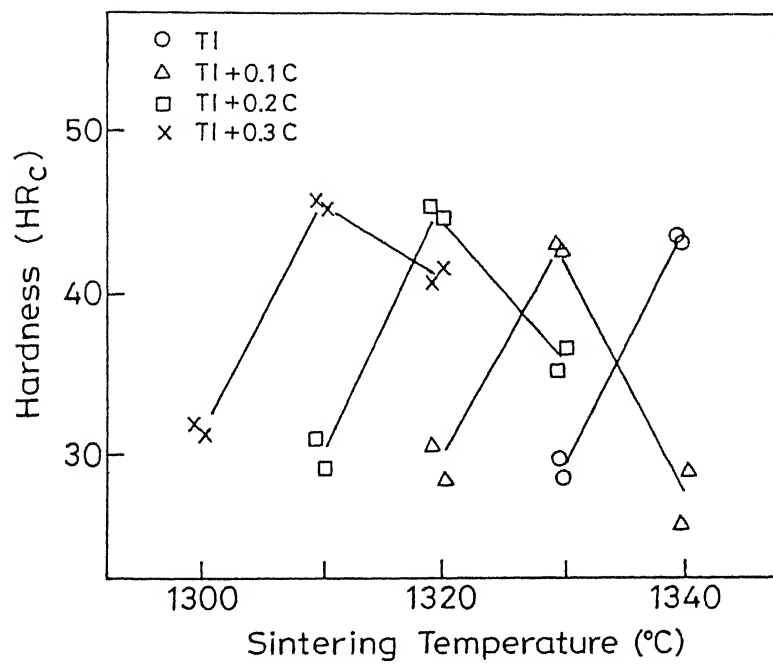


Fig 1.7 Effect of sintering temperature on hardness for T1 high speed steel by addition of carbon.[29].

from sintering in retort type gas atmosphere furnaces are too low to give any hardening effect, whereas samples sintered in mesh belt furnaces have sufficiently high cooling rates to achieve full hardening. In case of continuous furnaces, cooling rates are always more than sufficient to achieve maximum hardness as HSS are air hardening materials.

During heat treatment higher peak hardness is obtained by using higher austenitizing temperatures to dissolve more of the primary carbide phase. The finer carbide size distributions give rise to significantly higher amounts of carbide dissolution, resulting in higher peak tempered hardness ($>1000 \text{ HV}_{30}$). The hardness does not change significantly with subsequent tempering because the precipitation of secondary carbides has little effect on bulk properties.

Brewin et al. [39], using water atomized M3/2 HSS, found that the addition of copper by infiltration in HSS, the hardness rises steadily with increasing copper content, since the density increases by infiltration. The apparent hardness of the admixed copper samples increases steadily up to 8% copper but further addition of copper decreases the hardness due to presence of excess free copper which counteracts the solid solution strengthening effect of the copper in the matrix. Presence of slag particles in the HSS does not show any systematic variation of the hardness [41]. It was found that increasing compaction pressure significantly increases the apparent hardness. The effect of process variables on apparent hardness is shown in Fig. 1.8.

Hot hardness, or tempered resistance, is largely determined by the composition and growth of the secondary hardening carbides and is promoted by vanadium, molybdenum, and cobalt [6].

The microhardness of as-atomized powder is rather high which is of about 800 or higher on the Vickers scale (corresponding to $R_c 60$). The microhardness increases with a reduction of the particle size and with increasing carbon content in the powder. This is attributed to an increase of the cooling rate in case of fine particles and to heterogeneization of the structure. In the neck contact zone of the sintered specimens the microhardness increases, whereas in the centre it decreases. This is attributed to a more intensive inflow of carbon atoms into the contact neck region, since the diffusivity of carbon is higher than that of metallic atoms [33,42].

1.7.3 Transverse Rupture Strength

Fracture strengths of HSS are, generally, determined by three or four point bending, transverse rupture strength (TRS) or modulus of rupture tests that assume linear elastic deformation. This is usually identified as the bend strength, with the quaint term 'modulus of rupture in bending' also being used [3]. The values of TRS depend on

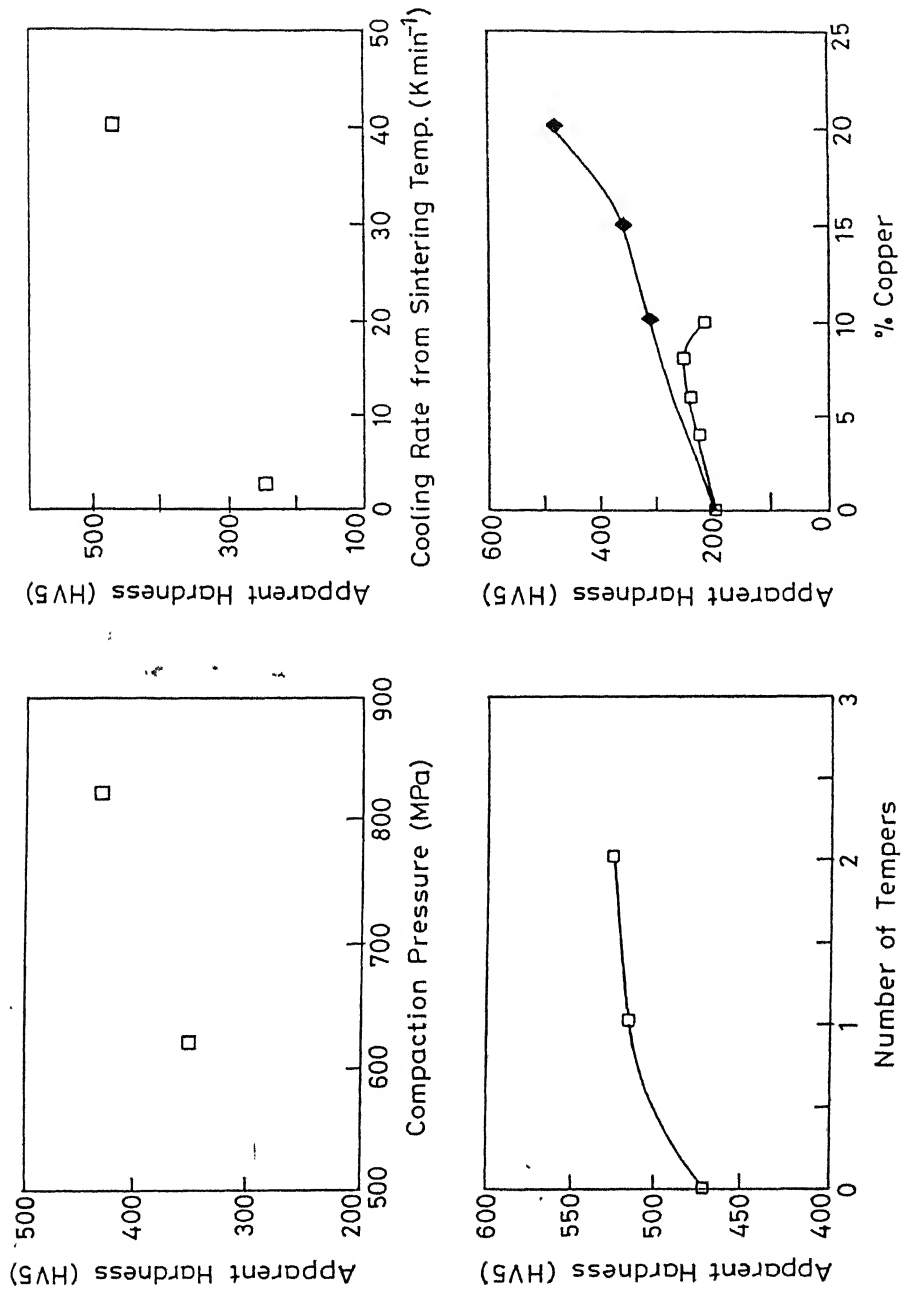


Fig 1.8 Effect of process variables on apparent hardness of M3/2 high speed steel (a) compaction pressure, 1120°C, 30 min; (b) cooling rate, 1120°C, 30 min; (c) number of temperings, 60 min. tempering at 560°C, sintering temperature 1120°C, sintering time 30 min; (d) Cu content, 1120°C, 60 min vacuum, \square = admixed, \blacklozenge = infiltrated; [39].

the size, method of loading and geometry of the test specimen, since failure is generally associated with the presence of some critical size defect which initiates crack propagation, such as brittle carbides, inclusions or pores. The specimen fractures when the stress attains the critical value for the particular size of the defect present or when the defect grows to a critical size by some subcritical growth process.

Primary carbides are frequently responsible for crack nucleation and proper control of their size, distribution, and shape during processing is an essential requirement in order to obtain high TRS. Fine carbide distributions are desirable, since smaller carbides form smaller cracks which may not be critical. M_6C type carbides often tend to be coarser and more angular in shape than MC type carbides. Hence, the formers are more harmful and frequently act as fracture initiation sites than latters. Slag inclusions have a strong influence on the TRS, since they act as fracture initiation sites. The TRS is proportional to the inverse square root of the crack initiation inclusion size. Residual porosity, found in directly sintered materials, acts as fracture initiation sites and reduces the TRS. Compaction pressure has a minor effect on TRS [3,39,41].

Brewin et al. [39], using water atomized M3/2 HSS, proposed that the dominating factor in TRS is sintering time. A 100% increase in TRS can be achieved by altering the sintering time from 30 to 60 minutes. The TRS can also be increased by increasing the sintering temperature. However, higher sintering temperature causes coarser carbide distributions to occur which reduce TRS. It was found [43] that in case of vacuum sintered HSS, both oversintering and undersintering by 5°C reduce TRS by 25%, since the former leads to carbide growth and latter increases porosity.

Addition of copper-phosphorus to HSS give lower TRS than their equivalent standard HSS because such steels can not be hardened to the same extent by heat treatment [39]. However, addition of elemental copper (up to 6% by admixing powder or up to 15% by infiltration) increases TRS because presence of copper increases the density. Effect of various process variables on TRS is schematically shown in Fig. 1.9.

Several processing methods, namely, undersintering followed by containerless-HIP'ping or hot working can be used to increase the TRS of sintered HSS or at least to keep TRS as high as possible by refining carbides. It has been found that post sintering HIP treatment can increase TRS of T15 and M3/2 HSS by 20-30%. If the T15 HSS is undersintered to densities in excess of 95% and HIP'ped, the improvement amounts to 50% compared with sintering to full density. The TRS of HIP'ped steels can reach values as high as 5 GPa while the directly sintered grades do not normally exceed 2 GPa [3,43].

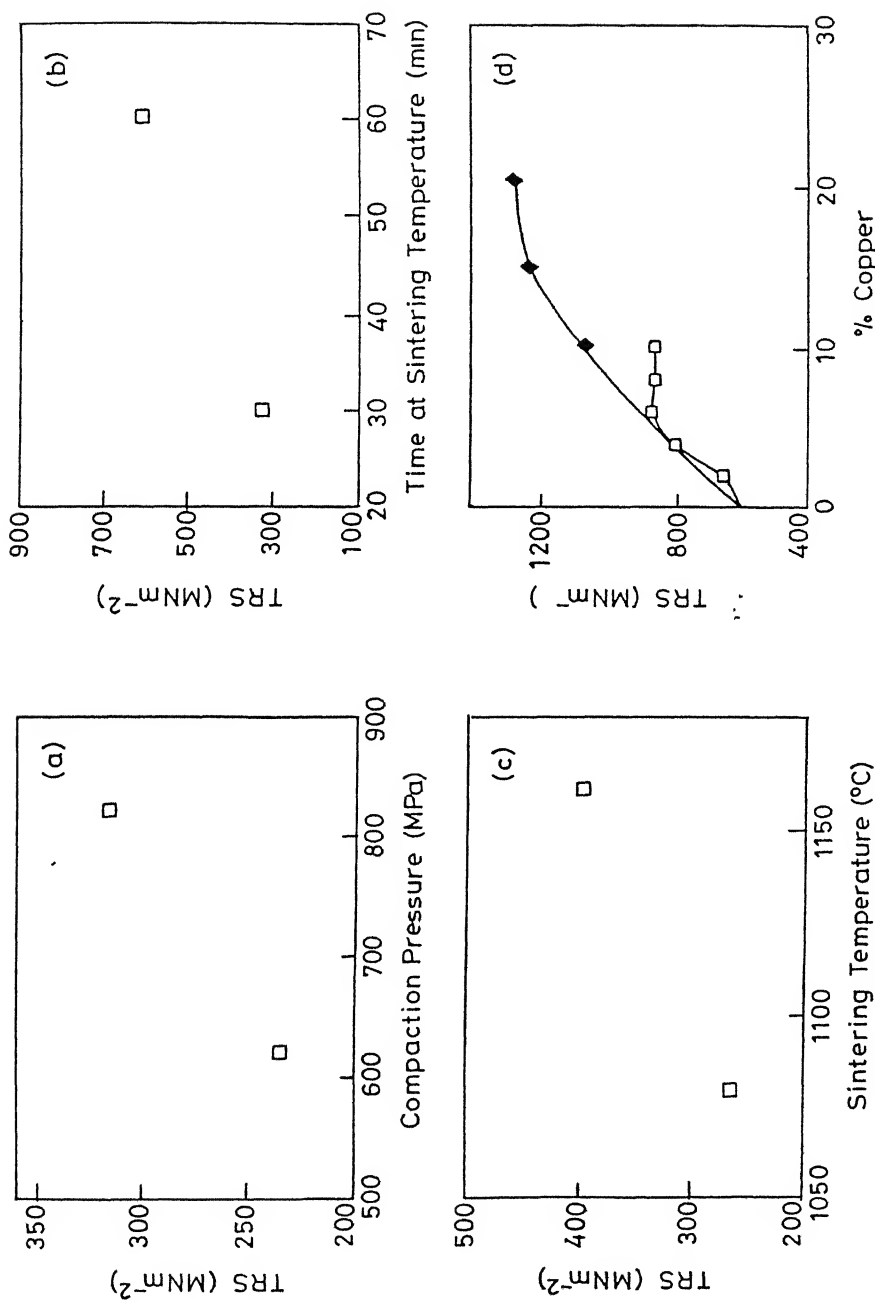


Fig 1.9 Effect of process variables on TRS of M3/2 high speed steel (a) compaction pressure, 1120°C, 30 min. cooling rate 40 K min⁻¹, 90N₂-10H₂; (b) sintering time, 1120°C, cooling rate 2.5 K min⁻¹, 80N₂-20H₂, compaction pressure 620 MPa; (c) sintering temperature, 1120°C, 15 min, cooling rate 2.5 K min⁻¹, 80N₂-20H₂, compaction pressure 620 MPa, (d) Cu content, 1120°C, 60 min, vacuum, compaction pressure 620 MPa, □ =admixed, ◆ =infiltrated; [39].

1.7.4 Fracture Toughness

Critical stress intensity factor (K_{IC}) represents the fracture toughness of the material and it is a material property. (K_{IC}) is not sensitive to microstructure of HSS in term of the type, size and shape of any primary carbides. Crack propagation, and hence the fracture toughness, only become sensitive to microstructure when the spacing between the microstructural features that can initiate cracking, such as primary carbides, pores or inclusions, are comparable to the size of the plastic zone at the crack tip and when they are present in sufficiently large numbers to influence crack growth across the whole crack front. Fracture toughness can only be affected when sufficient numbers of small sub-critical cracks formed within this crack initiation sites lie within the plastic zone and when the spacing between them is small. Localized plastic deformation and eventual fracture of any intervening matrix then become easy enough for small cracks to unite into the large propagating cracks which determine fracture toughness. Thus, for the same values of hardness, sintered HSS tend to have similar (K_{IC}) values compared to their wrought counterparts because similar carbide spacing exist in both materials despite any differences in carbide size [3]. Fracture toughness of wrought and sintered HSS are shown in Table 1.2.

Martinez et al. [44], using water atomized T6 and T15 HSS, observed that additional HIP'ping after sintering has no influence on fracture toughness of HSS. However, the HIP'ped HSS (fine carbide distributions) shows lower (K_{IC}) values than the direct sintered materials (coarse carbide distributions), since, fine closely spaced carbides encourage easier crack propagation. The fracture toughness decreases as hardness increases but with increasing the amount of retained austenite, it increases. Fig. 1.10 and Fig. 1.11 shows the dependence of fracture toughness on the hardness and amount of retained austenite, respectively.

1.7.5 Fatigue

Several investigations revealed that the cycling life time of low cycle fatigue of HSS decreases with increasing hardness. The size and the distribution of the primary carbides are probably of importance in the initiation of the fracture. The fatigue crack propagation rate appears to be primarily dependent on the strength and ductility of the martensite-austenite matrix. The average life time is dependent on the austenitizing temperature and thus, also on the final hardness after tempering [45].

The crack-start, during rotating bending of HIP'ped and vacuum sintered HSS specimens, depends on the size of the largest hard phase (carbide, inclusion) or pore which are normal to the rotating bending stress. Because they resemble discontinuities within

Grade	Condition [†]	K_{IC} (MNm ^{3/2})
M2	WL	18,15-20
	WT	24
	FS	30
	Forged	15-20
T1	WL	21
	WT	22
	FS	25
T6	WL	16
	WT	18
	FS	31
T42	WL	12
	WT	12
	FS	13
M3/2	As sintered, fully heat treated	19
M3/2-TiC-MnS composite	As sintered, fully heat treated	21.4
M3/2-NbC-MnS composite	As sintered, fully heat treated	22.7
M3/2-Cu ₃ P*	As sintered	14.5
M3/2-TiC-Cu ₃ P* composite	As sintered	13.9
C23	HIPed heat treated	18.7
ASP 30	HIPed heat treated	14.8
ASP 60	HIPed heat treated	12.9

† W: wrought; L: longitudinal; T: transverse; FS: sintered to full density.

* Sinter assisted by copper phosphorus.

Table 1 2 Fracture toughness of sintered and wrought high speed steels [3]

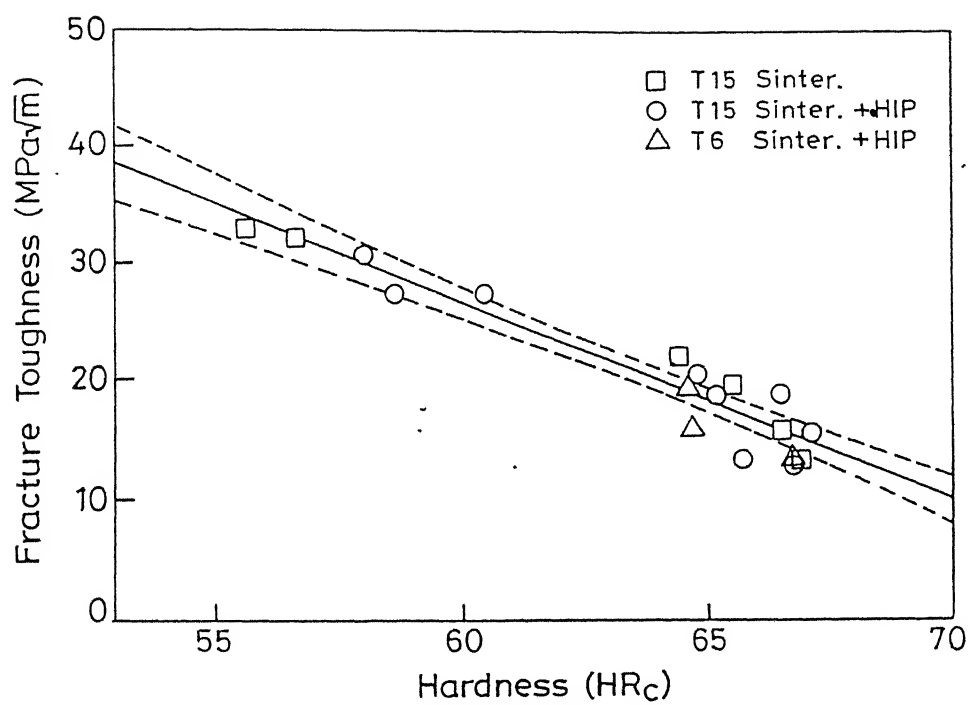


Fig 1.10 Dependence of fracture toughness on hardness of T6 and T15 P/M high speed steels [44].

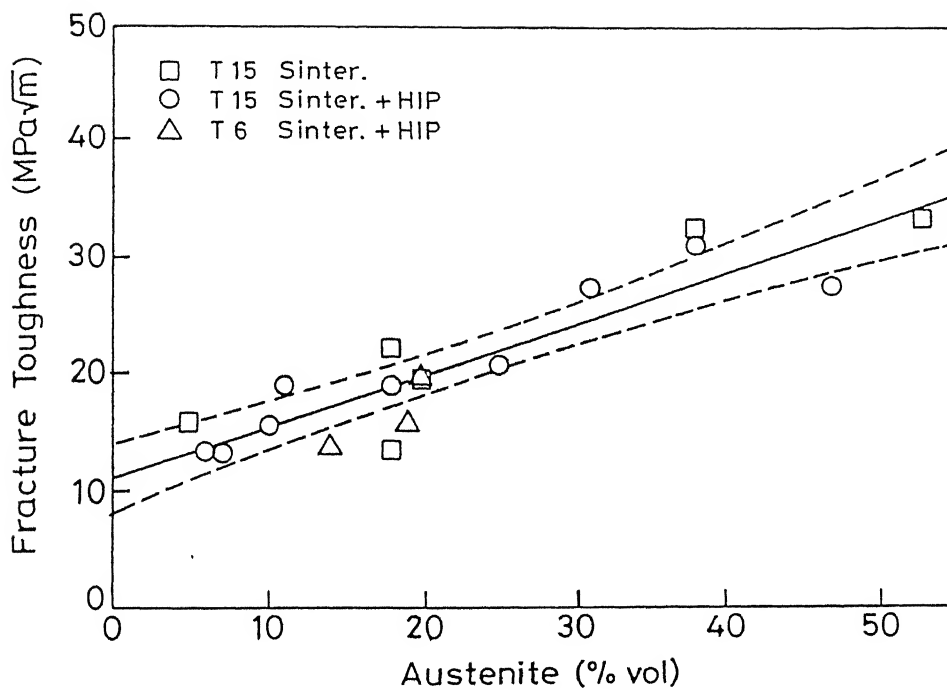


Fig 1.11 Dependence of fracture toughness on the amount of retained austenite of T6 and T15 P/M high speed steels. Chain lines represent the 95% confidence limits [44].

the hardened matrix and act as stress concentrators [46]. Due to the frequency and location of the largest discontinuity or defect, the crack is initiated at or below the surface. In HIP'ped HSS, non-metallic inclusions are larger than carbides and pores and, therefore, give rise to crack start. In vacuum sintered HSS, crack starts at pores and after hot working at non-metallic inclusions. Because of the small volume fraction of inclusions and pores the probability of subsurface crack initiation is higher in P/M HSS. Life to fracture in rotating bending primarily results from the life to crack initiation and therefore, a function of purity, density and carbide size. Fatigue life is increased as the local stress intensity of discontinuities at or below the surface decreases. This can be done by the size reduction of hard phases and pores. Smaller pores without inclusions and a sufficient degree of hot working are beneficial for vacuum sintered steels.

It was found that the P/M HSS show much better fatigue properties than conventional HSS. This is related to much more fine and homogeneous microstructure of the former in comparison to the latter. The specimen with ground surface decreases the fatigue life than the specimen with a polished surface. The fatigue strength decreases with increasing slag inclusion size [41], because in most cases fracture initiation is found to occur at slag inclusions. A compressive stress has a large negative influence on the fatigue life. The life time of the conventional and P/M HSS (ASP30 and M2 grades) specimens cycled in both tension and compression is considerably shorter than the life time of either steel exposed to tension stress only (Fig. 1.12.).

Failure due to rolling contact fatigue (RCF), generally, results in a loss of surface materials due to the action of stresses at or below the point of contact of the load. Porosity has a significant role in the failure of sintered materials subjected to RCF. The endurance limit of the materials at lower densities is controlled by the pore distribution. Angular and interconnected pores provide ready sites for fatigue crack initiation and subsequent propagation. It was found that for full density sintered T15 HSS, the endurance limit can reach above 380 MPa. This is primarily due to the absence of porosity, the fine microstructure and high cleanliness of the powder [47].

1.7.6 Superplasticity

The strain rate sensitivity of the deforming stress ' m ' is the primary criterion of the appearance of superplasticity. It characterizes the inherent capability of the material to resist the formation of a neck. The greater is ' m ', the higher is the deformation resistance of the specimen. P/M HSS are prone to superplastic deformation which is stipulated by the high values of ' m '. Gogaev et al. [48], using 'M' grade P/M HSS, found that with strain rates of 10^{-4} - 10^{-2} s $^{-1}$, the values of ' m ' could vary from 0.35-0.38 to 0.52-

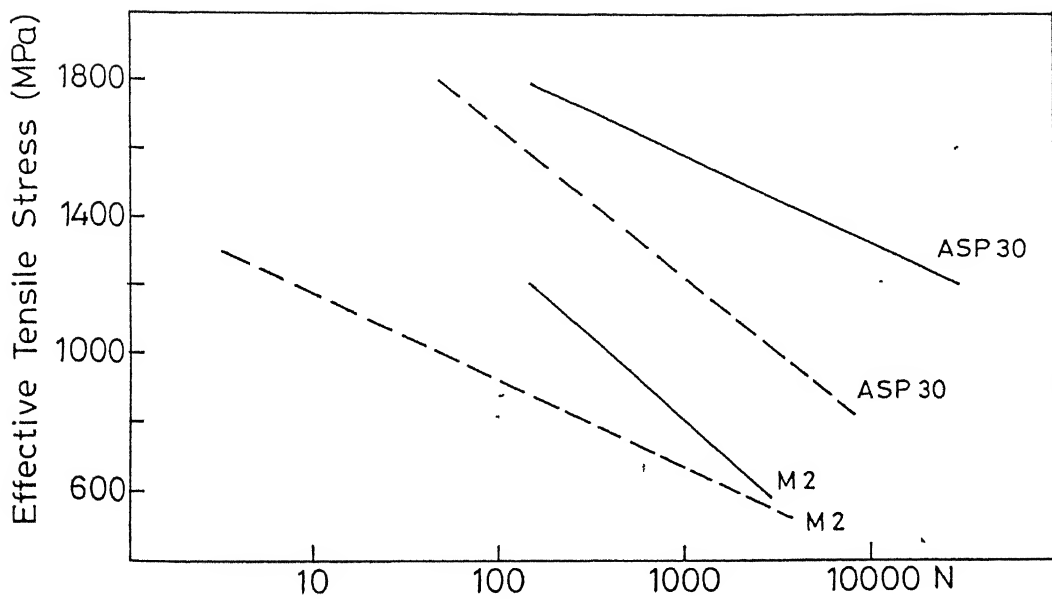


Fig 1.12 Fatigue life as a function of effective tension stress of different grades of P/M high speed steels. Effective compressive stress 3100 MPa (dotted lines) and 0 MPa (solid Lines) [45].

0.57 ($T=1100^{\circ}\text{C}$ and $\epsilon=20\%$) with a reduction in strain rate. However, the inclination to superplasticity is restricted by pore accumulation during deformation which is associated with microstructure and is governed by deformation mechanism. The higher the value of initial porosity and the lower the value of 'm', the lower the plasticity of material. The grain boundary condition plays a significant role in superplastic deformation and fracture processes. Presence of impurities and precipitates at the grain boundaries reduce the superplastic effect [49].

1.7.7 Electrical Property

The electrical resistance of the P/M materials (ρ_k) can be determined from the well known equation $\rho_k = \rho(1-1.5\theta)$, where θ is porosity and ρ is the electrical resistance of the material in absence of porosity. The sintering temperature has a major effect on the density and hence, the electrical resistance of the material. Andrievskii et al. [42], using R12M3K5F2 ('T' grade HSS), found that increasing the sintering temperature of the HSS, the density increases with the formation of a liquid phase and correspondingly, the electrical resistance decreases and at a sintering temperature of $1225-1250^{\circ}\text{C}$ the electrical resistance is $50-60 \mu\Omega.\text{cm}$.

1.8 P/M Based Particulate Composites

Hard ceramic particles are easily incorporated into HSS where advantage can be taken of their excellent P/M characteristics to produce full density metal-matrix composites with compositions and structures that would be impossible to produce by any other means. The purpose of developing metal-matrix composites is the improvement of wear resistance of the base material in order to have the toughness of the metallic matrix and the hardness of the ceramic particles in the same material [50,51].

Sinterability is reduced by the introduction of finer ceramic particles and by increasing the volume fraction of ceramic additions [52]. Because these lead to increase in the number of interfaces that required to be wetted by the liquid phase formed during sintering. The liquid phase also flows into cracks and clusters of ceramic particles. Thus, if the same quantity of liquid phase is always present complete wetting between the ceramic and liquid phases become more difficult to achieve. Ceramic particles can also form an obstruction to particle movement and thereby, hinder particle rearrangement. In order to improve sinterability and lower the sintering temperature, sintering aids (Cu_3P alloy, graphite etc.) are added.

The hardness of composite materials is expected to be affected not only by the hard phases added to the base material but also by porosity level in the sintered parts.

Additions of hard particles do not increase the hardness significantly [51]. However, hardening and tempering cause a slight increase in hardness due to secondary hardening. Increasing ceramic additions cause a gradual decrease in TRS due to poorer sinterability and increased porosity. Moreover, ceramic particles act as crack initiators. The heat treatment reduces TRS slightly. The fracture toughness (K_{IC}) is not affected by the presence of the ceramic particles since carbide, ceramic particle and pore spacing being beyond the limits of the plastic zone. However, the heat treatment causes a reduction in fracture toughness due to increase in the matrix hardness. Additions of ceramic particles also restrict the grain boundary movement and therefore, yield finer prior austenite grain size [52].

Thermodynamically less stable carbides, such as SiC and Cr_3C_2 , can easily dissolve in the matrix during sintering and not retained as discrete hard particles. However, other carbides, such as WC, Mo_2C , NbC and VC, react with the matrix to produce new carbide phases with compositions similar to those of the primary carbides present in HSS. Thermodynamically stable carbides, such as TiC, can retain more or less of their original form [50].

Sinterability of the HSS plus titanium based ceramic composites depends on the wettability and reactivity of the ceramic particles. Oliveira et al. [52], using water atomized M3/2 HSS, reported that sinterability increases in the order of $TiC > TiN > TiO_2$, which is similar to their wettability behaviour. Addition of TiC particles to HSS enhances the wear properties because the hard ceramic particles are retained and well bonded into the microstructure by chemical reaction with the matrix [50]. TiC additions decrease the sinterability by raising the sintering temperature and reduce the TRS and increase the hardness slightly. Effect of TiC additions on the sintering behaviour of M3/2 HSS is shown in Fig 1.13. However, with the addition of TiC microhardness decreases due to the loss of dissolved carbon from the matrix since the reactions between the TiC and matrix cause the conversion of M_6C into MC carbides [53]. Fine TiC particles enhance more retained austenite formation than coarse TiC particles because of the localized dissolution of carbon from TiC. The composites containing coarse grained TiC additions give the best overall combination of microstructure, hardness and TRS [51]. Bolton et al. [54] found that addition of TiC particles to M3/2 HSS has little effect on heat treatment and does not significantly improve overall hardness. Despite the fact that TiC encourages MC carbides to form in place of M_6C carbides, this does not have any great influence on hardness in the heat treated composites except to slightly reduce secondary hardening effects. TiN additions raise the sintering temperature and reduce TRS [50]. TiN usually increases hardness and can be superior to TiC in raising hardness for the sintered and heat treated composites. However, addition of above 10 vol.% TiN

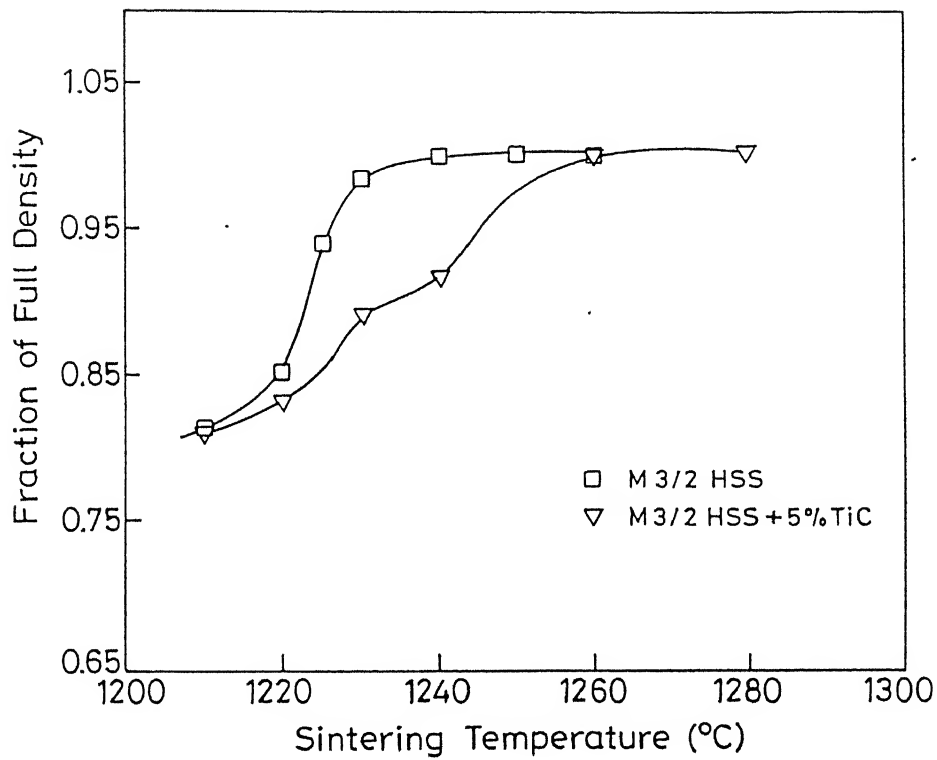


Fig 1.13 The effect of TiC additions on the sintering behaviour of M3/2 high speed steel [50].

to M3/2 HSS decreases hardness because of presence of porosity [51]. TiN particles remain chemically stable in the HSS matrix. Some reactions occur between the liquid and ceramic phase that lead to the formation of MC carbides at the ceramic/matrix interfaces [52]. This results in the TiN particles being well bonded into the steel matrix. Kar and Upadhyaya [55-60] extensively studied sintering of T15 and T42 grade HSS through supersolidus sintering. They also studied their based composites containing TiC and TiN. With the increase in TiC/TiN particle content, the density of T15 and T42 HSS decreased. The T42 based composites showed better densification as compared to the corresponding T15 based composites. This was related to the enhanced wetting behaviour in T42 HSS melt containing ~3% molybdenum as compared to practically nil in T15 HSS. The optimum sintering temperatures required to achieve full density in TiN containing composites based on either HSS (T15 or T42 grade) were lower than those containing TiC, although TiC has better wettability by iron/steel melt as compared to TiN. The increased addition of TiC/TiN also led to the coarsening of the microstructure and agglomeration of ceramic particles which lowers its strengthening effect. The TiC containing composites showed better overall properties (e.g. hardness, TRS, elevated temperature compressive yield strength and tool life) as compared to TiN containing ones. Saha et al. [60] found that except T15 HSS-4Ti(C,N) composite, the optimum sintering temperature for achieving nearly full density (>98% TD) of T15 or T42 HSS based composites increased with increase in carbonitride content. Generally, all T42 HSS - Ti(C,N) composites show better hardness compared to T15 HSS-Ti(C,N) composites. This is because of presence of higher amount of cobalt (10%), less carbide and grain coarsening, and lower optimum sintering temperature in T42 HSS based composites as compared to T15 HSS based composites which give the beneficial effect.

The composites containing TiO_2 are very porous because of poor wetting between liquid and ceramic phase. Chemical reaction between the TiO_2 and liquid phase also causes decarburization of the matrix which further contributes to loss in sinterability and decrease in hardness. Properties of HSS and TiC containing composites in various rates of heat treatment is shown in Table 1.3.

NbC and VC carbide additions improve hardness and give a general improvement of wear resistance and/or cutting performance [50]. But they can cause difficulties during powder mixing stage. Although, strengths are reduced by NbC/VC additions, their effect appears to be less detrimental than that of TiC additions. NbC gives significant increase in heat treated hardness by improving the secondary hardening response during tempering. Higher peak hardness can be obtained with M3/2 HSS + NbC composites both in the as sintered and heat treated conditions [53]. The M_6C carbides become partially replaced by a niobium rich MC carbides. Although, NbC additions are found

Composite	Property*	As sintered, fully dense, no heat treatment	Sintered & double tempered (550°)	Full heat treatment quench & double temper
M3/2 HSS	A	580	660	845
M3/2 HSS	B	2.20	2.45	1.30
M3/2+8.5 vol% TiC	A	605	665	865
M3/2+8.5 vol% TiC	B	1.80	1.70	1.25
M3/2+Cu ₃ P	A	720		690
M3/2+Cu ₃ P	B	1.89		1.36
M3/2+Cu ₃ P+8.5 vol% TiC	A	700		750
M3/2+Cu ₃ P+8.5 vol% TiC	B	1.01		1.08
T15	B			1.30
T15+10 vol% TiC	B			1.70
T15+TiC	B			1.2
M2+TiC	B			0.80
T42	B			1.20
T42+10 vol% TiC	B			1.10
T42, HIPed	A			820
T42, HIPed	B			5.0
T42+26 vol% TiC, HIPed	A			950
T42+26 vol% TiC, HIPed	B			2.5

* A = Hardness H_v 30 Kg; B = strength, TRS (GPa)

Table 1.3 Properties (average values) of (P/M) HSS and HSS + TiC composites in various states of heat treatment [49]

to raise the sintering temperature of M3/2 HSS but they also increase the width of the 'sintering window' and restrict the formation of coarse carbide grain boundary films and eutectics [61]. The apparently high thermal stability of alumina (Al_2O_3), despite its high hardness, prevents it being strongly bonded within a ferrous matrix. However, minute amounts of alloying elements (e.g. Silicon), that are simultaneously soluble in both Al_2O_3 and HSS, are apparently sufficient to develop acceptable levels of reinforcement/matrix bonding [62]. Improved and fully sintered composites can also be obtained by coating the Al_2O_3 particles by TiN before sintering, which helps the liquid phase to wet the Al_2O_3 particles [50,52]. It has been found that this type of coating can improve the hardness and TRS of the M3/2 HSS based composites with values similar to those obtained by the baseline M3/2 HSS. This is because of better bonding that occurs between the matrix and the TiN coated Al_2O_3 . Here an interfacial layer of vanadium rich MC type carbides (or carbonitrides) is formed at this interface whereas uncoated Al_2O_3 does not form this type of layer. Relatively low volume fractions of Al_2O_3 particles can be successfully incorporated into HSS matrix by sintering. But the best results are obtained by attrition milling of the powders. After sintering and heat treatment the resultant composites are superior in wear resistance than base steel and have TRS comparable to normal vacuum sintered HSS. Higher amount of Al_2O_3 decreases TRS because ceramic particles act as crack initiators, either by debonding at the particle/matrix interface or by cracking within the particles. Copper phosphide has been added as sintering aid to enhance sintering [46].

Besides, other ceramic particles, such as AlN, BN, TaC, SiC, WC, Mo_2C , HfC, ZrC and Cr_3C_2 , can be incorporated to HSS matrix. They increase the cutting life of HSS tool material [16].

1.9 Service Behavior

1.9.1 Grindability

The finishing steps in the production of cutting tools is usually the abrasive grinding. Without proper grindability, the benefit of using an improved wear surface achieved by the hardening is countered by increased grinding cost. In cases where dimensional control is very important, it is absolutely necessary to perform final grinding on the hardened piece. The cost of material removal is quite high in this step and therefore, every measure is taken to improve the grindability [63,64].

The grindability of P/M HSS is superior to that of conventional HSS of the same composition because of the small size and uniform size distribution of carbides in P/M steels [6]. Grinding wheel break down occurs when the wheel runs into the large lumps

of carbides which, in fact, lead to wear of the wheel. Since, these large lumps do not exist in a P/M HSS, wheel wear is minimized [64]. The relative grindability of several conventional and P/M HSS is shown in Fig 1.14. The grindability ratio (ratio of the volume of metal removed to the volume of wheel worn) is clearly superior for P/M HSS than conventional HSS. This ratio generally decreases for both the conventional and P/M HSS as their alloy and carbon contents increase. Presence of sulphur in the HSS improves grindability.

1.9.2 Machinability

In normal cutting operations, slower speeds are used. In such operations, P/M HSS give a significant machinability advantage over the conventional products. To evaluate machinability, comparative cut-off tests are performed. Fig. 1.15 shows the cut-off machinability of conventional and P/M M2 HSS in the annealed condition [63].

1.9.3 Cutting Performance

The cutting performance of sintered HSS is equal, or sometimes, superior to that of equivalent conventional HSS heat treated to the same hardness.

In continuous cutting, some improvement in wear rates for sintered tools can be obtained compared to conventional material. The performance consistency of the directly sintered material is much improved compared to wrought product. Fig. 1.16 shows the continuous cutting test of sintered and wrought BT6 HSS [65].

In intermittent cutting, tool life is determined on the basis of flank wear. Under this cutting condition, the P/M tools give more consistent results and appear to be less prone to premature failure than wrought tools. The flank wear of sintered tips with a density greater than 98% is superior compared to conventional tools, without any chipping and breaking of the working edge [65,66]. The intermittent cutting behaviour of wrought and sintered BT6 HSS is shown in Fig 1.17.

Tool life data from spade drilling tests of sintered and conventional M3/2 HSS are presented in Fig. 1.18. The tests were continued until failure occurred and the result for the conventional material was defined as 100%. The sintered spade drills hardened to 64.5 HR_c give a tool life improvement of 38% while those hardened to 65 HR_c performed 65% better than conventional tools. At higher cutting speeds the percentage improvement is lower, although better performance of sintered insert is maintained.

Results from single point turning tests are shown in Fig. 1.19. In all cases the inserts are superior compared to the conventional ones. The performance of sintered T42 HSS seems to be intermediate between sintered and conventional T15 HSS.

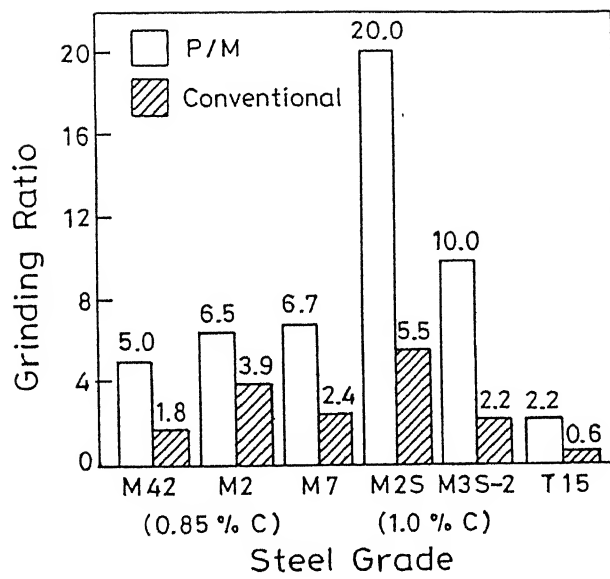


Fig 1.14 Comparative results of grindability tests of various P/M and I/M IISS grades [5].

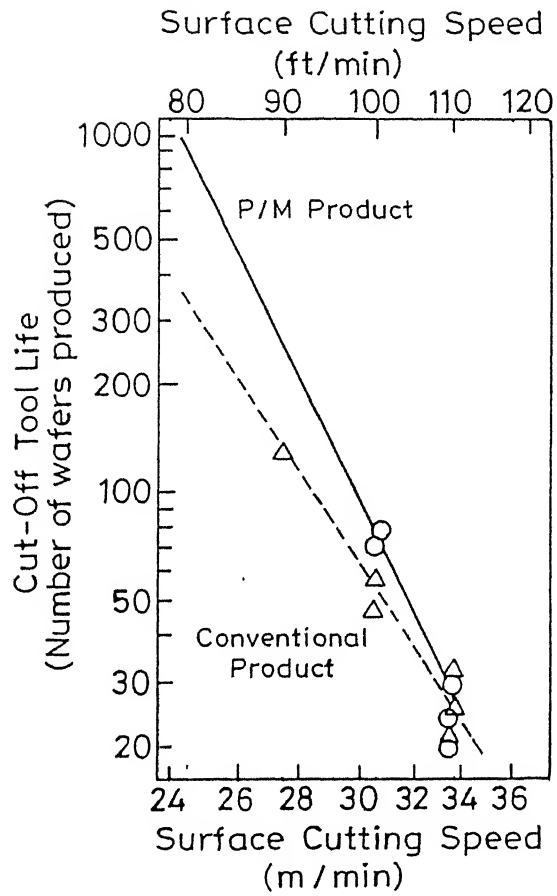


Fig 1.15 Cut-off machinability of P/M and conventional M2 in the annealed condition (R_b 100); [63].

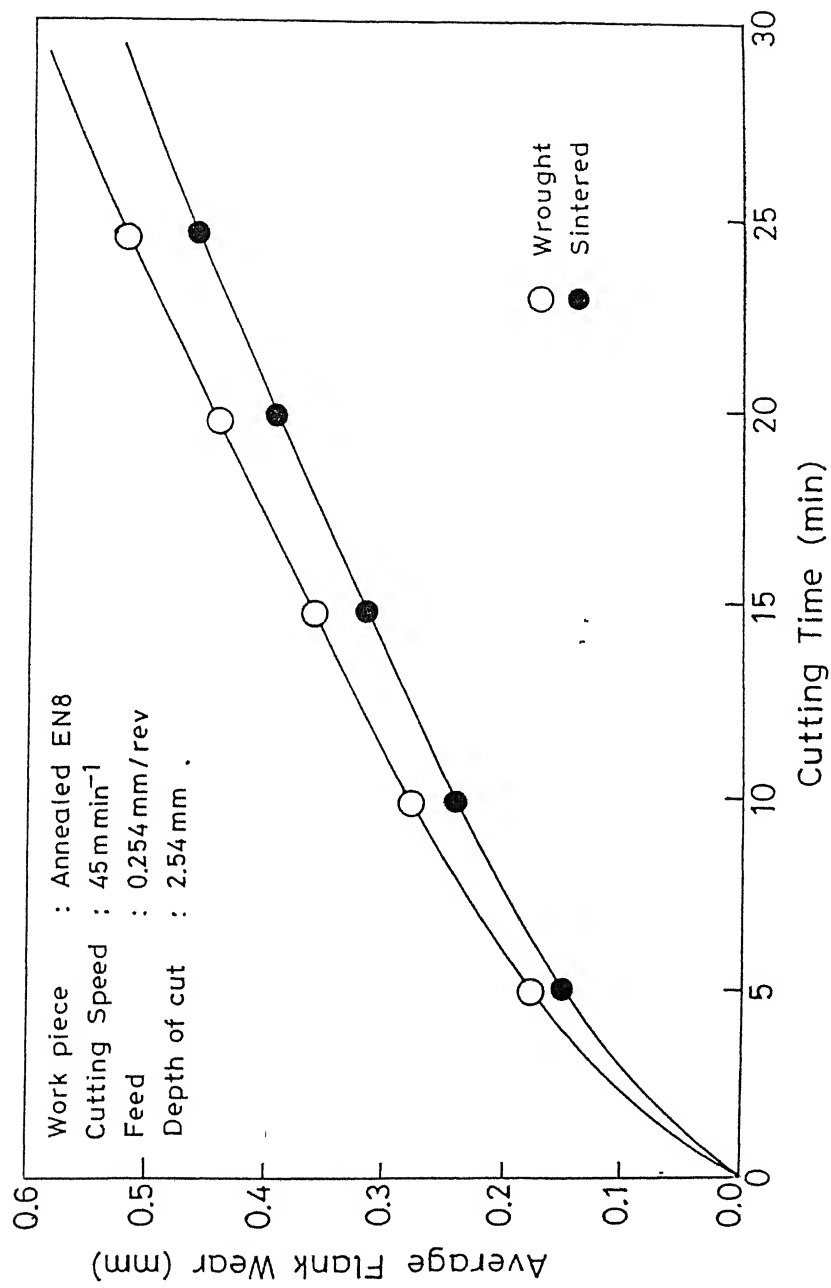


Fig 1.16 Continuous cutting test response of sintered and wrought BT6 high speed steels [65].

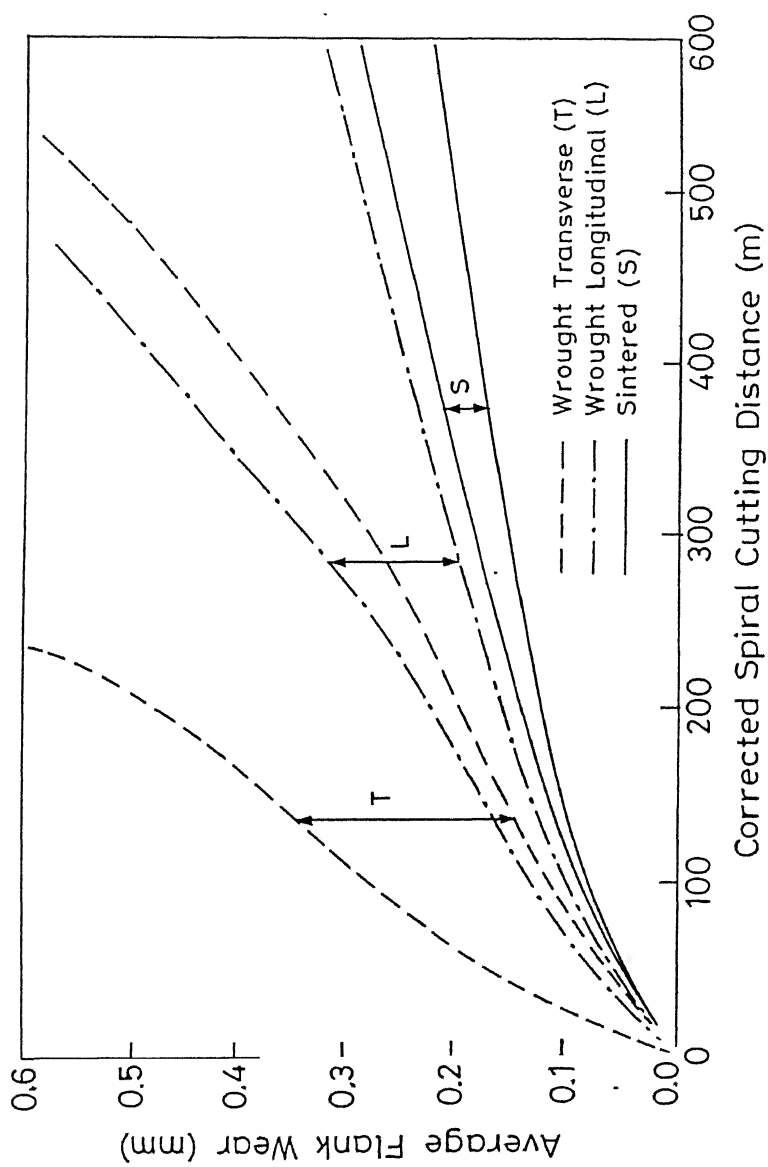


Fig 1.17 Intermittent cutting behaviour of wrought (transverse/longitudinal) and sintered BT6 high speed steel. Cutting speed 30 m min^{-1} , slotted ENB workpiece. (Feed 0.254 mm/rev , Depth of cut 2.54 mm); [65].

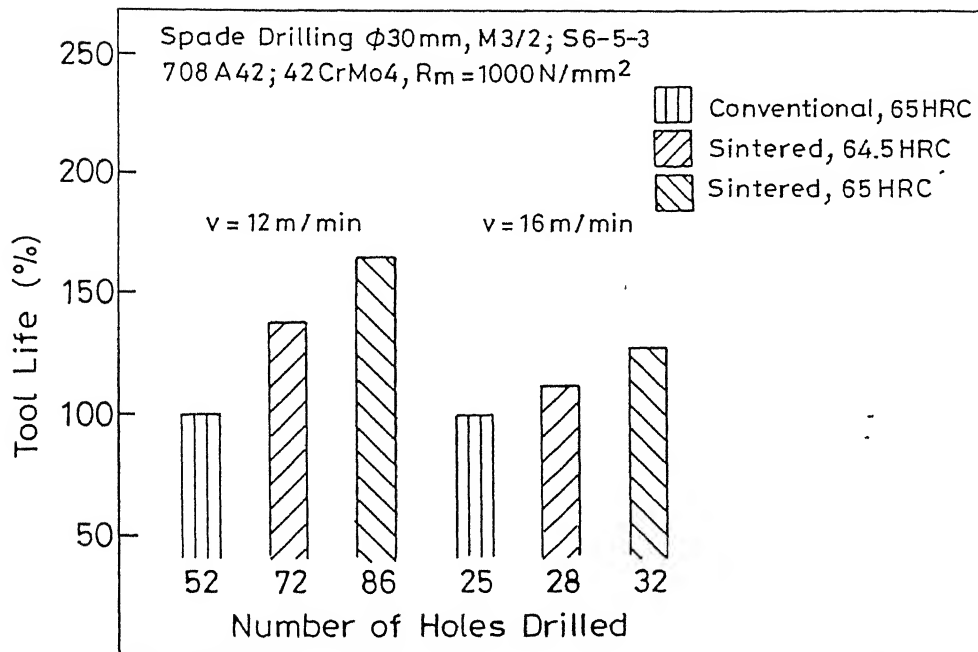


Fig 1.18 Cutting performance of sintered M3/2 (S6-5-3) high speed steel during spade drilling [2].

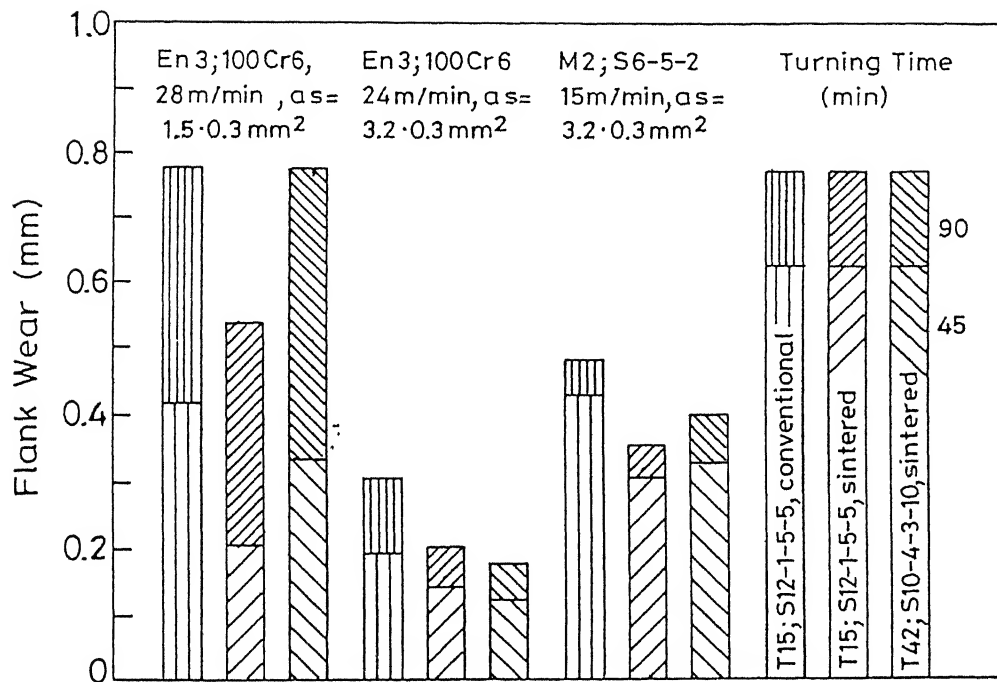


Fig 1.19 Cutting performance of sintered high speed steels during turning in single point turning test [2].

Cutting performance of sintered HSS during milling is shown in Fig. 1.20. The sintered versions perform slightly better than the conventionally processed material. This behaviour changes only negligibly when the feed is increased, although the difference between the wrought and sintered T42 HSS becomes more pronounced [2].

In cutting wear takes place as an adhesive process between the tool and work piece [64]. The wear behaviour of cutting tools made of cast R6M5 ('M'grade) and sintered R6M5F3 ('M'grade) and R12MF5 ('T'grade) steels are shown in Table 1.4. In the examined cutting range the advantage of the powdered steels are quite evident, irrespective of their residual porosity ($\sim 3\%$) [38].

Fracture, chipping and microchipping are phenomena which frequently affect the performance of cutting tools [67]. Increased toughness is extremely important in chipping resistance and edge life in interrupted cutting situation [64]. P/M HSS have higher toughness due to the uniform microstructure and therefore, improve the chipping resistance. Microchipping appears to be an important wear controlling mechanism affecting the performance of HSS tools in intermittent cutting operations. This adversely affect the cutting edge causing stresses to increase and other wear mechanisms to accelerate [67]. In conventional HSS, when surface defects from tool preparation are eliminated, individual carbides and stringers act as stress raiser. In P/M HSS inclusions act as stress raiser [68] and cutting performance is strongly affected by inclusions due to chipping which shortens the life time of the tools. The degree of chipping depends on the inclusion frequency and distribution rather than the size of individual slag particles [41]. Tronberg et al. [69] reported that by using ESH (electro slag heating) process on a large tundish in the atomization process of HSS, a marked reduction of the size and number of non-metallic inclusions are achieved. This process offers the combined advantage of generating the heat required for maintaining a stable temperature throughout the whole atomization while at the same time providing a hot top slag for efficient separation of inclusions and protection against melt oxidation. Thus, ESH process increases the cleanliness of HSS and therefore, improves the microchipping resistance.

1.9.4 Wear Resistance

HSS offer excellent wear resistance both for abrasive and adhesive wear conditions at ambient or elevated temperatures. The abrasive and adhesive wear of P/M HSS are comparable to the wrought HSS [70].

The abrasive wear rate data for P/M HSS plotted as a function of the apparent hardness are shown in Fig 1.21. These data indicate that HSS grades with apparent hardness values of 400-500 VHN have significantly greater wear resistance than the

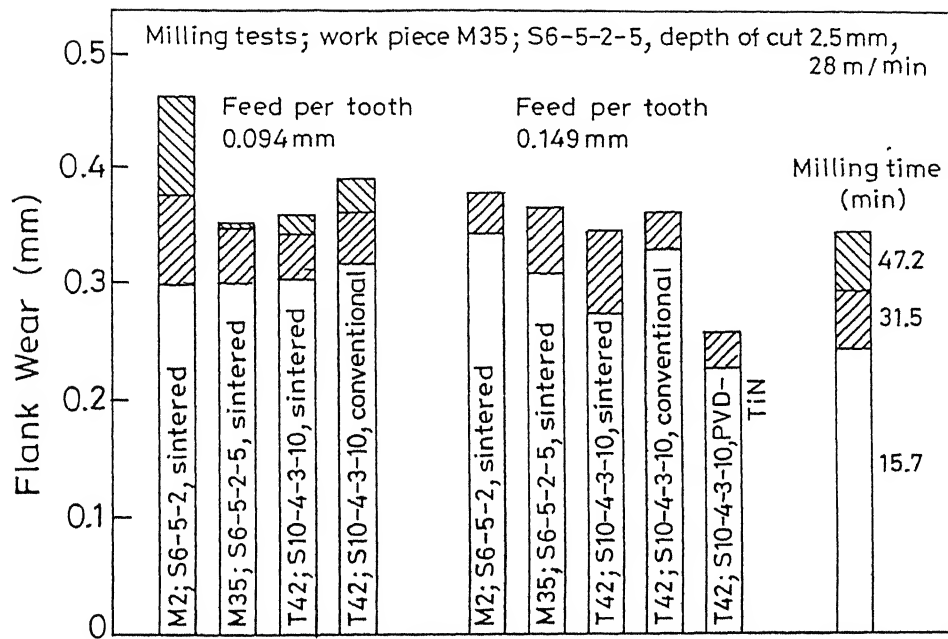


Fig 1.20 Cutting performance of sintered high speed steels during milling of M35 (S6-5-3-5) work piece [2].

Cutting Speed, min^{-1}	Tool Life			Tool Life	
	Cast HSS R6M5	R6M5F3	R12MF5	R6M5F3	R12MF5
32.6	64.5 ± 1.7	107.5 ± 2.6	118.5 ± 2.1	1.65 ± 0.08	1.85 ± 0.08
51.8	43.0 ± 1.4	52.5 ± 2.5	55.4 ± 2.2	1.20 ± 0.09	1.29 ± 0.09
65.3	29.0 ± 1.2	31.0 ± 1.9	39.0 ± 1.9	1.05 ± 0.06	1.35 ± 0.06

$h_3=0.4$ mm, cutting depth 2 mm, feed 0.13 mm/rev; reliability of results 0.95

Table 1.4 Wear behaviour of sintered R6M5F3 ('M' grade) and R12MF5 ('T' grade) high speed steels during cutting [30]

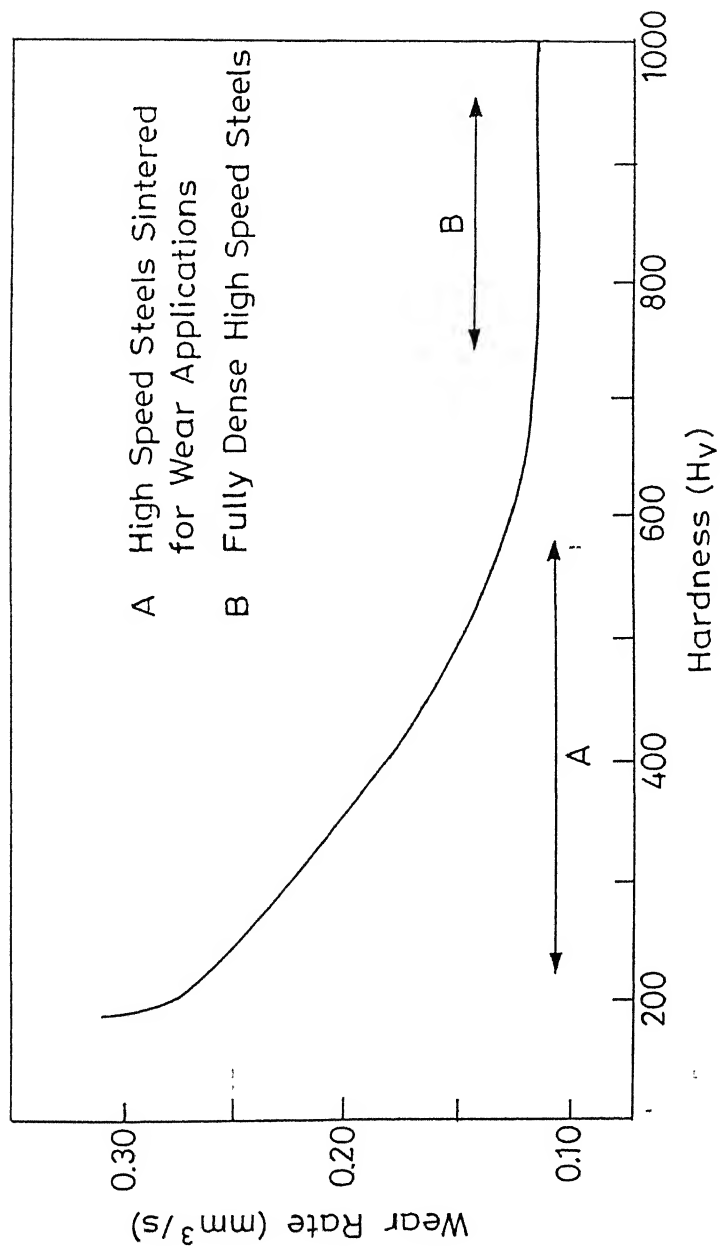


Fig 1.21 Abrasive wear rate versus hardness for high speed steels [70]

grades having apparent hardness values of 300-350 VHN

The adhesive wear test data of the modified P/M HSS of M3 grade (Fe-1.1C-4.0Cr-2.0V-6.3W-5.0Mo) are shown in Fig 1.22. The modified HSS grades have greater wear resistance than the medium carbon steel. Further, the modest improvement in wear resistance as the apparent hardness increases, implies that the wear behaviour of the sintered HSS grades is consistent with that of conventional wrought HSS.

1.10 Applications

Products which have been successfully realized from sintered HSS are cutting tools, wear resistance components and structural parts [6.17.50,70-72].

P/M HSS are primarily used for cutting tools, such as cutters, drills, broachers, reamers, taps, chasers, hobs, etc. Application in which full density vacuum sintered HSS are currently in use include screw machine tooling, gear cutting tools and indexable cutting tool inserts. Besides, another successful cutting tool application is a large range of sintered HSS trimming dies for the bolt industry which are used to cut hexagonal shapes out of the cold formed round bolt heads.

HSS have been less commonly applied as wear components. The relative difficulty in machining and grinding of HSS as compared to other tool and alloy steels, has reduced their cost effectiveness and limited their application to relatively simple shapes such as pump vanes, guides and wear liners. Other wear components, which are widely used, include rotor ring in a diesel fuel injection pump, valve seat inserts for internal combustion engines, rocker arm button for a diesel engine with an overhead cam, cam ring for rotary distribution diesel fuel injection pump and punches and dies. In addition, valve train parts made from P/M HSS are also used in the automotive industry.

P/M HSS have also been used as structural parts. Extruder tube, which is used in an extrusion machine for the coating of welding electrodes, and moulding tool, which is used in glass industry for bottle production, are successfully manufactured from the P/M HSS. HIP'ping and direct sintering plus HIP'ping routes are also promising for aerospace applications, such as gas turbine engine main shaft bearings. Besides, as forming tools, HSS are used in abundance in stamping, cold forming, cold extrusion, warm or hot forming and extrusion, plastic moulding insert, die casting die inserts, etc.

1.11 Scope of the Present Investigation

The cutting ability and wear resistance property of HSS depend on hardness, toughness and wear resistance. These properties are best achieved by an alloy consisting of uniform

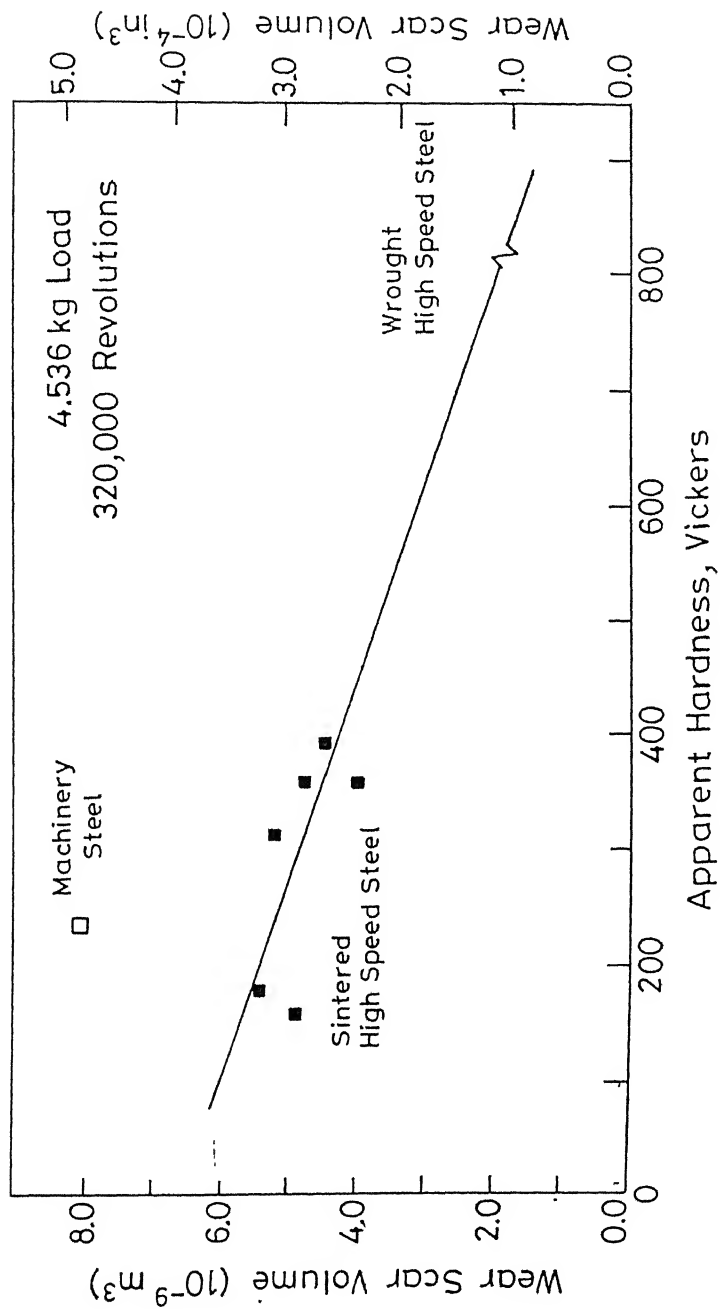


Fig 1.22 Wear scar volume plotted as a function of hardness [70].

dispersion of fine, hard and stable particles in a tough matrix. The HSS contain higher amount of carbide forming alloying elements such as W, Mo, Cr, V and Co. These alloying elements combined with carbon form a dispersion of hard alloy carbides in a relatively tough tempered martensitic matrix.

The wear resistance of HSS is directly related to the volume fraction of hard phase present in the matrix. Although the alloying elements present in the HSS, especially vanadium, form hard carbide dispersoid, the addition of inert ceramic particles like alumina with high hardness may still further improve wear resistance. The HSS can be easily enriched by such ceramic particles through P/M route to produce full density metal-matrix composites with composition and structure that would be difficult to produce by any other means.

In the present investigation Al_2O_3 has been selected as hard dispersoid in the T15 HSS matrix due to its high hardness (2100 kg/mm^2). The liquid phase sintering route has been followed as it is less capital intensive and could be easily adopted in a plant processing conventional sintered products.

T15 grade high speed steel provides wide sintering gate, so the temperature control during liquid phase sintering is relatively easy. This grade also contains higher amount of carbide forming elements and therefore, provides ideal matrix for further studies.

Chapter 2

Experimental Procedure

The detailed experimental procedures carried out in the present investigation are presented in this chapter

2.1 Powders and Their Characteristics

T15 HSS Powder (Water Atomized)

Source:- Sinter-Metallwerk Krebsoge, Germany.

Chemical Composition (mass %)

Carbon	1.59	Chromium	4.23
Cobalt	4.99	Copper	0.08
Manganese	0.26	Molybdenum	0.55
Nickel	0.15	Tungsten	12.50
Vanadium	4.75	Oxygen	1000 p.p.m.

Physical Characteristics

Apparent Density	2.1g/cm ³
Flow Rate	42.7s/50g
Compressibility (at 455 MPa)	5.52g/cm ³

Sieve Analysis

Mesh	% Cumulative Mass Fraction
+100	0.08
+150	7.53
+200	29.10
+350	64.30
-350	35.70

α -Al₂O₃ Powder

Source: Linde A. Union Carbide Corporation, U.S.A.

Av size: 0.3 μ m

Electrolytic Copper Powder

Source: Amrut Industry, Mumbai, India

Size: -400 mesh

2.2 Powder Mix Preparation

With the as received T15 HSS powder, different volume fractions of Al₂O₃ (0, 2, 4, 6 and 8%, respectively) were blended in a Turbula Mixer, type T2C, for 30 minutes. With one part of these composite compositions, 5 wt.% copper was blended for 30 minutes. The uniformity of mixing was checked under an illuminated magnifying lens.

In order to assess the mechanism of sintering, a model experiment was carried out. The T15 HSS powder was sieved and a rather narrow particle size range 63-106 μ m was taken. With this powder different compositions (T15, T15+5 wt.% Cu, T15+2 vol.% Al₂O₃, T15+2 vol.% Al₂O₃+5 wt.% Cu) were prepared by blending in the same way as described above.

2.3 Room Temperature Compaction

The blended powders of different compositions were pressed into green compacts in the shapes of cylindrical and rectangular specimens on a compression testing machine of 50 tons capacity, of Fuel Industries and Engineers Pvt. Ltd., model CTM-50, India make. A fixed compaction pressure of 600 MPa was used which imparted a green porosity in the range of 28-30%. Green porosity was calculated on the basis of dimensional measurements.

2.4 Sintering

Sintering was carried out in a SiC resistance heated tubular furnace. The furnace of 4.4 cm internal diameter had a constant temperature zone of 7 cm. length. The sintering was carried out under a dynamic H₂ atmosphere. Green compacts were placed on a fused alumina tile, which in turn was kept on a graphite boat within the constant temperature zone. The furnace temperature was controlled within $\pm 5^\circ\text{C}$ using a analog ON/OFF type controller.

The three different temperatures of 1250°C, 1280°C and 1300°C were selected. A 5-8°C/min. heating rate was followed during heating. The holding period at the sintering temperature was maintained uniformly for 60 min for all the samples and then furnace cooled.

For the model experiments, the T15 HSS and T15-5 wt.% Cu composition samples were sintered at 500°C, 700°C, 900°C, 1100°C and 1300°C, respectively. The T15+2 vol % Al₂O₃ and T15+2 vol.% Al₂O₃+5 wt.% Cu composites were sintered at 1100°C and 1300°C, respectively.

2.5 Sintered Density Measurement

The sintered density of the samples was measured using water displacement method described by Arthur [73]. The sintered samples were impregnated with xylene in vacuum and the following formula was used to calculate the sintered density.

$$Density = \frac{W_c}{W_{xa} - W_{xw}}$$

where W_c = weight of the compact in air,

W_{xa} = weight of xylene impregnated compact in air,

W_{xw} = weight of xylene impregnated compact in water.

The sintered density were expressed as percentage of the theoretical density, which was calculated using the rule of mixture.

2.6 Heat Treatment

The sintered samples were subsequently heat treated in the same type of furnace as used for sintering studies. All heat treatment operations such as transformation annealing, austenitizing, oil quenching and triple tempering were done in air. To prevent the samples from decarburisation, they were wrapped in a special graphite coated foil (sintercast protec tool wrap of stainless steel) before placing into the furnace. The critical temperature and different holding time for all the heat treatment operations were followed as described by Kar [74]. For the samples sintered for model experiment no heat treatments were done.

2.6.1 Transformation Annealing

The purpose of transformation annealing was to relieve the internal stresses developed in the sintered compacts during cooling from the sintering temperature and to provide a refined grain structure prior to further hardening and tempering treatments. Samples were held at 900°C, for 1 hr and at 760°C for 4 hrs. From 760°C, the samples were air cooled to room temperature.

2.6.2 Hardening

An uniform austenitizing temperature of 1200°C was selected for all the samples. Each batch of annealed samples was slowly heated to 850°C and soaked for 60 min. after that faster heating was done to 1200°C. Holding time at the austenitizing temperature was kept fixed for 10 min. in each case. After this, the samples were quenched in mineral oil to room temperature.

2.6.3 Tempering

Oil quenched samples were subsequently triple tempered isothermally in still air. The tempering temperature was kept 550°C and the tempering period was kept uniform for 1 hr. each time. After tempering the samples were air cooled to room temperature.

2.7 Hardness

Macrohardness of the sintered as well as heat treated samples after every stage of heat treatment were measured on Vickers hardness testing machine, model HPO-250 of "Fritz Heckert". Leipzig make, using a load of 10 kg (98.1 N). At least 10 indentations were taken on each specimen and the average value was reported.

The microhardness of all samples prepared for model experiment was measured on Leitz microhardness testing machine, Wetzlar, Germany make, using load of 0.015 kgs. (147 mN). At least ten indentations were taken on each specimen and average value was reported.

2.8 Transverse Rupture Strength (TRS)

For the measurement of TRS, the rectangular samples sintered at the three selected temperatures were ground to proper dimensions. The ground samples were placed in the standard TRS test fixture (ASTM B406-81). The tests were carried out at room temperature on the 'Instron 1195' (Material Testing System) machine at a cross head

speed of 0.5 mm/min. The TRS was calculated according to ASTM standard B-528-76, as follows:

$$TRS(MPa) = \frac{3PL}{2t^2w}$$

where P is the force in Newton required to rupture the specimen, L is the distance between the bottom supports in mm W and t are the width and thickness of the specimen in mm, respectively

2.9 Sliding Wear Test

The sliding wear test of the all sintered samples was carried out on a pin on disc machine, model TR-20 of Ducom, Bangalore. India make. This machine consists of two sections: pin on disc section and controller. The specifications are given below:-

Disc material	En-32 steel hardened to 65 HR _c
Pin size	5 to 12 mm diagonal
Disc size	ϕ 215 mm X 8mm
Wear track diameter	ϕ 50 mm min. to ϕ 180 mm max.
Sliding speed range	0.26 m/s to 10 m/s
Disc rotation speed	100 to 1200 rpm
Normal load	20 kg. max.
Frictional force	0-20 kgf.

Rectangular sintered samples having approximate dimensions of 5.1x8.0x25.0 mm³ were held to the lever arm by specimen holder. the flat surface of the samples and the grinding disc were cleaned by acetone to remove the dust and lubricants. The pin (i.e. sample) was loaded by putting weight on the pan attached to the lever arm over the pulley. The applied load on the pin was normal to the surface of the disc. This force effectively maintained contact between the sample and the disc by gravitational force. The distance of the center of the sample from the center of the grinding disc was fixed. This is known as the track distance and from this the length of the path traversed in any run can be calculated. The rpm of the disc was brought to the desired level by varying the supplied voltage to the motor. The motor was allowed to run for the fixed period. When the rotation had started, loading turn the pin against the disc and the friction sensor recorded the changes in frictional force as a function of time. In this experiment, the surface of the pin wears away and the amount of wear is recorded by the displacement sensor which actually shows the change in height of the sample during testing. In the subsequent wear run the disc surface was carefully cleaned to remove the wear debris and a fresh sample was inserted. The operating conditions during testing were as follows:

Sliding speed	400 rpm
Sliding distance	2625 m
Track dia.	140 mm
Applied load	1.5 kg and 2.5 kg

2.10 Magnetic Properties

2.10.1 Saturation Magnetization

This property was measured after sintering and every stage of heat treatment on Sigma metal. model SM 75 of Lab Magnet Physik, Bombay, India make. This instrument consists of electromagnet and a digital panel meter. The electromagnet is used to generate a magnetic field of about 10 Kilogauss in its air gap which is enough to saturate any sample. A pair of detection coil is mounted on the poles of the electromagnet. The sample of which the saturation magnetization (σ_s) is to be measured is weighted and then introduced in the air gap and when withdrawn from it, an e.m.f. is induced in the coil mounted on the poles. This induced voltage is integrated using an I.C. amplifier and the output of which is read in a digital panel meter which gives the flux indicator reading. This output is then compared with the output of a known weight of nickel sample. The saturation magnetization of Ni is known and taken as a standard value. The σ_s value of the unknown sample is then calculated from the formula given below:

$$\text{Saturation Magnetization}(\sigma_s) = \frac{X_2 K}{W_2} \dots (i) \text{gauss}$$

$$\text{where } K \text{ is the sensitivity} = \frac{685 \times W_1}{X_1} \dots (ii) \text{gauss/digit}$$

Where X_1 and W_1 are flux reading and weight of standard nickel sample, respectively and X_2 and W_2 are flux reading and weight of the tested sample respectively. Note: 685 gauss/g in equation (ii) is the $4\pi\sigma_s$ of the saturated nickel sample. For the sintered samples prepared for the model experiment the saturation magnetization was also measured.

2.10.2 Magnetic Coercivity

The coercivity of the sintered as well as triple tempered samples was measured on the unit 'coercicheck' of Electromagnets and Tool Room, India make. The unit consists of three subassemblies i.e. magnetizer, solenoid and the coercimeter. The function of the magnetizer is to magnetize the samples to saturation. When this magnetized sample is placed inside the solinoid, it energised. The coercimeter unit applies a callibrated

demagnetizing force to the solenoid so as to demagnetize the sample. This demagnetized force from the coercimeter is displayed in a digital display unit as the coercive force for the sample in Oersteds.

2.11 Microstructural Studies

Microstructural studies, both qualitative and quantitative, included optical and scanning electron microscopy.

2.11.1 Optical Metallography

Quantitative metallography study of the samples sintered at 1280 and 1300°C was performed on an optical microscope, Laborlux 12 ME, Leitz Wetzlar, Germany make where grain size of the samples was measured and the average values were reported. The same measurement was done for the model samples sintered at 1300°.

Samples for qualitative metallographic studies were selected after every stage of processing such as sintering, oil quenching and after triple tempering. Microstructure was prepared using the conventional process starting from the belt grinding followed by wet polishing on 'Lunn Major' unit over 120, 250, 500 and 1000 grit size SiC coated paper, successfully. This was followed by disc polishing (struers DAP-2 unit) using alumina powder of 0.3 μ m particle size. Polished samples were then etched by using nital (5% HNO₃+95% methanal) as etchant. The photographs of the etched samples were taken on an optical microscope, Metallux 3, Germany make, at different magnifications.

2.12 SEM study

The unetched surface of the samples subjected to wear test was observed under 'JEOL' JSM-840A scanning electron microscope. Scanning electron microscopy examination of the worn surface of the test pieces was made to assess the wear mode.

Chapter 3

Experimental Results

3.1 Effect of sintering temperature and copper addition on T15 HSS and T15-2vol%Al₂O₃ composite.

3.1.1 Densification Behaviour

The densification behaviour of T15 HSS and its containing 5wt%Cu at various sintering temperatures is shown in Fig.3.1. In case of T15 HSS, up to 1100°C sintering temperature, very little densification was observed. But after 1300°C sintering, rapid densification occurred. With the addition of copper in the steel, a similar trend was observed. However, in case of 1300°C sintering, the effect of copper on densification was much more pronounced. The interconnected porosity of T15 HSS remained almost unchanged up to 1100°C sintering. But in case of 1300°C sintering, it dropped rapidly. The closed porosity of T15 HSS, irrespective of sintering temperature, varied in a very narrow range. Addition of copper in T15 HSS followed the similar trend to that of T15 HSS. However, in case of 1300°C sintering, the interconnected porosity rapidly dropped to below 1% and the closed porosity increased substantially. The densification behaviour of T15 HSS and T15-2vol%Al₂O₃ composite with addition of 5wt% Cu at two sintering temperatures i.e. 1100 and 1300°C is shown in Fig.3.2. In case of 1100°C sintering temperature, the composite showed very poor densification. After 1300°C sintering, improvement in densification was not substantial. The addition of copper (5wt%) in T15 HSS, in case of 1100°C sintering, did not change the densification behaviour. But after 1300°C sintering, a slight improvement of densification was observed. The interconnected and closed porosity of T15 HSS and T15-2vol%Al₂O₃ with addition of 5wt% Cu at 1100 and 1300°C sintering temperatures is shown in Fig.3.3. After 1100°C sintering, the interconnected porosity of T15-2vol%Al₂O₃ composite was slightly higher than that for T15 HSS. The same trend was also observed in case of 1300°C sintering. However,

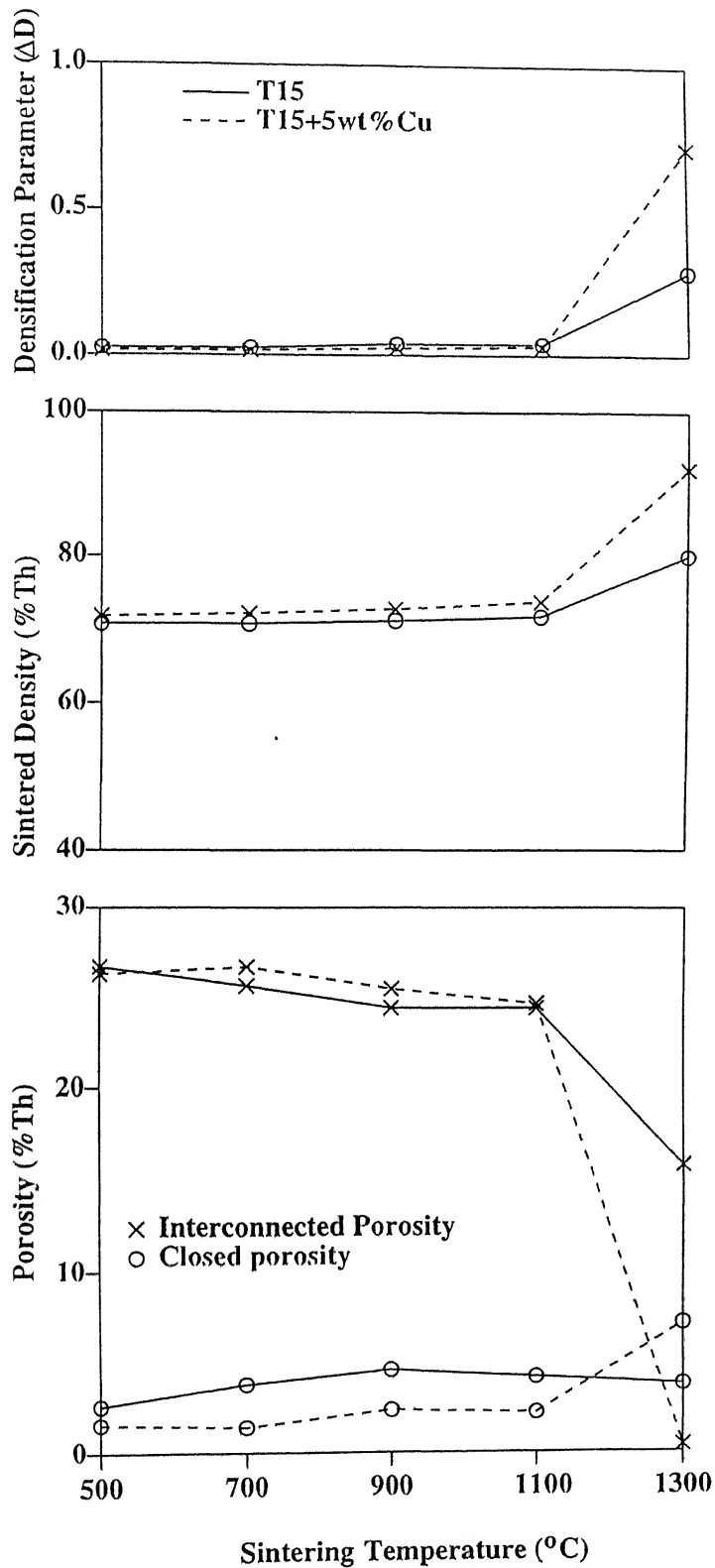


Fig. 3.1 Effect of sintering temperature on (a) Densification parameter (b) Sintered density and (c) sintered porosity of T15 HSS with or without the addition of 5 wt% copper

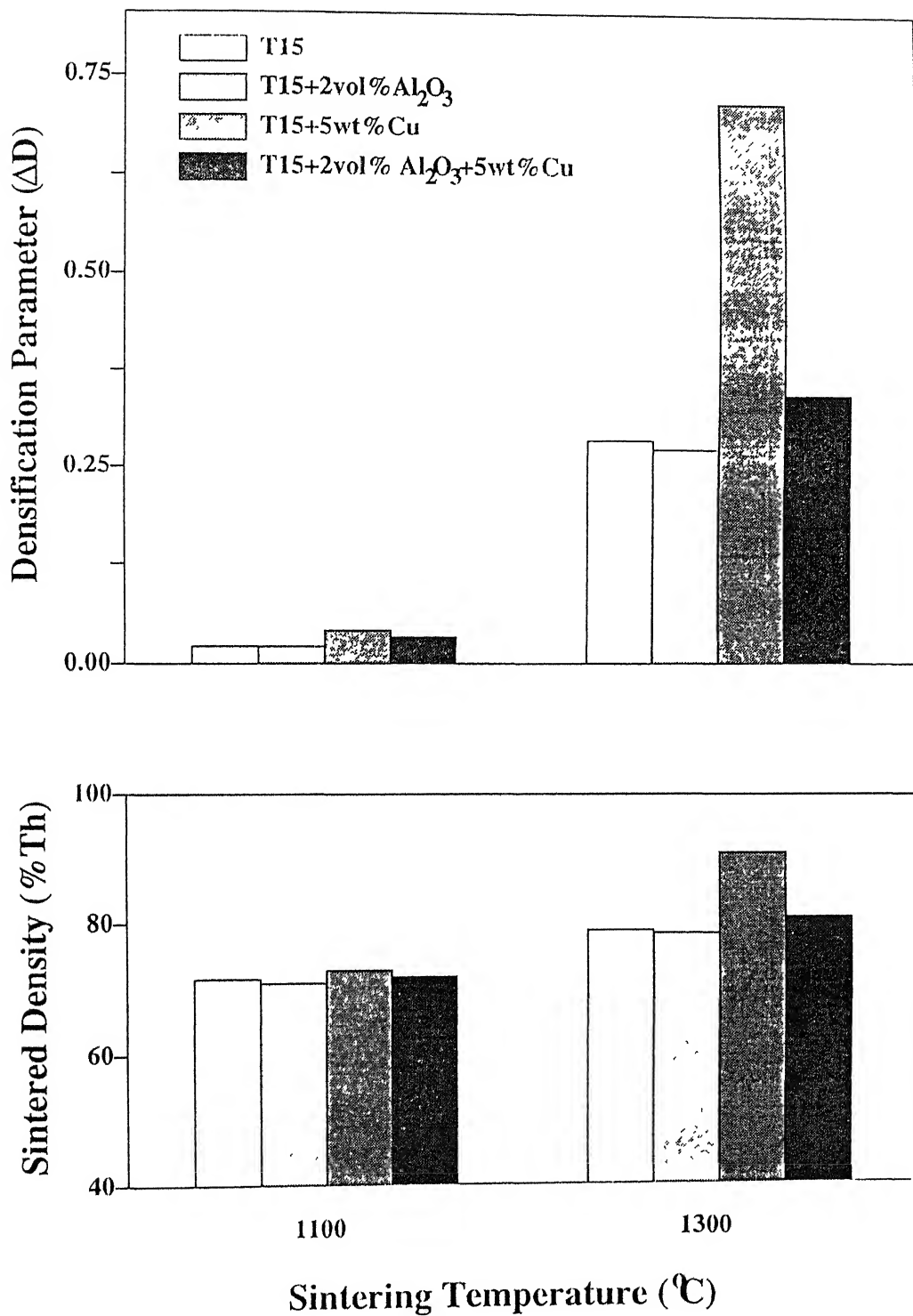


Fig. 3.2 Effect of sintering temperature on (a) Densification-parameter and (b) Sintered density of T15 HSS and T15-2 vol% Al_2O_3 compositions with or without the addition of 5 wt% copper.

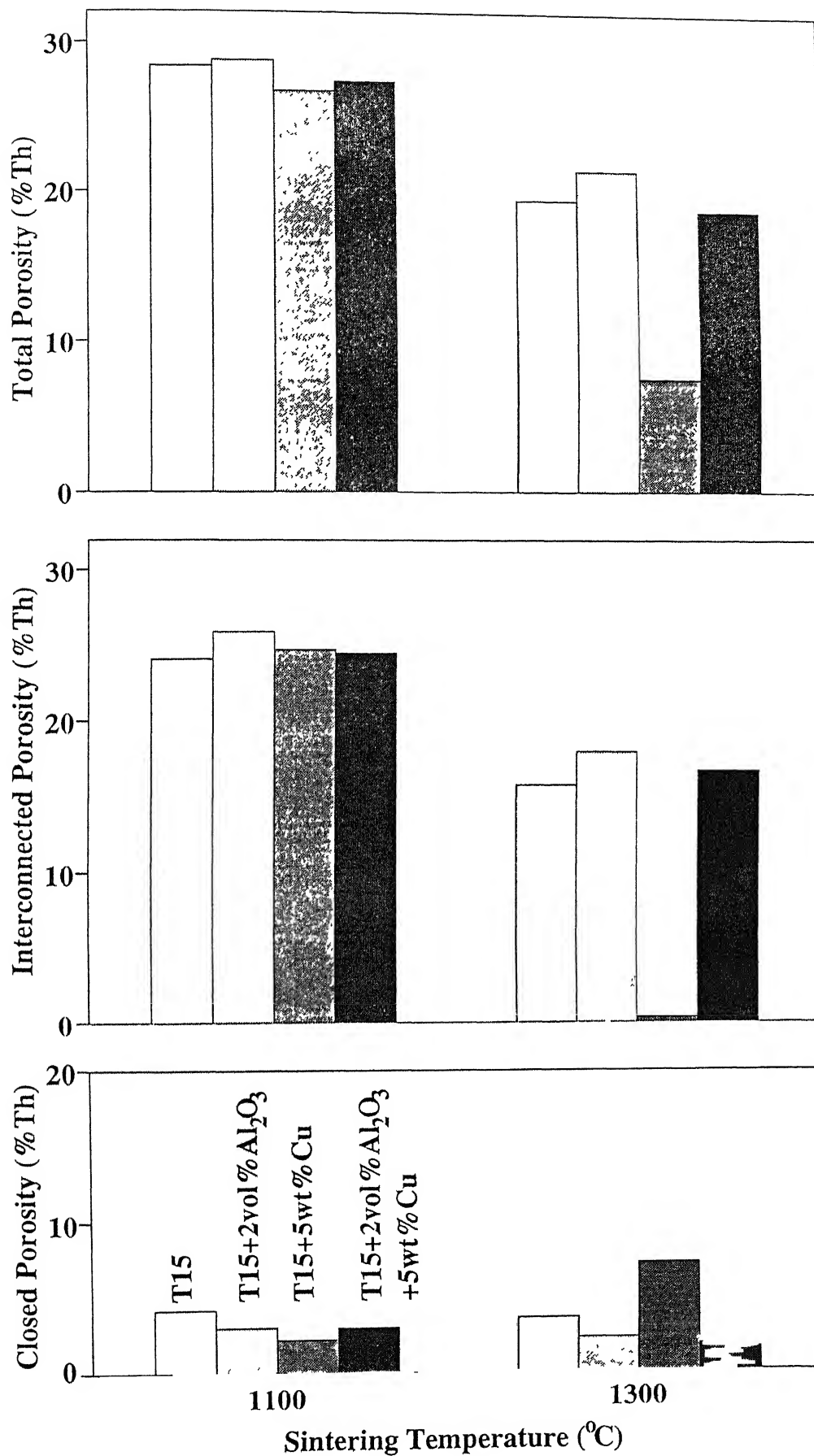


Fig. 3.3 Effect of sintering temperature on the porosity of T15 IIS and T15-2 vol% Al₂O₃ compositions with or without the addition of 5 wt.% copper.

high temperature sintering showed a drop in interconnected porosity compared to low temperature sintering. In case of both the sintering temperatures, the closed porosity of the composite was observed slightly below than that of T15 HSS. The addition of copper in the composite, irrespective of sintering temperature, decreased the interconnected porosity slightly. However, the closed porosity remained unchanged.

The interconnected and closed porosity variation of T15 HSS and T15-2vol%Al₂O₃ with addition of 5wt% Cu after repressing/resintering of sintered samples (1300°C) is shown in Fig.3.4. After repressing of the 1300°C sintered samples, the interconnected as well as closed porosity of the investigated alloys decreased slightly. However, in case of T15 HSS, the drop in interconnected porosity was higher compared to that of other compositions. After resintering, the interconnected porosity of all the investigated alloys decreased slightly and the closed porosity remained unchanged except in case of copper containing alloys where an increase in closed porosity was observed.

3.1.2 Vickers Macrohardness

The Vickers macrohardness variation of T15 HSS with or without addition of 5wt% Cu with respect to sintering temperature is shown in Fig.3.5(a). In case of either T15 HSS or T15-5wt% Cu sample, the as-sintered hardness followed the similar trend to that of densification with respect to sintering temperature. However, in case of 1300°C sintering temperature, the role of copper in increasing hardness was very much pronounced. The Vickers macrohardness variation of T15 HSS and T15-2vol%Al₂O₃ composite with addition of 5wt% Cu at two sintering temperatures i.e. 1100 and 1300°C is shown in Fig.3.5(b). In case of 1100°C sintering, the T15-2vol%Al₂O₃ composite showed similar Vickers hardness to that of T15 HSS. Addition of copper did not increase their hardness. After 1300°C sintering, the Vickers hardness of the composite dropped slightly. Here also addition of copper did not change the hardness. After repressing/resintering the Vickers hardness of the composites increased. Here the effect of copper in increasing hardness was also observed.

3.1.3 Vickers Microhardness

The Vickers microhardness variation of the matrix of T15 HSS with or without the addition of 5wt% Cu with respect to sintering temperature is shown in Fig.3.6(a). The peak hardness of T15 HSS was obtained in case of 1100°C sintering temperature. But after 1300°C sintering it rapidly decreased. The effect of copper addition also followed the same trend, such that in case of 1100°C sintering a peak hardness value of 770 HV_{0.015} was observed. However, after 1300°C sintering, it dropped slightly.

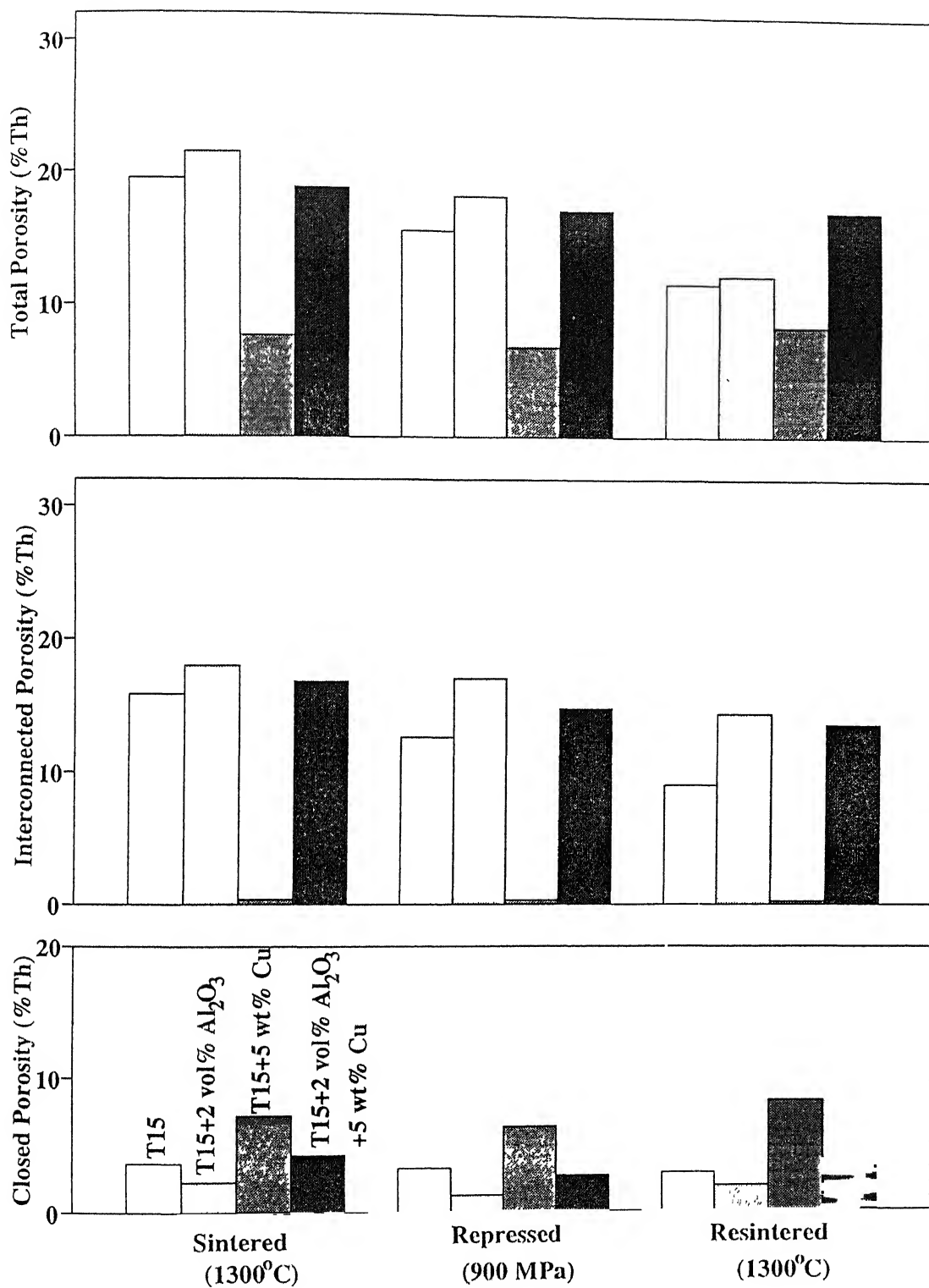


Fig. 3.4 effect of repressing and resintering on T15 HSS and T15-2 vol% Al₂O₃ compositions (sintered at 1300°C) with or without the addition of copper.

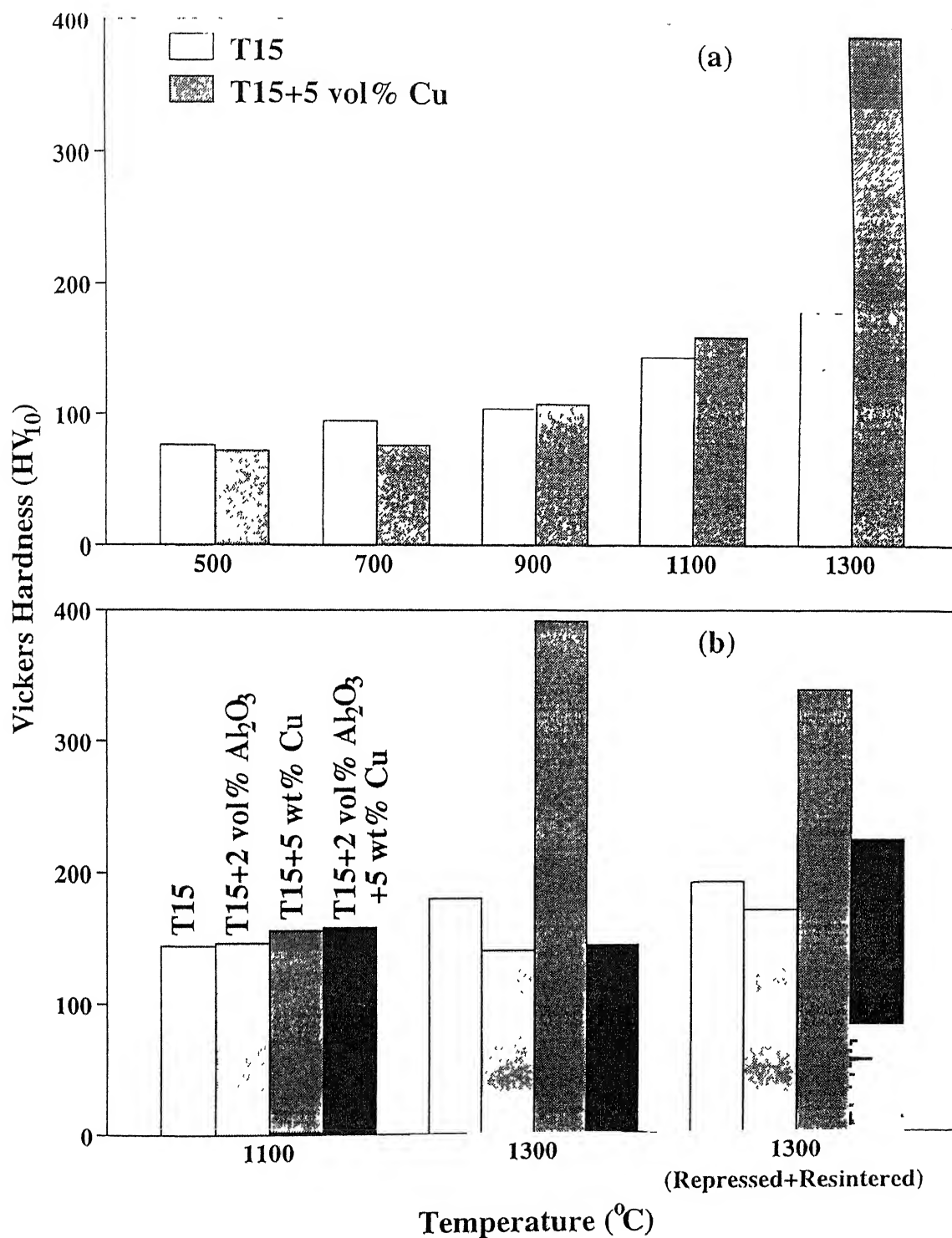


Fig. 3.5 Effect of sintering temperature on Vickers hardness of T15 HSS and T15-2 vol% Al₂O₃ compositions with or without the addition of 5 wt% copper.

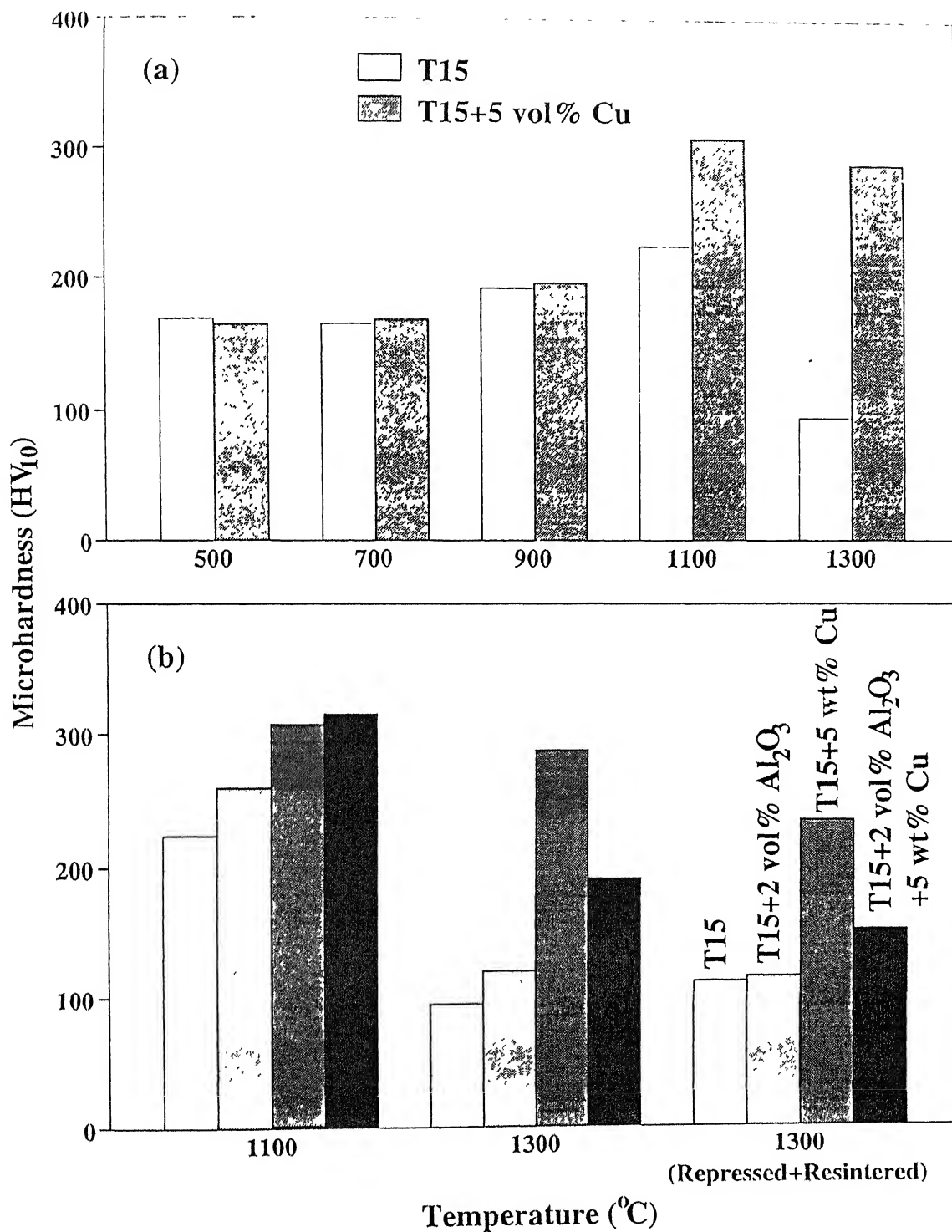


Fig. 3.6 Effect of sintering temperature on matrix microhardness of T15 HSS and T15-2 vol% Al₂O₃ compositions with or without the addition of 5 wt% copper.

The Vickers microhardness variation of T15 HSS and T15-2vol%Al₂O₃ with addition of 5wt% Cu at two sintering temperatures i.e. 1100 and 1300°C is shown in Fig.3.6(b). In case of 1100°C sintering, the microhardness of T15-2vol%Al₂O₃ composite increased compared to that of T15 HSS. Addition of copper also further increased this value. After 1300°C sintering, the microhardness of T15-2vol%Al₂O₃ decreased. Addition of copper to the composite also followed the same trend. After repressing/resintering, the microhardness of T15 HSS and T15-2vol%Al₂O₃ composite changed negligibly. But in case of copper containing composite it dropped.

3.1.4 Magnetic Properties

Saturation Magnetization (σ_s)

The variation in saturation magnetization (σ_s) of T15 HSS with or without addition of 5wt% Cu with respect to sintering temperature is shown in Fig.3.7(a). The σ_s of T15 HSS, up to 900°C sintering, remained unchanged. But further increase in sintering temperature i.e. 1300°C decreased it slightly. With addition of copper, the samples showed σ_s comparable to that for T15 HSS, except in case of 900 and 1100°C sintering where it dropped rapidly and the values as compared to those for T15 HSS were substantial. Fig.3.7(b) shows the variation of the saturation magnetization (σ_s) of T15 HSS and T15-2vol%Al₂O₃ composite with or without the addition of 5wt% Cu at two sintering temperatures i.e. 1100 and 1300°C. In case of 1100°C sintering, the σ_s of T15-2vol%Al₂O₃ composite decreased compared to that of T15 HSS. Addition of copper further decreased σ_s . After 1300°C, the σ_s of either composite (with or without copper) increased. After repressing/resintering, compared to other alloys, only T15 HSS showed a considerable change in σ_s , where an increase in the value was observed.

Magnetic Coercivity

The variation in magnetic coercivity of T15 HSS with or without the addition of 5wt% Cu with respect to sintering temperature is shown in Fig.3.8(a). For either composition (T15 HSS or copper containing HSS), the coercivity followed the similar trend to that of microhardness. Both the compositions showed the peak values in case of 1100°C sintering. Like microhardness, here also the effect of copper in increasing the coercivity of the alloy was observed.

The variation in coercivity of T15 HSS T15-2vol%Al₂O₃ composite with or without the addition of 5wt% Cu at two sintering temperatures i.e. 1100 and 1300°C is shown in Fig.3.8(b). In case of 1100°C sintering, the coercivity of T15-2vol%Al₂O₃ composite was higher than that of T15 HSS. Addition of copper further increased the coercivity.

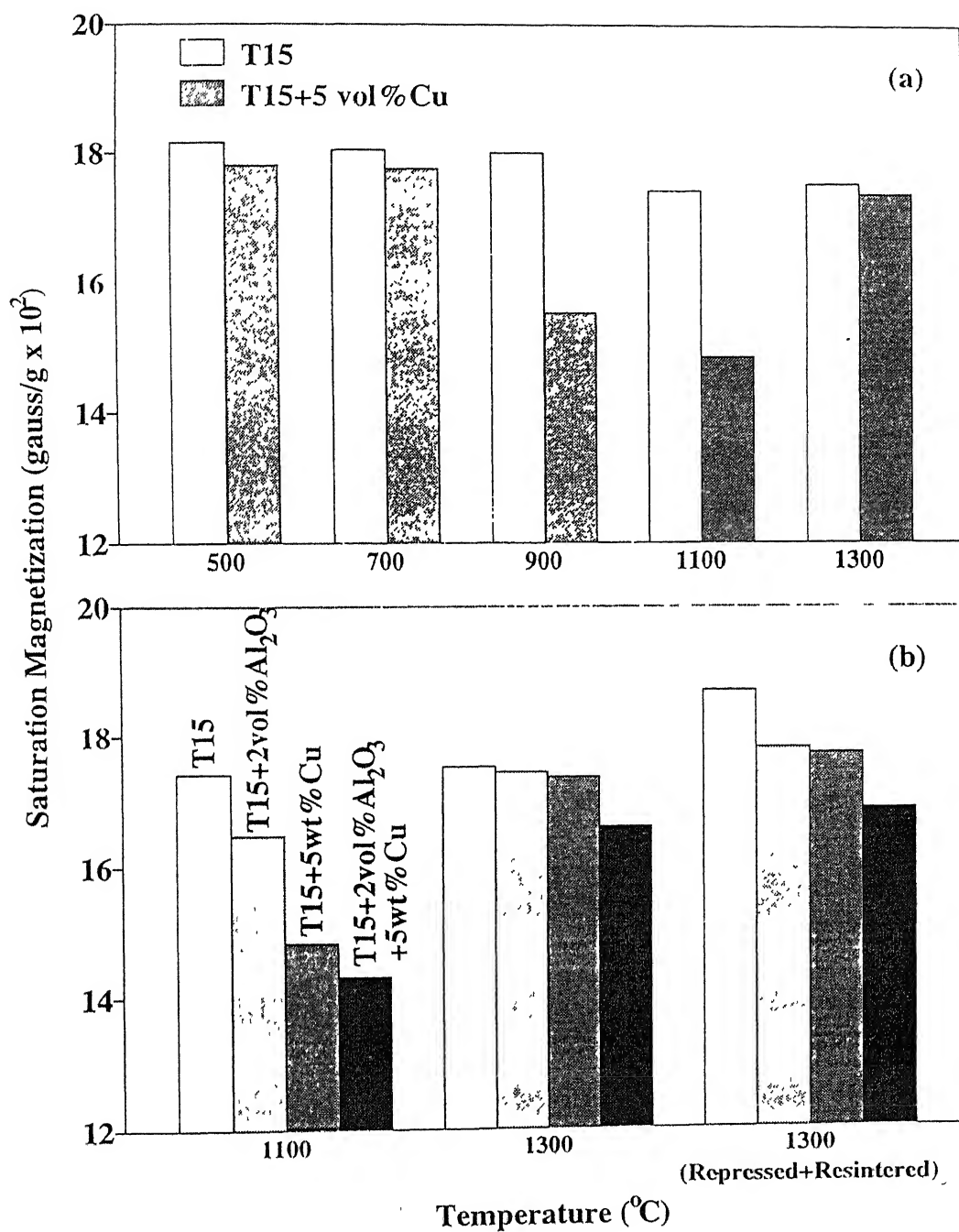


Fig. 3.7 Effect of sintering temperature on saturation magnetization of T15 HSS and T15-2 vol% Al₂O₃ compositions with or without the addition of 5 wt% copper.

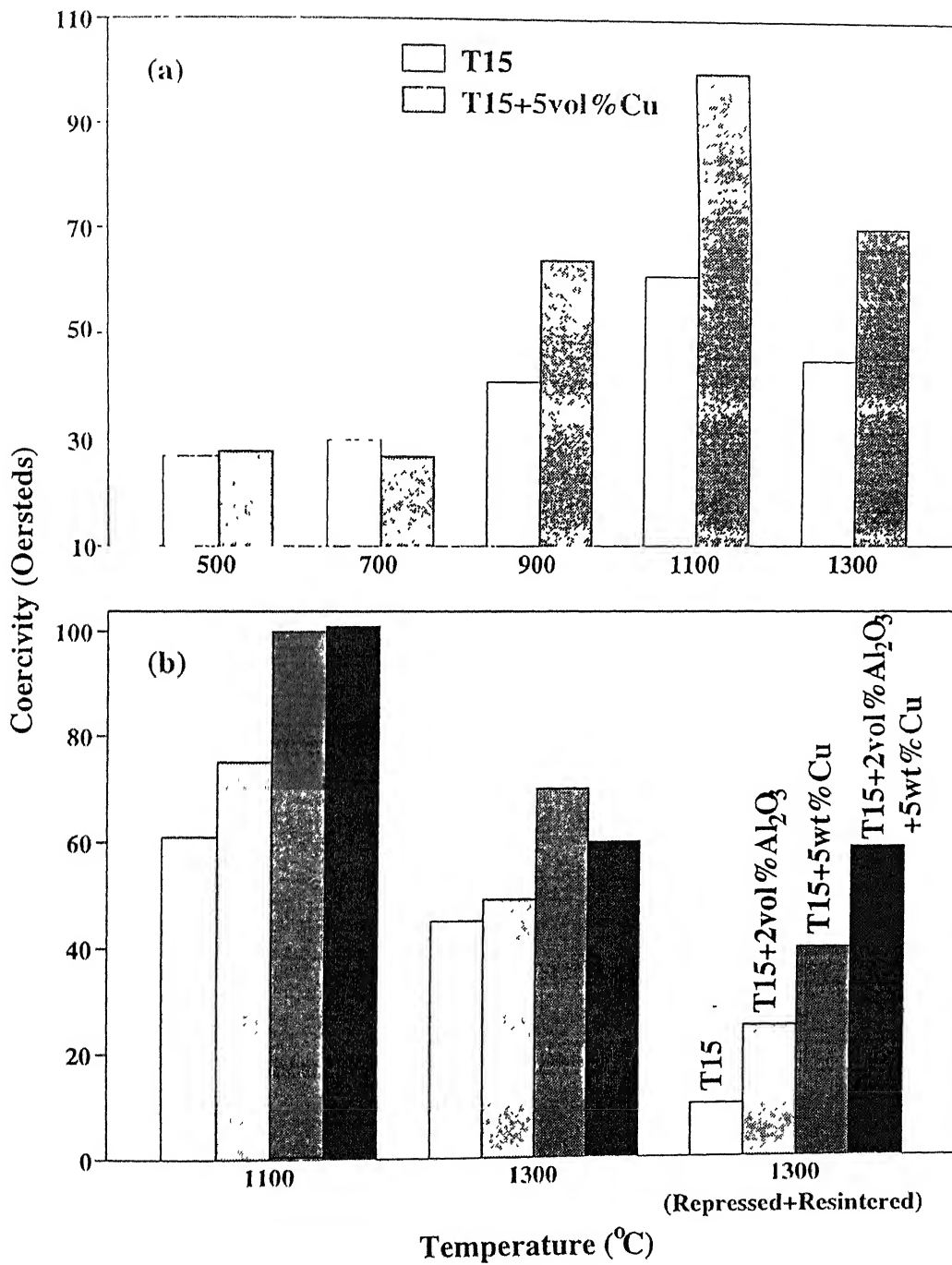


Fig 3.8 Effect of sintering temperature on magnetic coercivity of T15 IIS and T15-2 vol% Al₂O₃ compositions with or without the addition of 5 wt% copper.

In case of 1300°C sintering, the coercivity of either composite dropped compared to that of 1100°C sintering. After repressing/resintering the coercivity of all the compositions except T15-2vol%Al₂O₃-5wt%Cu decreased.

3.1.5 Microstructural Analysis

The optical microstructures of T15 HSS with or without addition 5wt% Cu at various sintering temperatures are shown in Fig.3.9. In case of the microstructure of T15 HSS sintered up to 1100°C, many large pores were observed. The grains were not evident and only the bonding among the particles was seen in the microstructure. In case of 1300°C sintering, the microstructure was well developed and consisted of fine matrix as well as carbide grains along with many large pores.

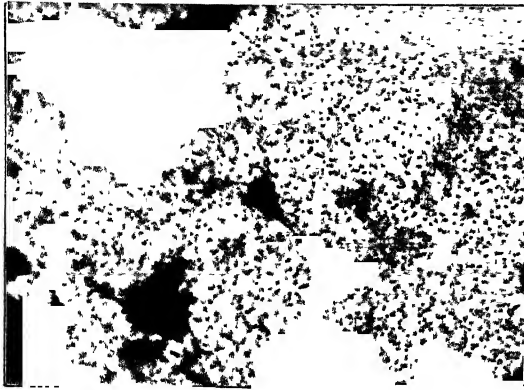
The microstructures of T15-5wt% Cu composition were similar to those of T15 HSS when sintered identically. However, in case of 1300°C sintering, instead of many large pores, some small isolated pores were observed.

The optical microstructures of T15-2vol% Al₂O₃ with or without the addition of copper sintered at two selected temperatures (i.e. 1100 and 1300°C) are shown in Fig.3.10. In case of 1100°C sintering, the microstructures of T15-2vol% Al₂O₃ as well as T15-2vol% Al₂O₃-5wt% Cu were similar to those compositions without Al₂O₃. In case of 1300°C sintering, the T15-2vol% Al₂O₃ and T15-2vol% Al₂O₃-5wt% Cu samples showed a well developed microstructure with fine matrix as well as carbide grains and some small, uniformly distributed pores.

The optical microstructures of T15 HSS and T15-2vol% Al₂O₃ with or without the addition of copper after repressing/resintering are shown in Fig.3.11. The microstructures of all the compositions remained almost identical after repressing/resintering in relation to as-sintered microstructures, except some coarsening of grains.

The effect of sintering and repressing/resintering on average grain size of T15 HSS and T15-2vol% Al₂O₃ composite with or without the addition of 5wt% Cu (all sintered at 1300°C) is shown in Fig.3.12. The effect of dispersoid as well as copper on T15 HSS in reducing the grain size was evident. After repressing/resintering the grain size of all the compositions slightly increased.

T15 HSS



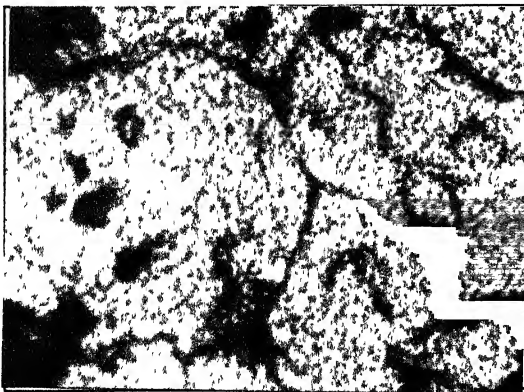
20 μ m

T15+5 wt% Cu



20 μ m

(a)



20 μ m



20 μ m

(b)



20 μ m



20 μ m

(c)

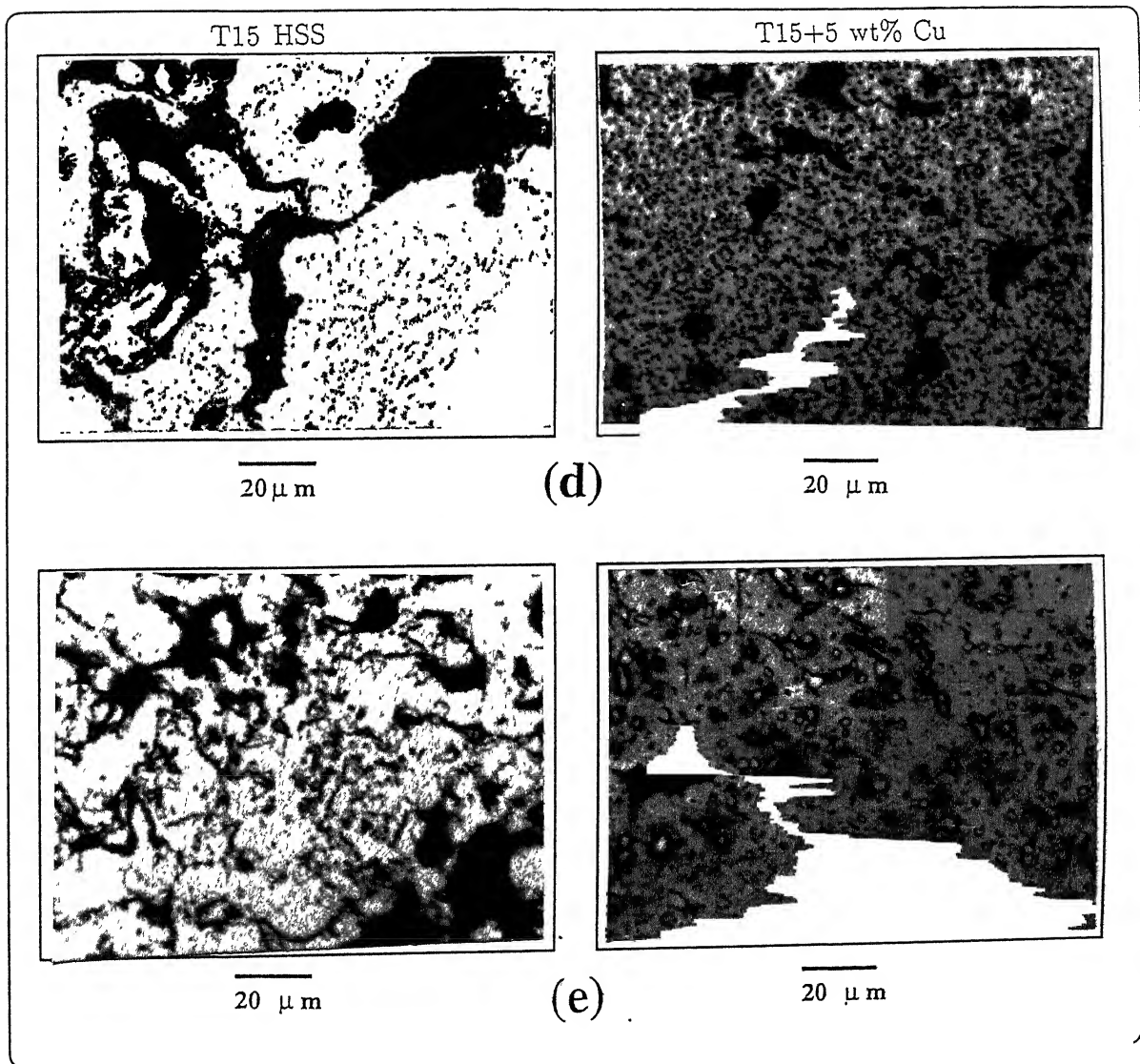


Fig. 3.9 The optical microstructures of T15 HSS with or without the addition of copper sintered at (a) 500 (b) 700 (c) 900 (d) 1100 and (e) 1300°C respectively.

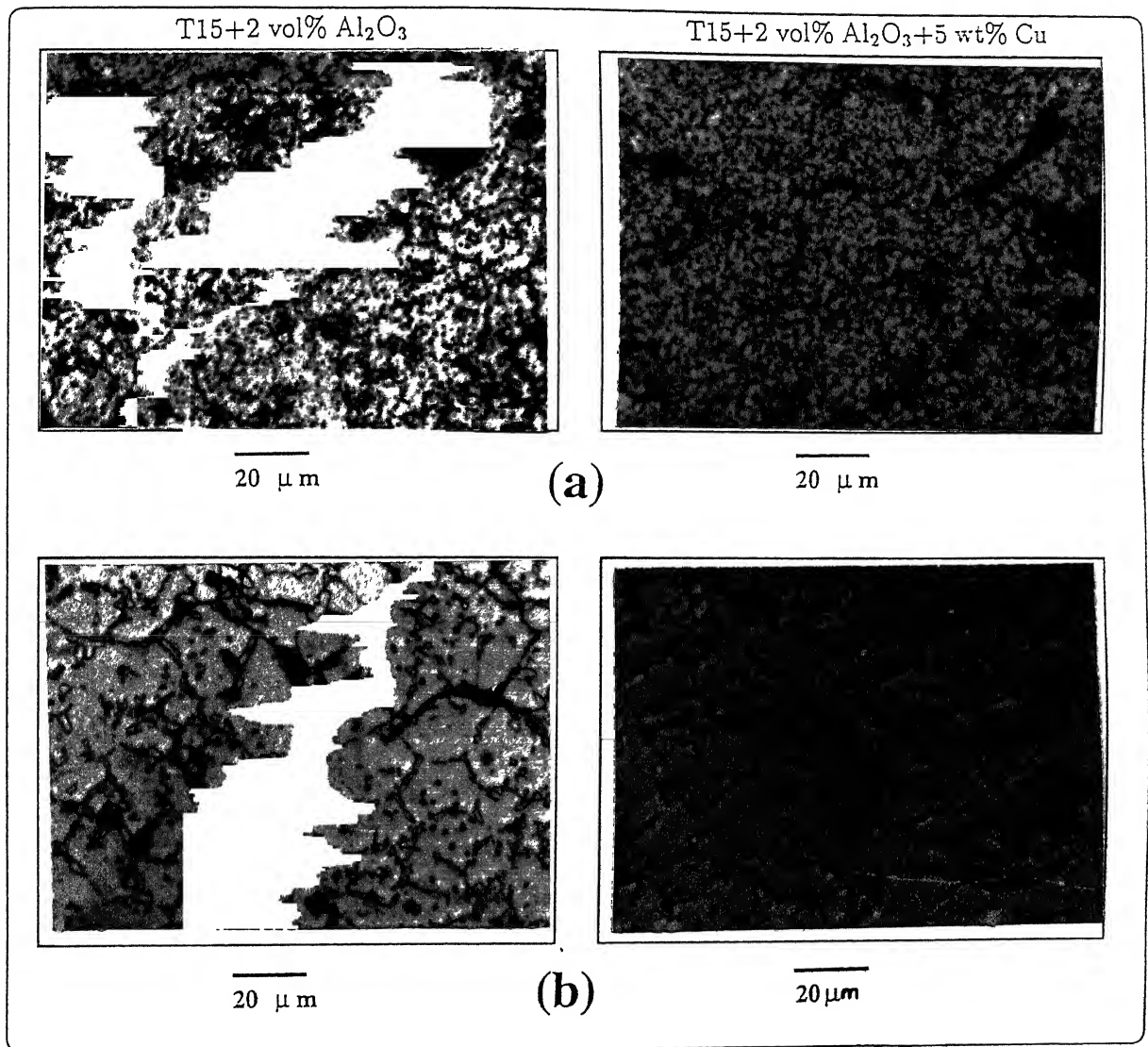
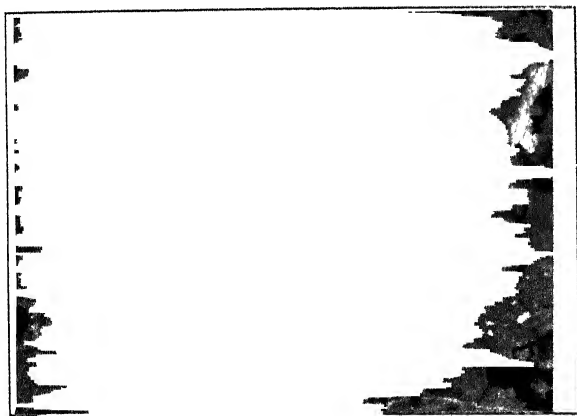
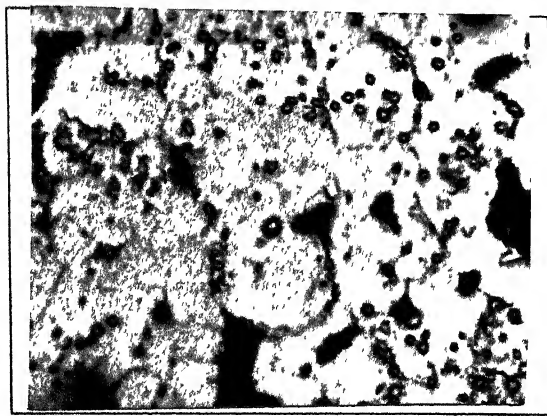


Fig. 3.10 The optical microstructures of T15-2 vol% Al_2O_3 composite with or without the addition of 5 wt% copper sintered at (a) 1100 and (b) 1300°C respectively.



(a)

20 μm



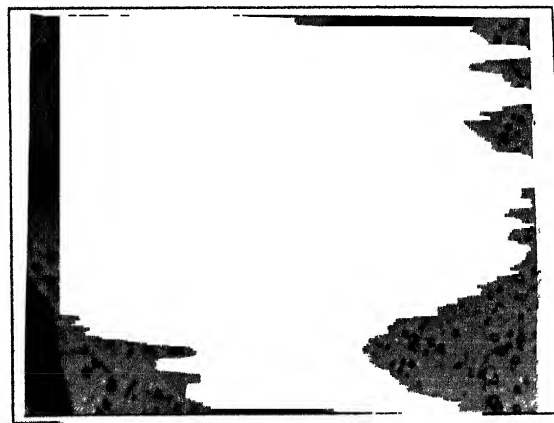
(b)

20 μm



(c)

20 μm



(d)

20 μm

Fig. 3.11 The optical microstructures of T15 HSS and T15-2 vol% Al_2O_3 compositions with or without the addition of 5 wt% copper (sintered at 1300°C) after repressing/resintering; (a) T15 HSS (b) T15+2 vol% Al_2O_3 (c) T15+5 wt% Cu (d) T15+2 vol% Al_2O_3 +5 wt% Cu.

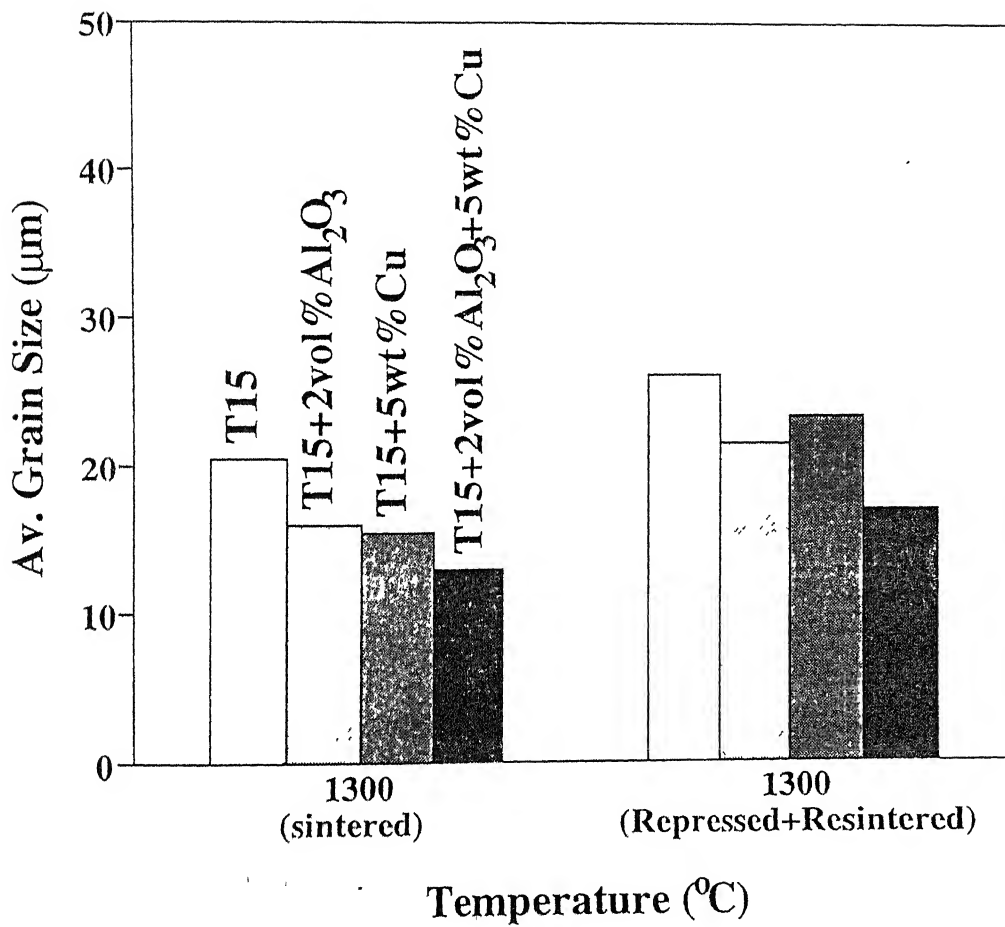


Fig 3.12 Effect of sintering and repressing/resintering on av. grain size of T15 IHS and T15-2 vol% Al₂O₃ compositions with or without the addition of 5 wt% copper (all sintered at 1300°C).

3.2 Effect of Al_2O_3 content and 5wt% Copper Addition on T15- Al_2O_3 composites

3.2.1 Densification Behaviour

The effect of Al_2O_3 content with or without 5wt% copper addition on densification behaviour of T15- Al_2O_3 composites at various sintering temperatures is shown in Fig.3.13. In case of 1250°C sintering temperature, T15- Al_2O_3 composites showed very poor densification and with increasing Al_2O_3 content it remained unchanged. In case of 1280°C sintering temperature, the sintered density decreased with increase in Al_2O_3 content. However, at any particular composition, the densification was much higher than that of 1250°C sintered composition. After 1300°C sintering, the densification followed the similar trend to that of 1280°C sintering. But in this sintering temperature and at any particular composition, the densification was slightly better than that of 1280°C sintered one.

With the addition of copper, irrespective of sintering temperature, the densification of all the compositions was observed lower than that of samples without copper. In case of 1250 and 1280°C sinterings, the samples with copper showed very little densification. The trend and magnitude of densification were found similar to those of 1250°C sintered samples without copper. After 1300°C sintering, the densification followed similar trend to that of 1300°C sintered samples without copper.

3.2.2 Vickers Hardness

The variation of Vickers hardness of T15 HSS and its Al_2O_3 containing composites with or without addition of copper sintered at various temperatures and at different heat treatment conditions is shown in Fig.3.14 -3.16. Irrespective of sintering temperature, any increase in dispersoid volume fraction of T15- Al_2O_3 composites decreased Vickers hardness, with the exception of 2 vol% Al_2O_3 composite where the role of hardening by the hard dispersoid is evident. For any particular composition, in general, higher sintering temperature showed higher Vickers hardness.

With the addition of copper, irrespective of the sintering temperature, the Vickers hardness increased. After 1250 and 1280°C sinterings, the trend remained similar to those of compositions without copper. But after 1300°C sintering, T15 HSS showed the maximum hardness of 460 HV_{10} .

After quenching, irrespective of sintering temperature, the hardness increased significantly as compared to the as-sintered hardness. For the 1250 and 1300°C samples, the as-quenched hardness followed similar trend to that of as-sintered samples. However, in

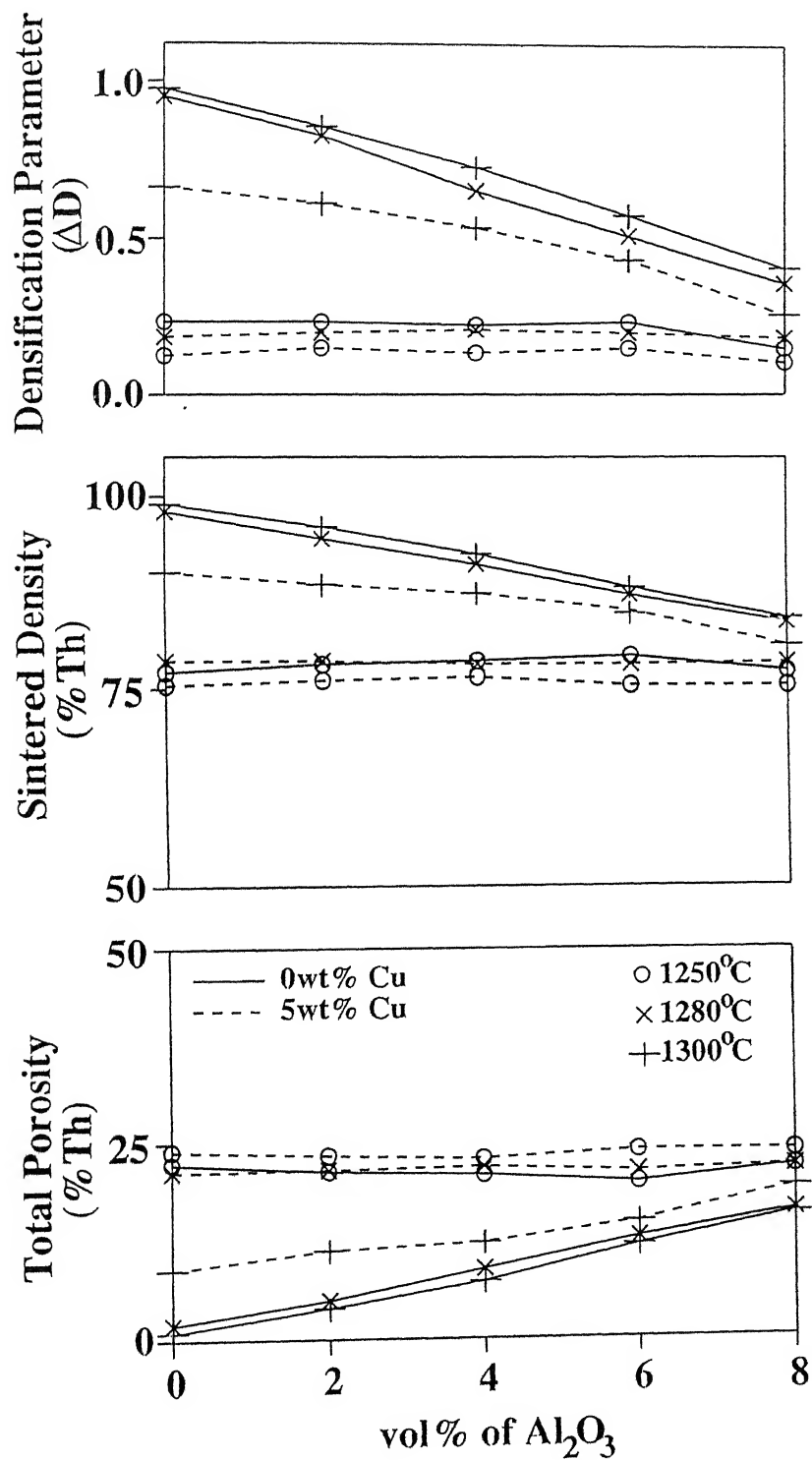


Fig. 3.13 Effect of Al_2O_3 addition on densification behaviour of T15 HSS with or without the addition of 5 wt% copper sintered at various temperatures.

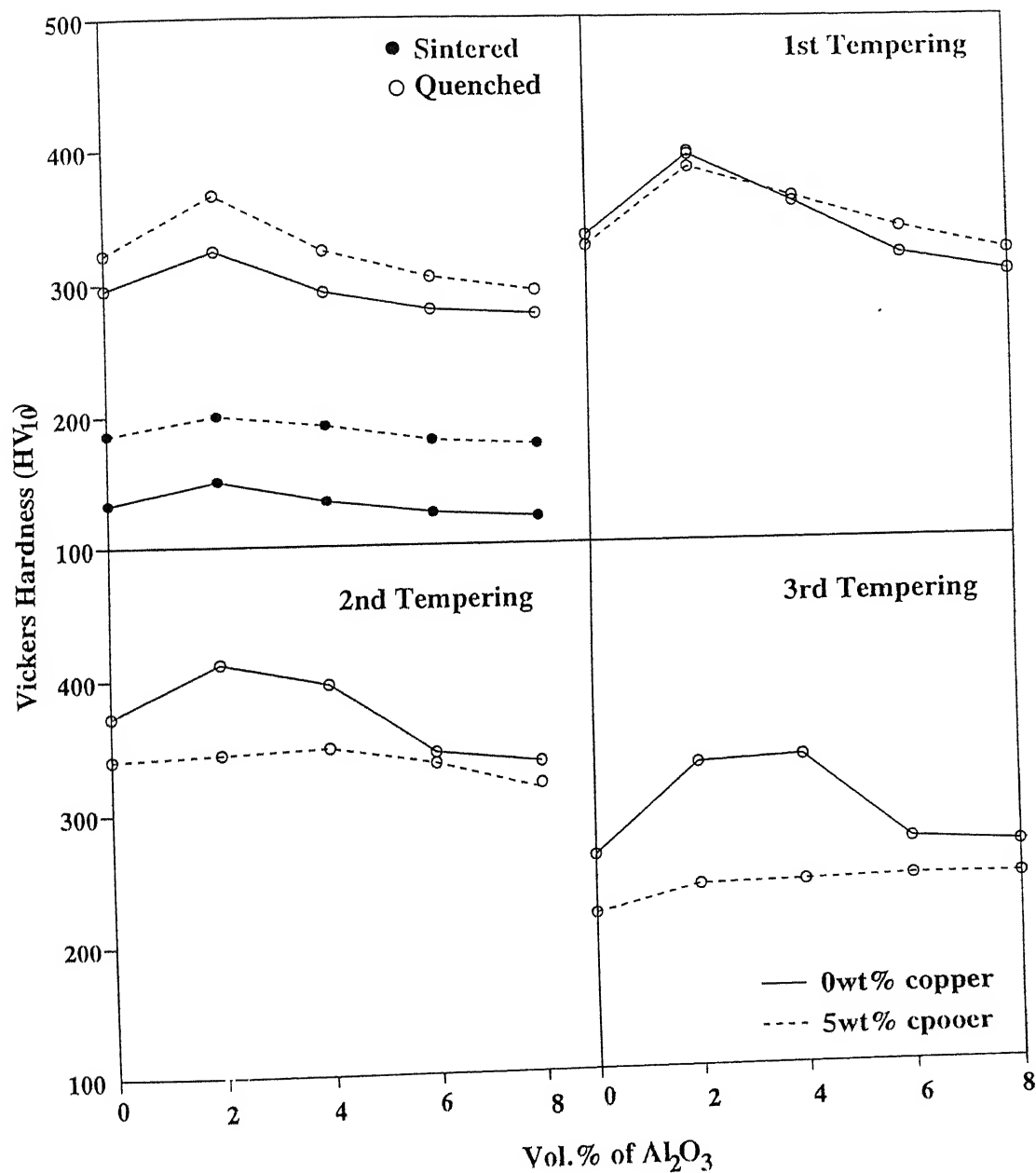
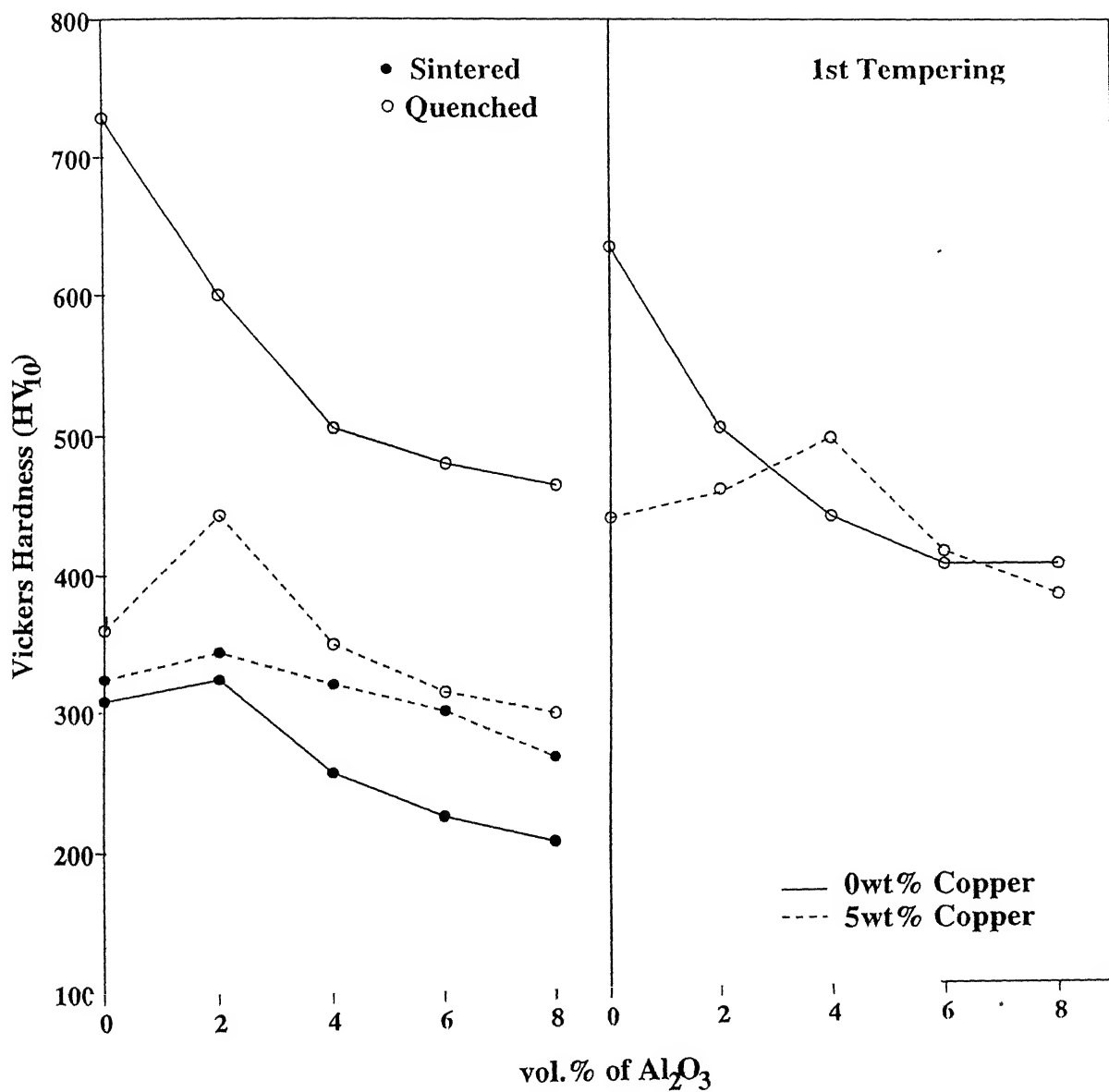


Fig. 3.14 Vickers hardness variation of sintered (1250°C) and heat treated T15 HSS and its Al₂O₃ containing composites with or without 5 wt% copper addition



Contd....

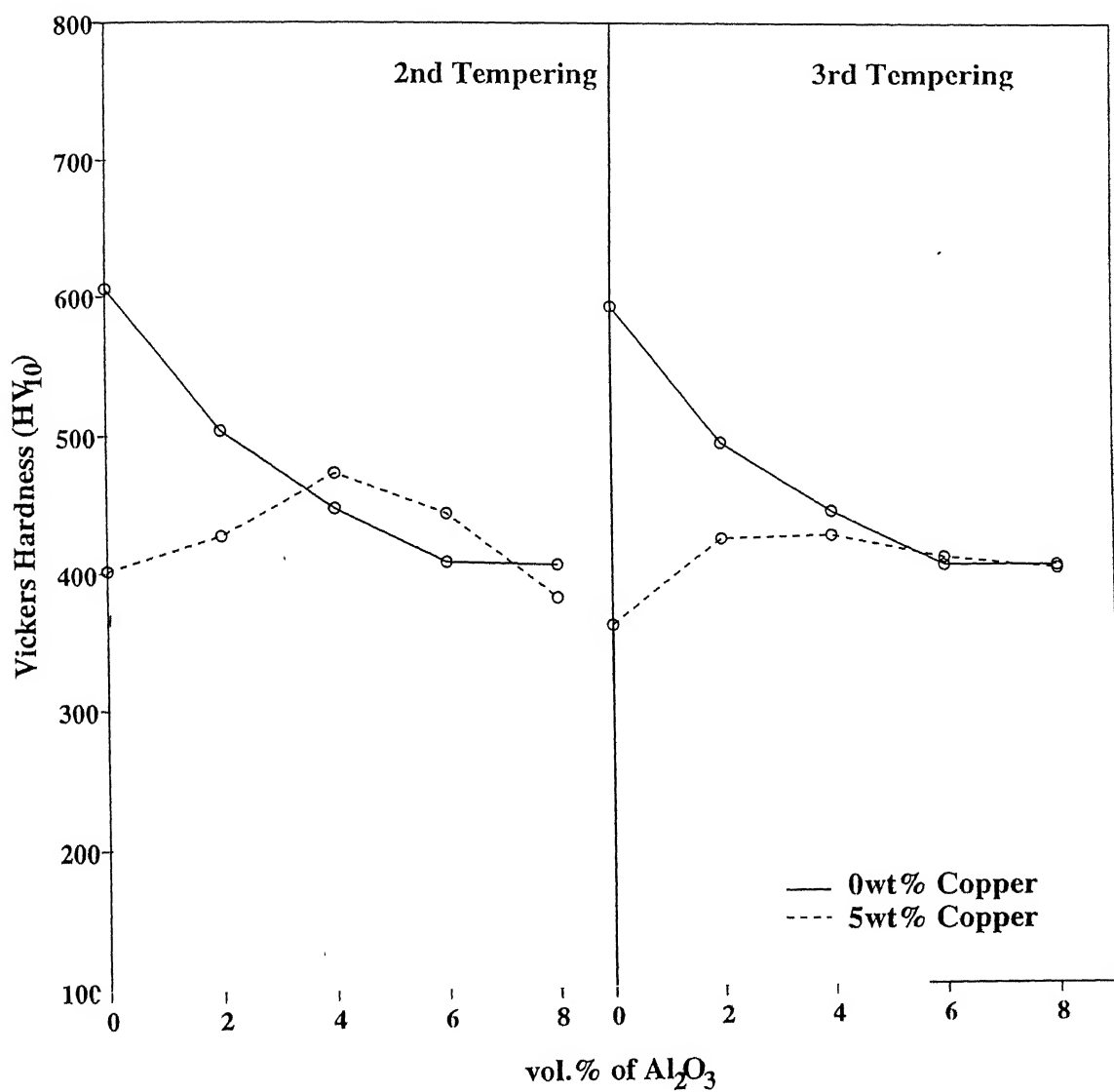
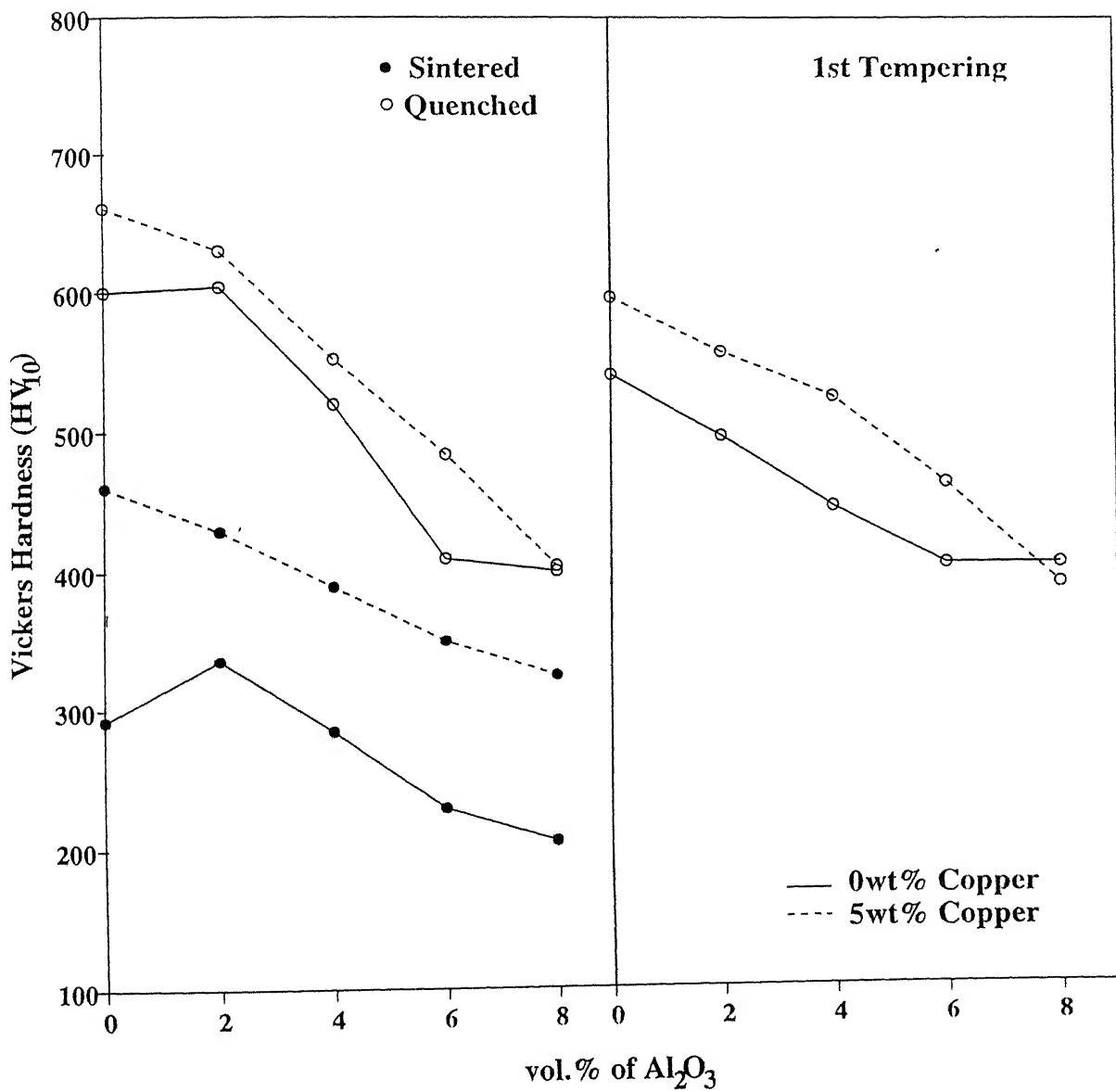


Fig 3.15 Vickers hardness variation of sintered (1280°C) and heat treated T15 HSS and its Al₂O₃ containing composites with or without 5 wt% copper addition.



Contd....

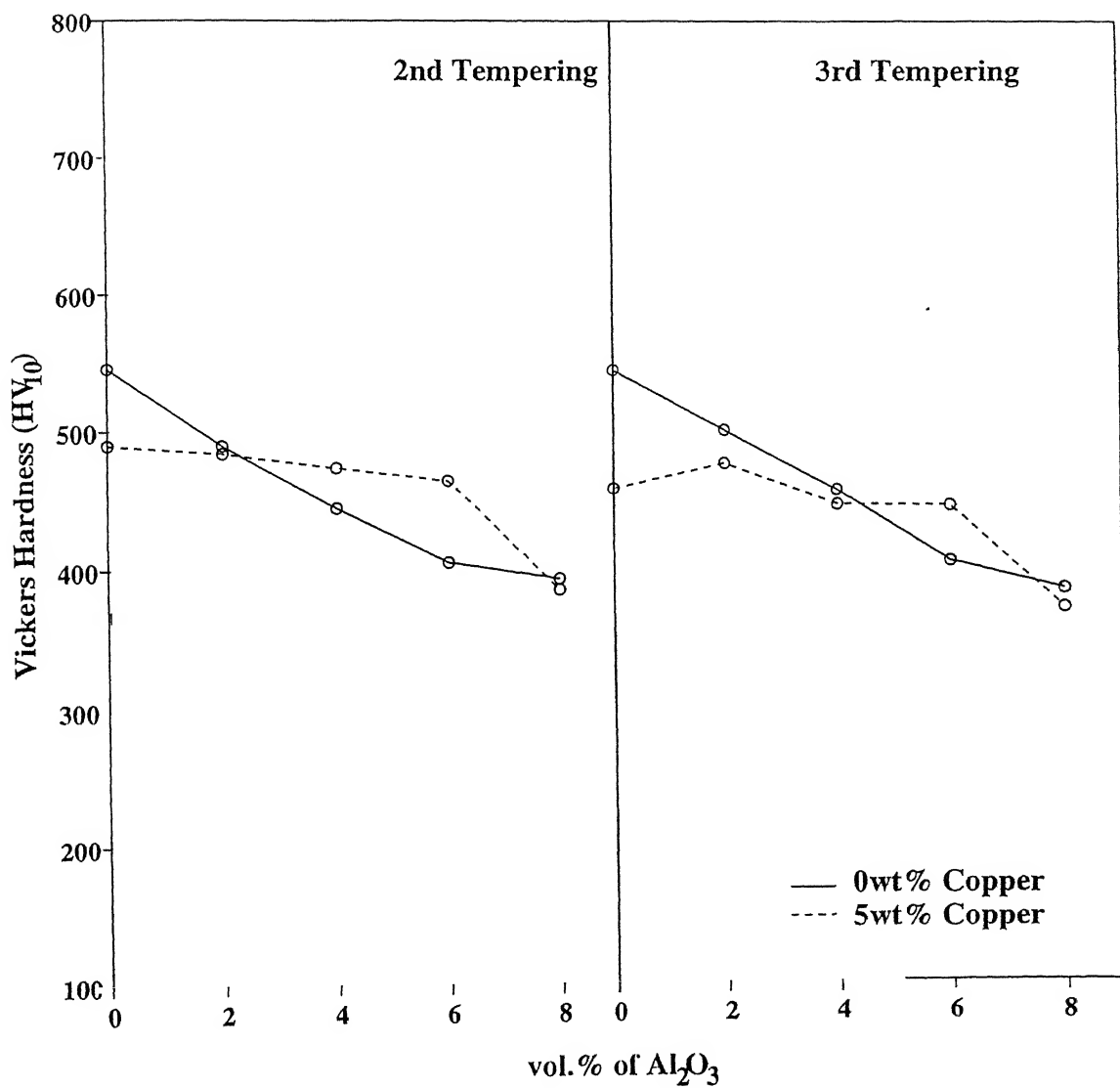


Fig. 3.16 Vickers hardness variation of sintered (1300°C) and heat treated T15 IIS and its Al₂O₃ containing composites with or without 5 wt% copper addition.

case of 1280°C sintered samples. after quenching. T15 HSS showed the best as-quenched hardness of 730 HV_{10} .

Irrespective of sintering temperature, the compositions with copper showed the similar trend of hardness variation to that of as-sintered ones. Here also hardness increased significantly after quenching.

During triple tempering, in case of 1250°C sintered samples, the hardness increased first and then dropped. After every tempering a peak value of hardness which ranging in between 2 and 4 vol% Al_2O_3 was observed. For the 1280°C sintered samples. after every tempering, the plot followed the similar trend that was observed for as-quenched samples. After 1st tempering it decreased and then remained unchanged. In case of 1300°C sintered samples, the trend of hardness during tempering was observed similar to that of as-quenched ones. After 1st tempering the hardness dropped and then remained unchanged.

Irrespective of sintering temperature, the hardness of all samples with copper gradually decreased with increase in the number of tempering and the difference in the hardness values between different composites become less pronounced.

3.2.3 Transverse Rupture Strength (TRS)

The effect of Al_2O_3 content on TRS of sintered T15 HSS with or without 5 wt% copper addition is shown in Fig.3.17. Irrespective of sintering temperature, TRS gradually decreased with increase in Al_2O_3 content. Maximum TRS value was observed after 1280°C sintering i.e. 2330 MPa for T15 HSS.

In case of 1250 and 1280°C sintering temperatures, addition of copper decreased TRS. But after 1300°C sintering, the reverse trend was observed.

3.2.4 Sliding Wear Behaviour

The sliding wear behaviour of sintered T15 HSS and its Al_2O_3 containing composites with or without 5 wt% copper addition at two different loads is shown in Fig. 3.18-3.29.

Sliding Wear Behaviour With Respect to Applied Load

At 1.5 kg load

In case of 1250°C sintering, in general, the wear loss variation of all compositions fell within a wide range. There was no clear-cut relationship of wear behaviour with respect to different compositions. However, 8 vol% composite showed severe wear loss. After 1280°C sintering, in contrast to 1250°C sintering, the wear loss variation of all

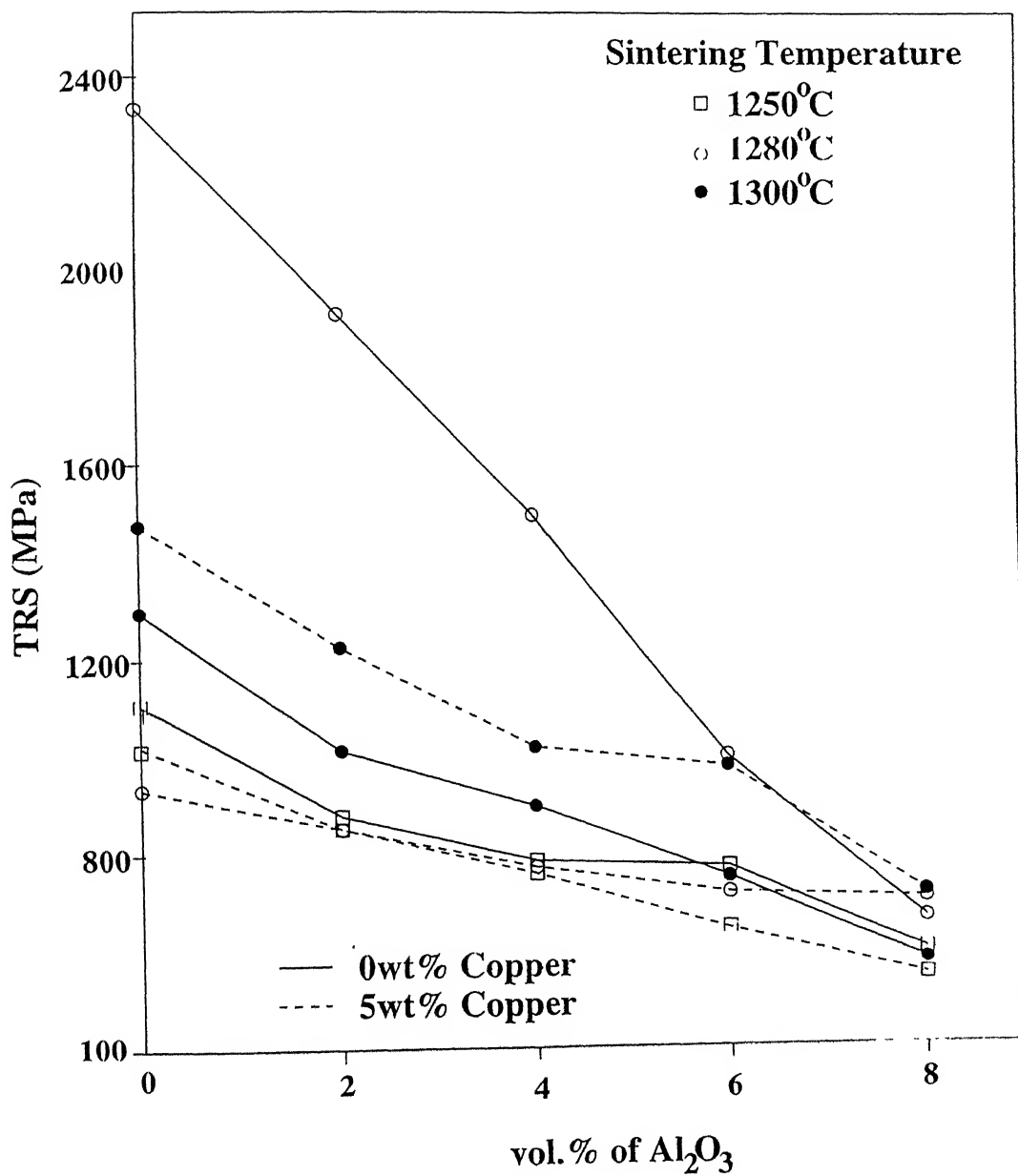


Fig. 3.17 Effect of Al_2O_3 addition on TRS of sintered T15 HSS with or without 5 wt% copper addition.

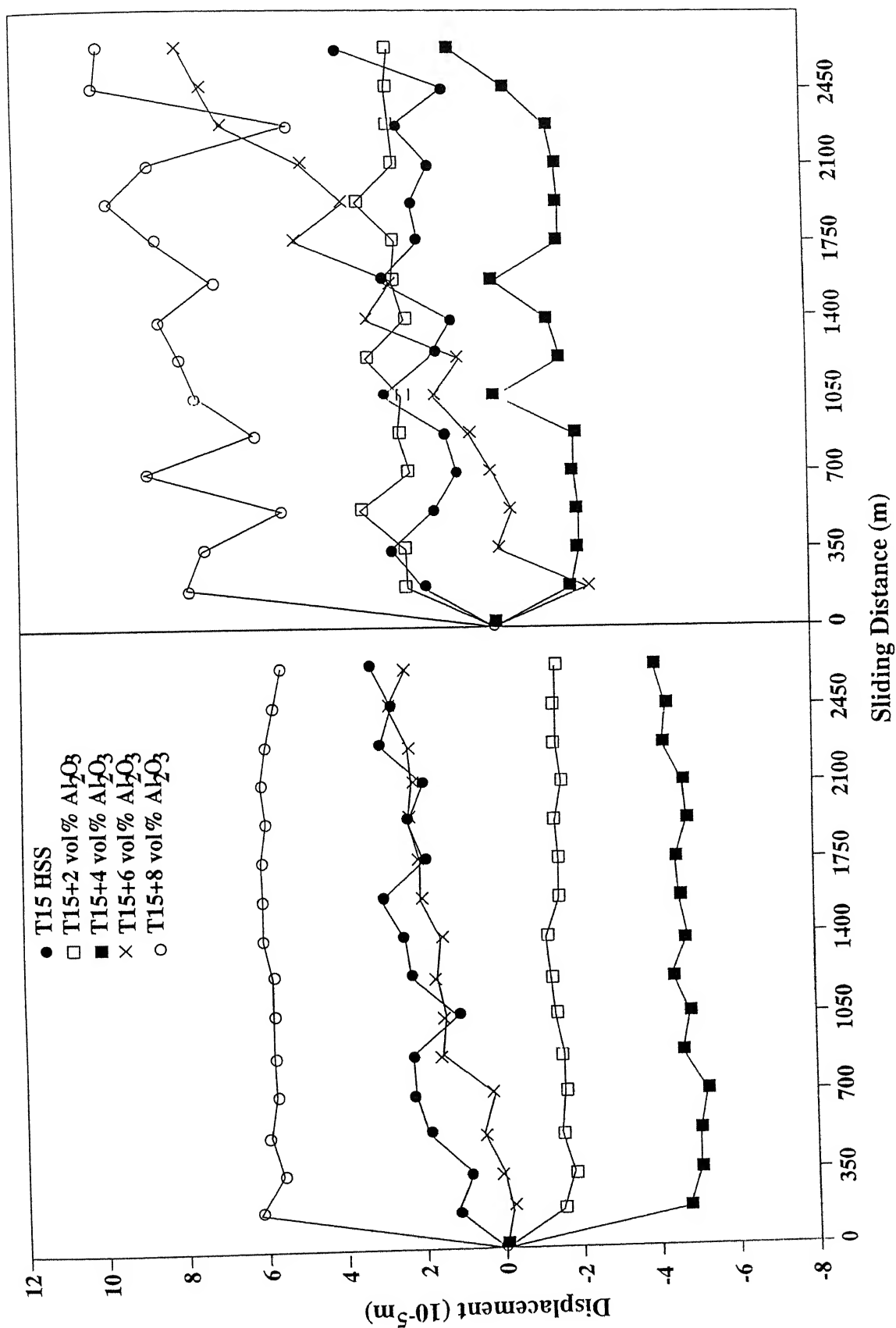


Fig. 3 18 Effect of Al_2O_3 content on sliding wear behaviour of T15 HSS sintered at 1250°C temperature and tested at 1.5 and 2.5 kg loads.

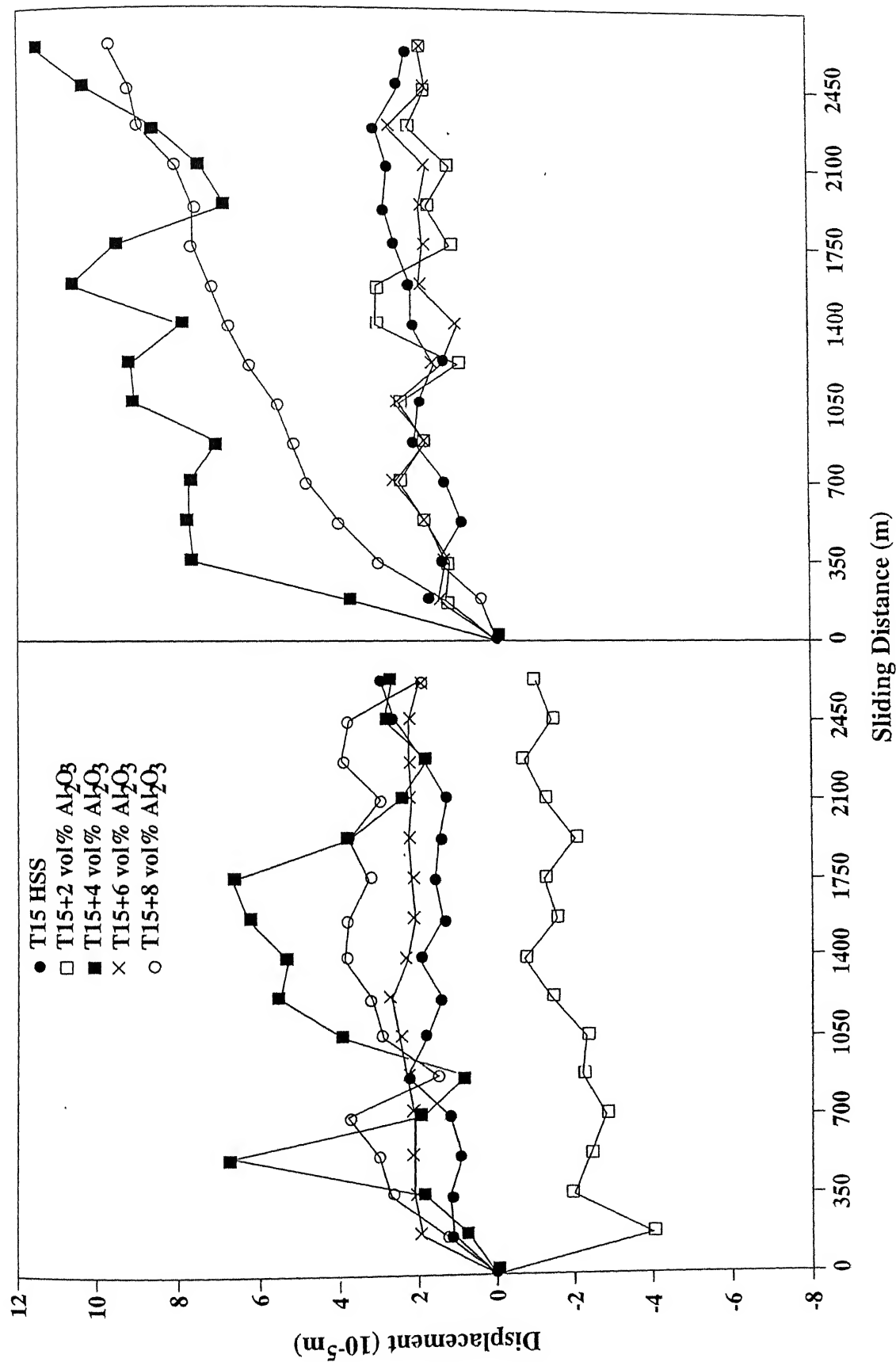


Fig. 3 19 Effect of Al_2O_3 content on sliding wear behaviour of T15 HSS with 5 wt% copper sintered at 1250°C temperature and tested at 1.5 and 2.5 kg loads

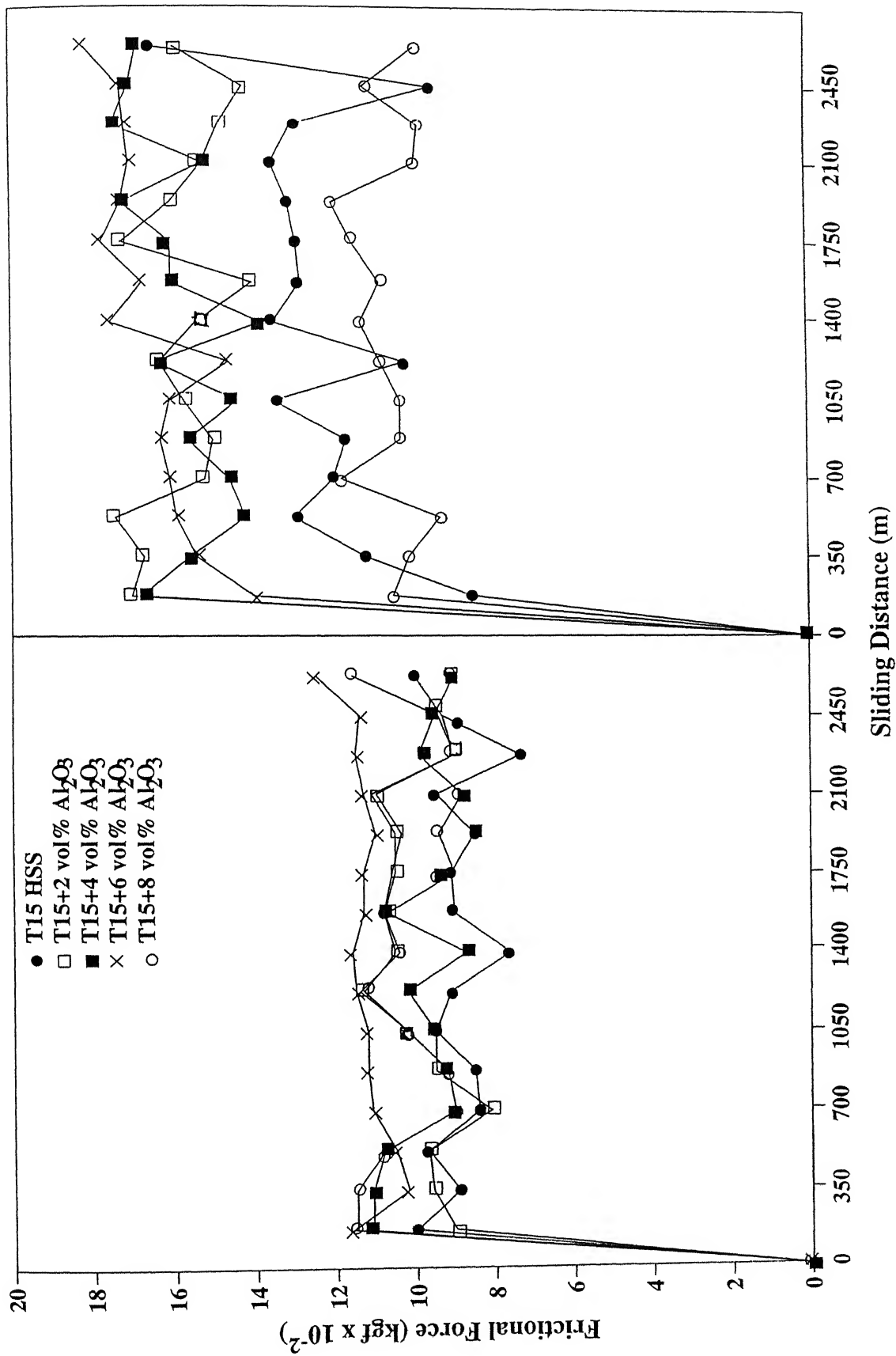


Fig. 3.20 Effect of Al_2O_3 content on frictional force of T15 HSS sintered at 1250°C temperature and tested at 1.5 and 2.5 kg loads.

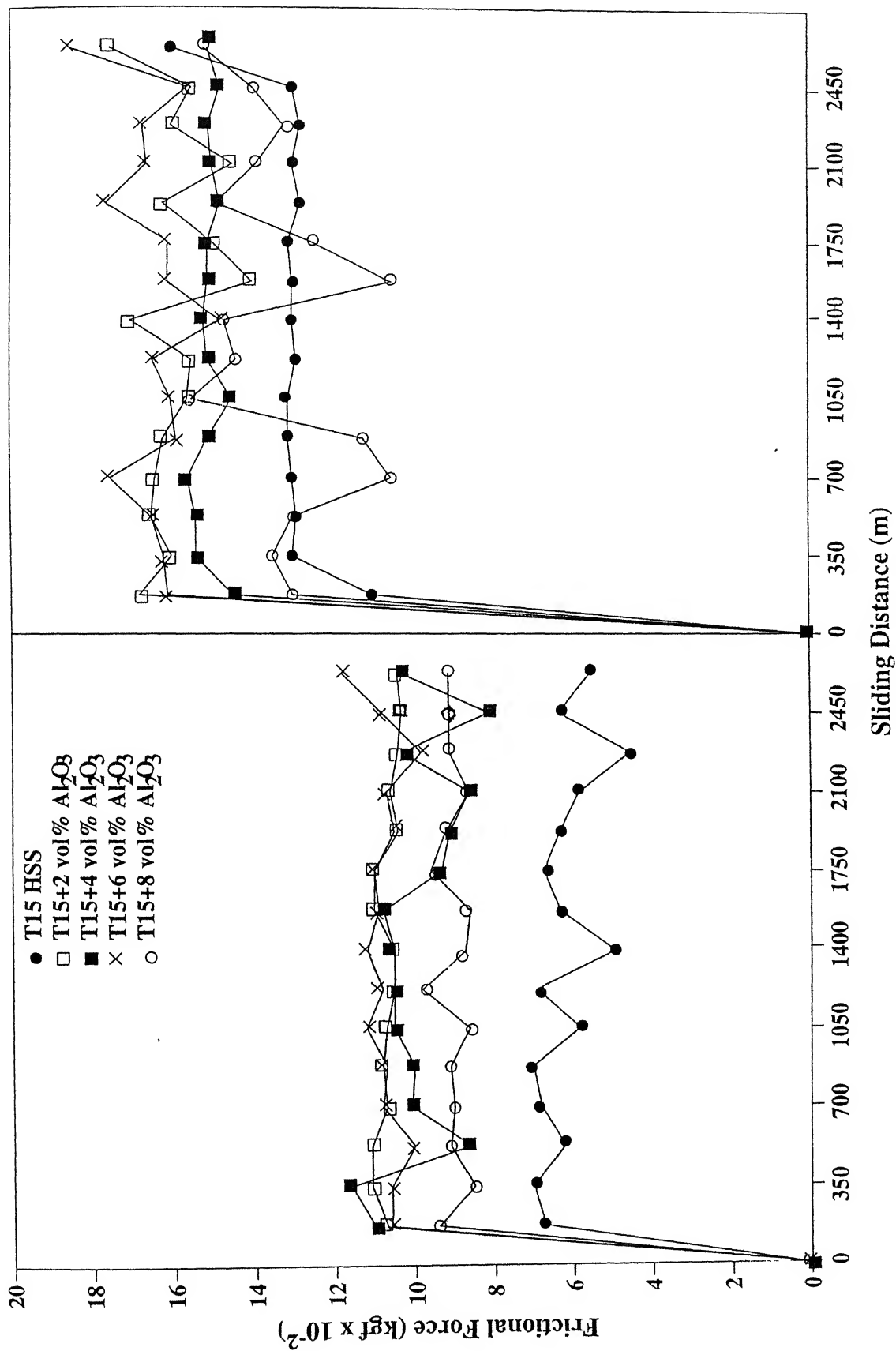


Fig. 3.21 Effect of Al₂O₃ content on frictional force of T15 HSS with 5 wt% copper sintered at 1250°C temperature and tested at 1.5 and 2.5 kg loads

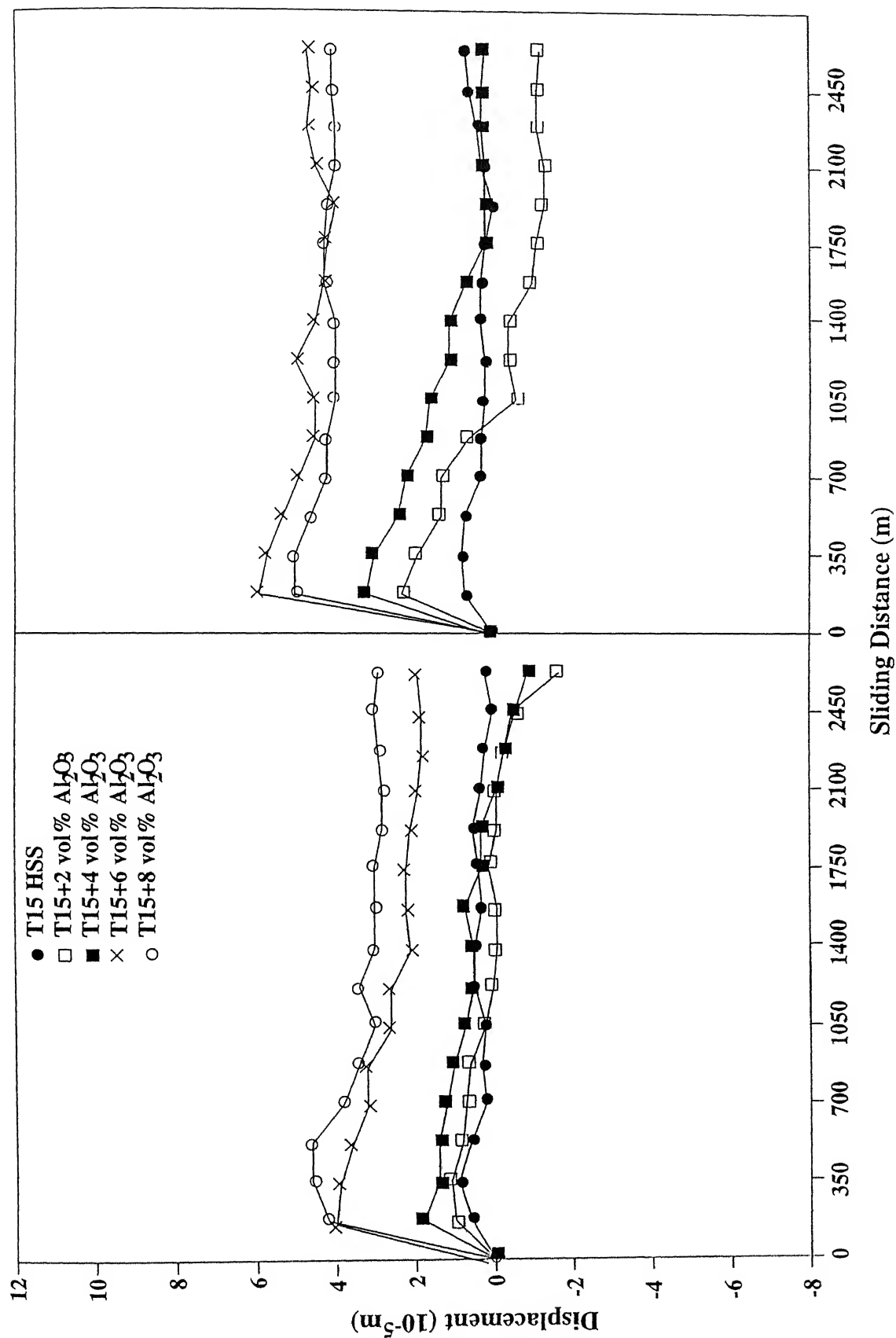


Fig. 3.22 Effect of Al_2O_3 content on sliding wear behaviour of T15 HSS sintered at 1280°C temperature and tested at 1.5 and 2.5 kg loads

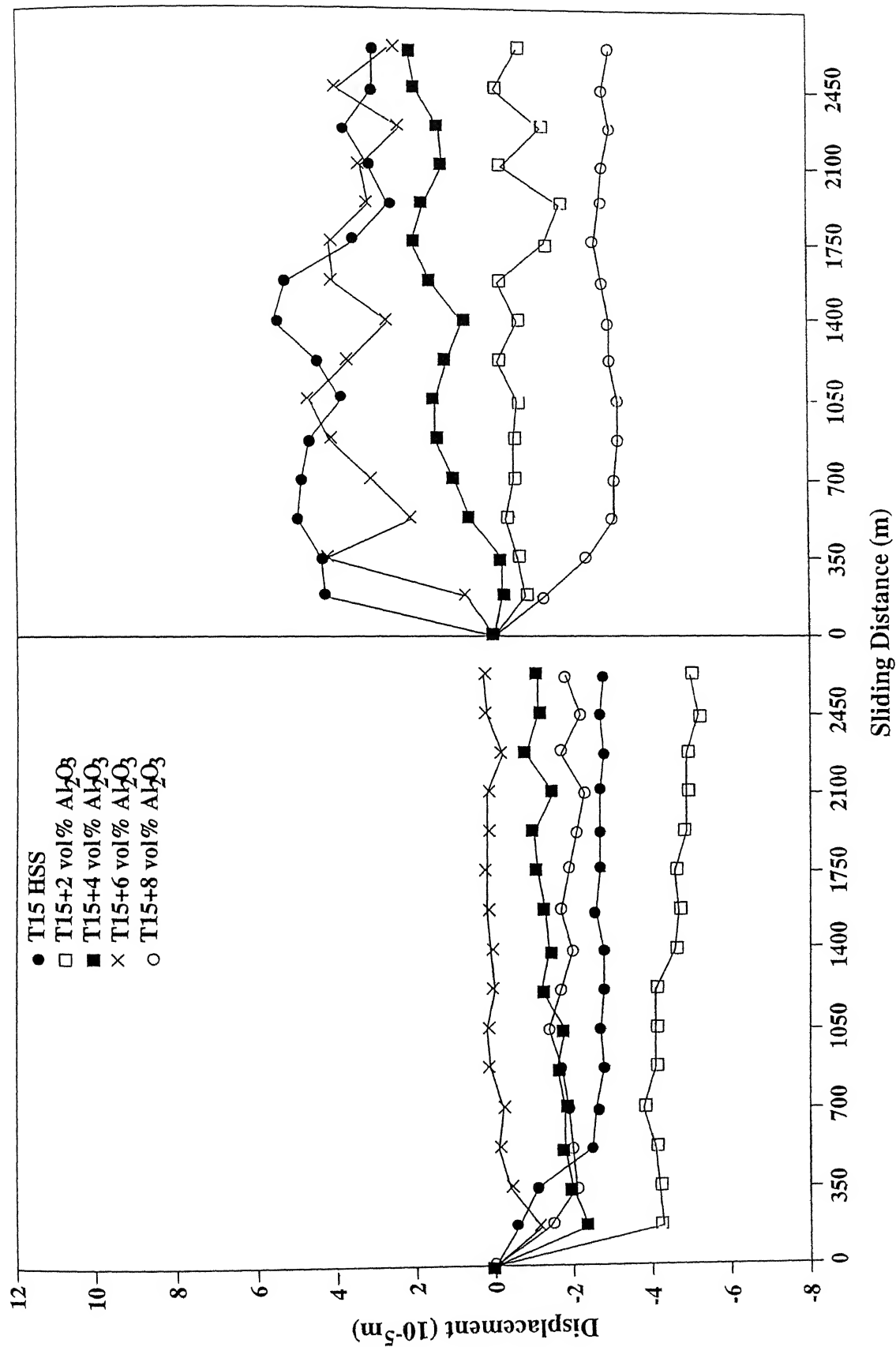


Fig. 3.23 Effect of Al_2O_3 content on sliding wear behaviour of T15 HSS with 5 wt% copper sintered at 1280°C temperature and tested at 1.5 and 2.5 kg loads

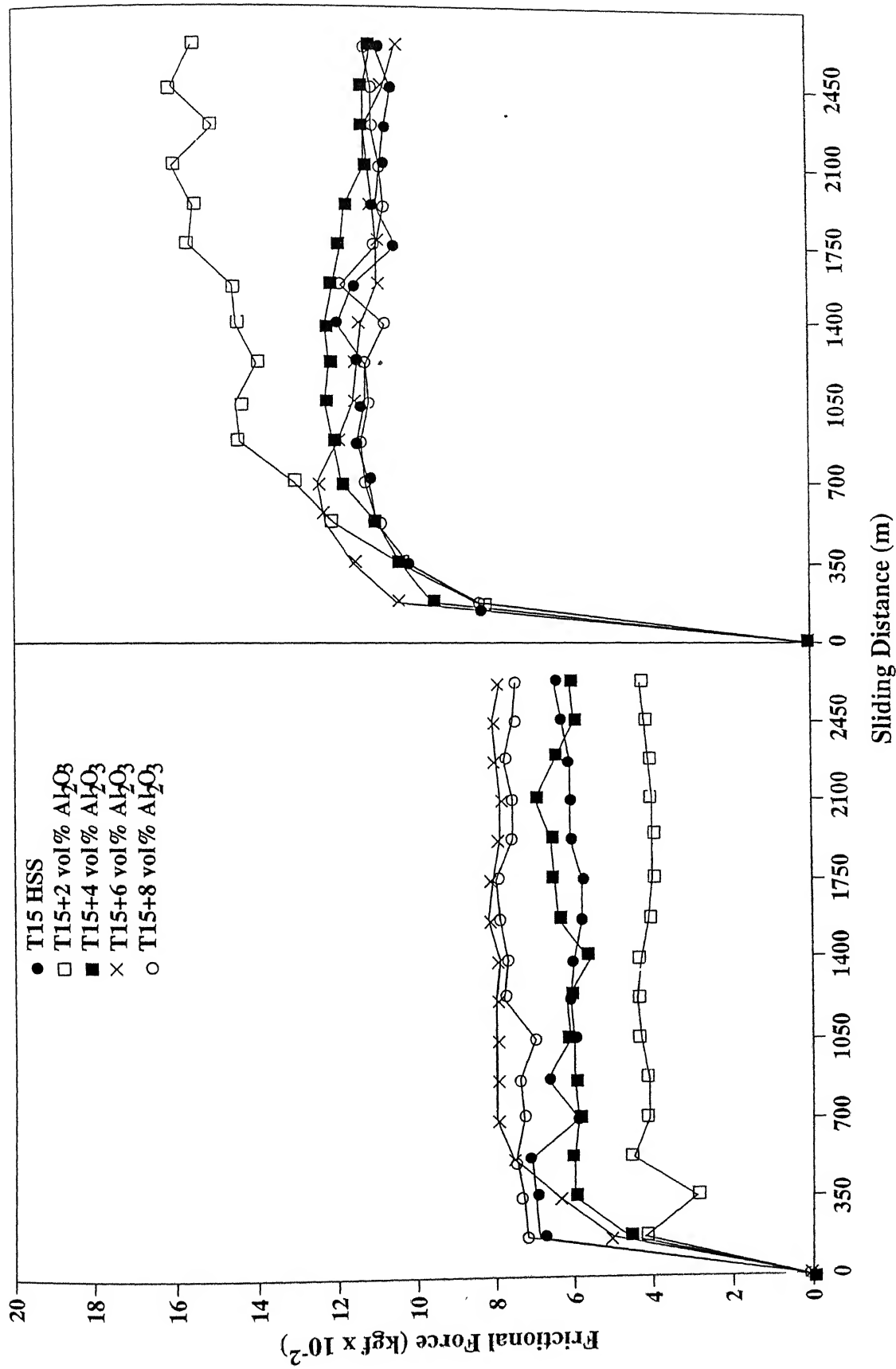


Fig. 3.24 Effect of Al_2O_3 content on frictional force of T15 HSS sintered at 1280°C temperature and tested at 1.5 and 2.5 kg loads

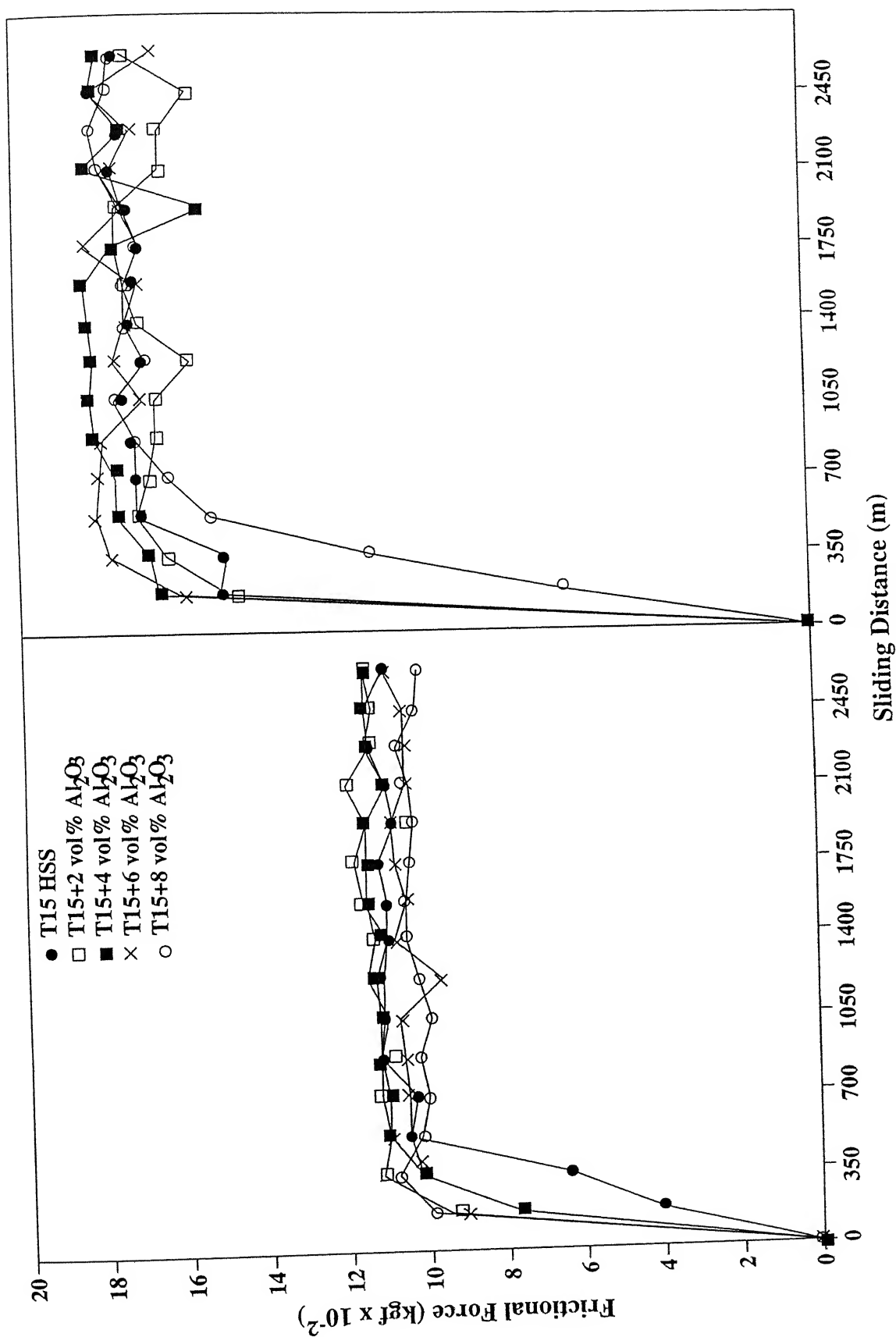


Fig 3.25 Effect of Al_2O_3 content on frictional force of T15 HSS with 5 wt% copper sintered at 1280°C temperature and tested at 1.5 and 2.5 kg loads.

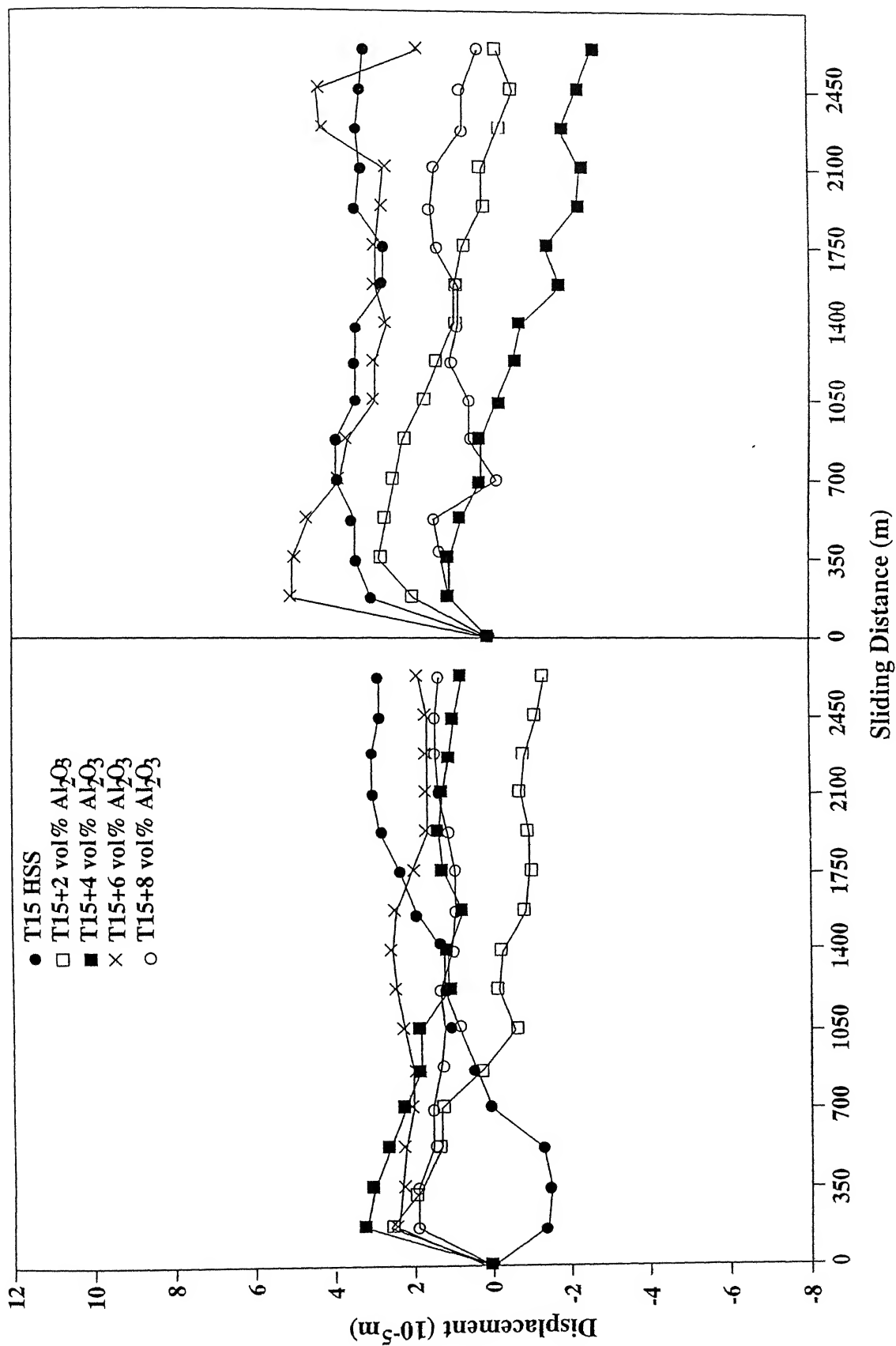


Fig. 3.26 Effect of Al_2O_3 content on sliding wear behaviour of T15 HSS sintered at 1300°C temperature and tested at 1.5 and 2.5 kg loads.

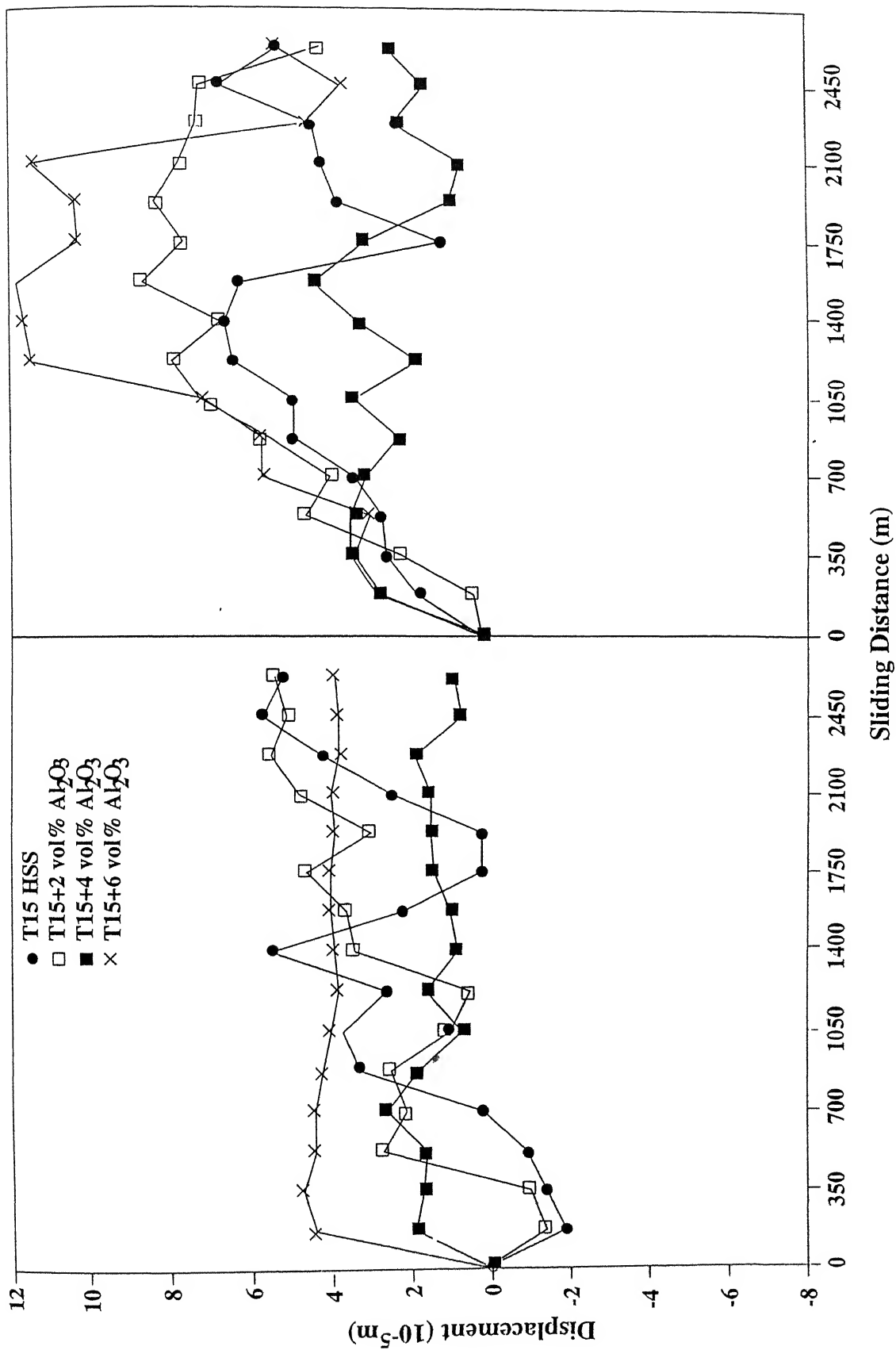


Fig. 3.27 Effect of Al_2O_3 content on sliding wear behaviour of T15 HSS with 5 wt% copper sintered at 1300°C temperature and tested at 1.5 and 2.5 kg loads.

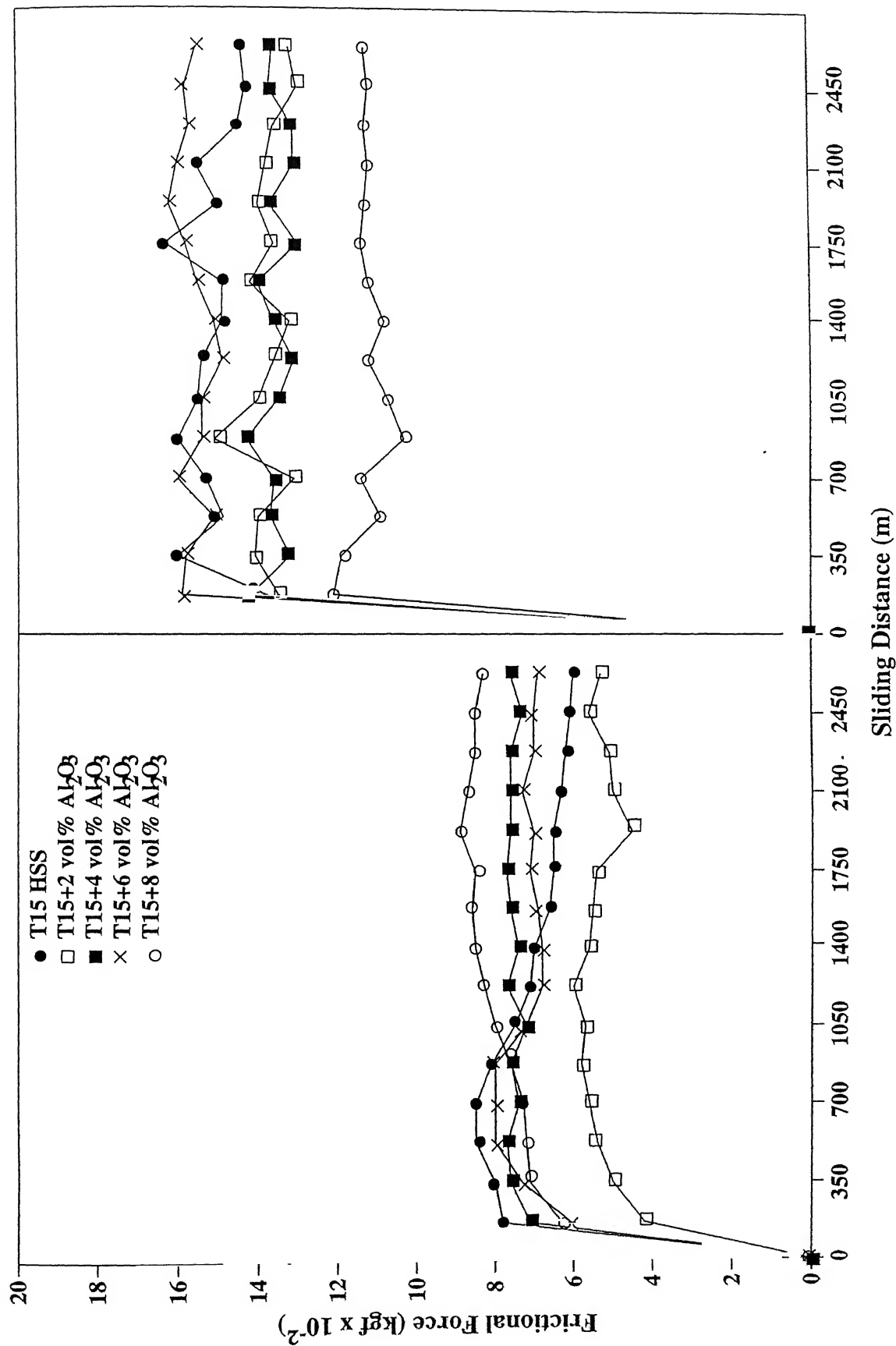


Fig. 3.28 Effect of Al_2O_3 content on frictional force of T15 HSS sintered at 1300°C temperature and tested at 1.5 and 2.5 kg loads.

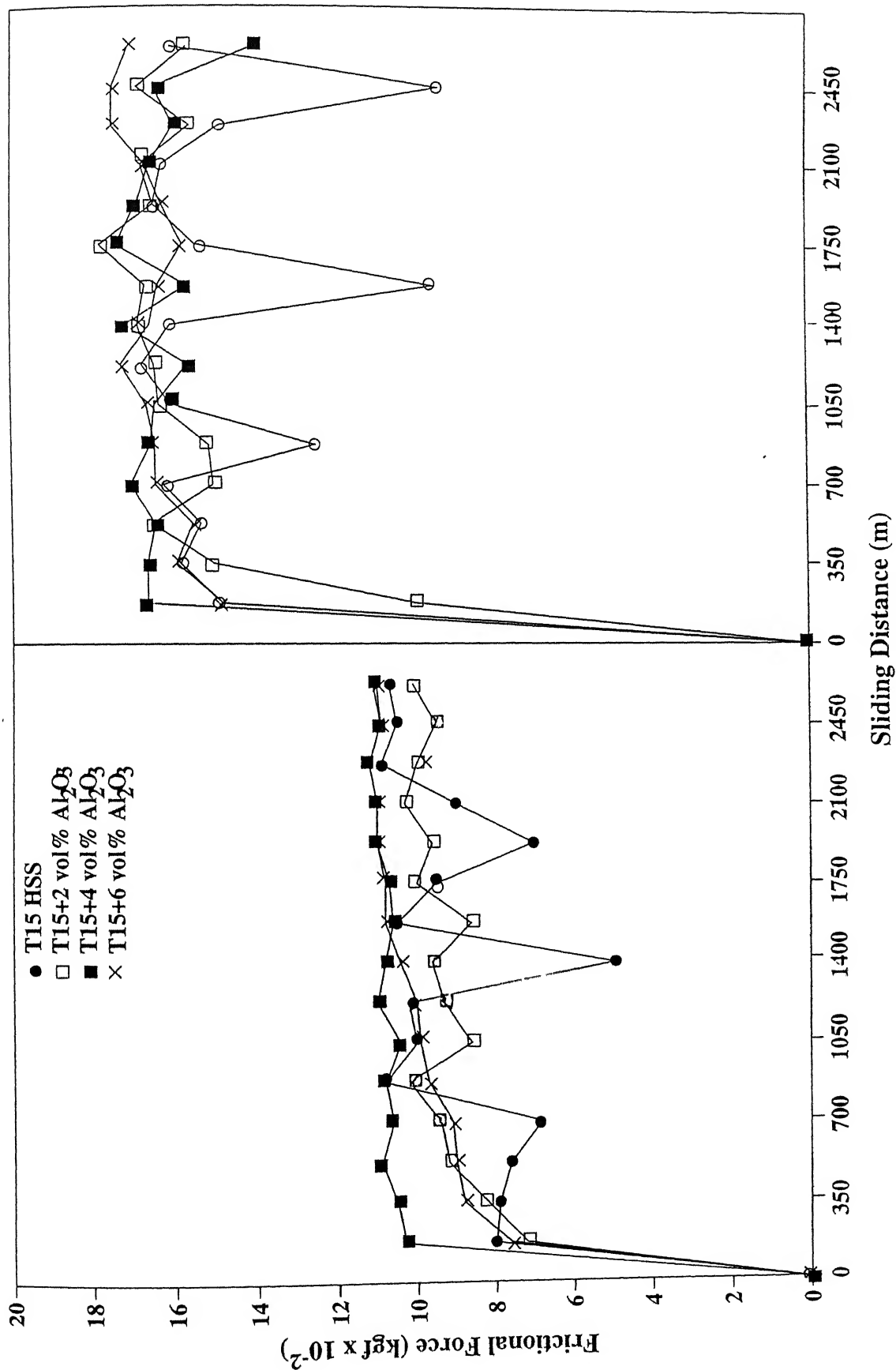


Fig. 3.29 Effect of Al_2O_3 content on frictional force of T15 HSS with 5 wt% copper sintered at 1300°C temperature and tested at 1.5 and 2.5 kg loads.

compositions fell within a narrow range. For all compositions, the initial wear was higher. However, straight T15, 2 vol% and 4 vol% Al_2O_3 composites did not show any appreciable wear loss. Also the wear loss of the T15 HSS was observed less than that for 1250°C sintered one. In case of 1300°C sintering, in general, the nature and range of wear loss variations of all compositions were similar to those for 1280°C sintered samples. However, T15 HSS showed an appreciable increase in wear loss with respect to sliding distance. It was interesting that, in general, 2 vol% Al_2O_3 composite showed better wear resistance behaviour and 6 and 8 vol% Al_2O_3 composites suffered higher wear loss among the all compositions, irrespective of the sintering temperature.

At 2.5 kg load

In general the wear loss was observed more at higher load for all the compositions irrespective of the sintering temperature. The range of wear loss variation of all the compositions was similar to that of samples subjected to lower load. Here also, in general, 6 and 8 vol% Al_2O_3 composites suffered higher wear loss. However, in case of 1250°C sintering, T15 HSS showed maximum wear loss among all the compositions. After 1280°C sintering, similar to that of lower load, T15 HSS did not show any appreciable wear loss and was less than that of samples sintered at 1250 and 1300°C, respectively.

Role of 5 wt% copper addition in T15- Al_2O_3 composites tested at 1.5 kg load

After 1250°C sintering, the magnitude of wear loss variation with composition was in a narrow range than that of compositions without copper. Similar to that for lower load (1.5 kg), there was no clear-cut relationship of wear behaviour with respect to composition. However only 2 vol% Al_2O_3 composite showed wear debris accumulation. After 1280°C sintering, in general, the wear loss variation of all compositions fell within a narrow range which was similar to that of compositions without copper. It was interesting that practically all compositions accumulated the wear debris in the contact region and also reached a steady state with respect to sliding distance. In case of 1300°C sintering, in general, the nature of wear loss variation was similar to that of compositions without copper. However with increasing Al_2O_3 content, the nature changed from sinusoidal to steady state with respect to sliding distance.

Role of 5 wt% copper addition in T15- Al_2O_3 composites tested at 2.5 kg load

In general, for all the composites, the wear loss was observed more at higher load

which was similar to composites without copper. The range of wear loss variation with composition, irrespective of the sintering temperature, was wider than that at lower load. In general, with sliding distance the wear behaviour was sinusoidal in nature and with increasing the Al_2O_3 content the wear loss increased. It was interesting that after 1300°C sintering, for all the copper containing composites, the wear loss was higher than that of corresponding composites without copper.

Sliding Wear Behaviour With Respect to Sintering Temperature

In case of 1250°C sintered specimens, the wear was observed more at higher load (2.5 kg). However, in case of 8 vol% Al_2O_3 composite there was an anomalous increase in wear loss. With the addition of 5 wt% copper, the wear loss variation was similar to that for compositions without copper but in magnitude the values were in a narrow range. There was no clear-cut relationship with the different compositions. However, in case of 8 vol% Al_2O_3 composite, the wear uniformly increased at higher load with respect to sliding distance. In general, with sliding distance, the wear behaviour was found sinusoidal in nature, but in some cases there was an uniform increase in the values with the sliding distance. In case of copper containing compositions, T15 HSS did not show any effect of increase in load. However, the wear loss of 2 vol% Al_2O_3 composite was observed more at higher load.

After 1280°C sintering, in general, the nature of wear loss variation with respect to sliding distance was similar at either load and with increase in load the wear loss was observed more. However, T15 HSS did not show any appreciable wear loss at either load and was less than that sintered at 1250°C . With the addition of 5 wt% copper, in general, the nature of wear loss variation with respect to sliding distance was similar to that without copper. With increase in load the wear loss was more. It was interesting that at low load practically all compositions, instead of wear, accumulated wear debris in the contact region and thereby, reduced the friction. However at higher load, except T15 HSS and its 2 vol% Al_2O_3 containing composite, all other compositions showed wear loss. The T15 HSS in this respect did not appear to have any difference after alloying with copper and at higher load 2 vol% Al_2O_3 composite showed some amount of wear loss.

In case of 1300°C sintering, at either load (1.5 or 2.5 kg), the wear loss variation fell within a narrow range and its variation with respect to sliding distance was similar at either load. However, in case of T15 HSS, the wear was uniformly increasing with respect to sliding distance at lower load. With the addition of copper, at higher load, the effect of composition on wear was more distinctive but at the same time copper containing composites exhibited wider fluctuation in the values. With sliding distance it

appeared that there was a sequence of material loss and accumulation which alternated during wear testing

Variation of Frictional Forces with Respect to Sintering Temperature

In case of 1250°C sintering, in general, at either load and for all compositions, the frictional forces did not reach to a steady state rather showed a wide fluctuation of values, especially at higher load. The nature was observed sinusoidal. At higher load, the frictional forces of all compositions were higher and varying in a wide range compared to that for lower load. With the addition of copper, at either load, the behaviour was similar to that of compositions without copper. However, at either load, T15 HSS showed much lower value of frictional force compared to that of composite compositions.

In case of 1280°C sintering, in general, the frictional forces of all composites reached a steady state at either load. However, at higher load (2.5 kg), in case of 2 vol% Al_2O_3 composite the frictional force increased with increasing sliding distance. With the addition of copper, a steady state was attained by all composites at either load. However, the frictional force increased for each composite at either load. Besides, the variation of the values of frictional forces of all composites was in a very narrow range at either load.

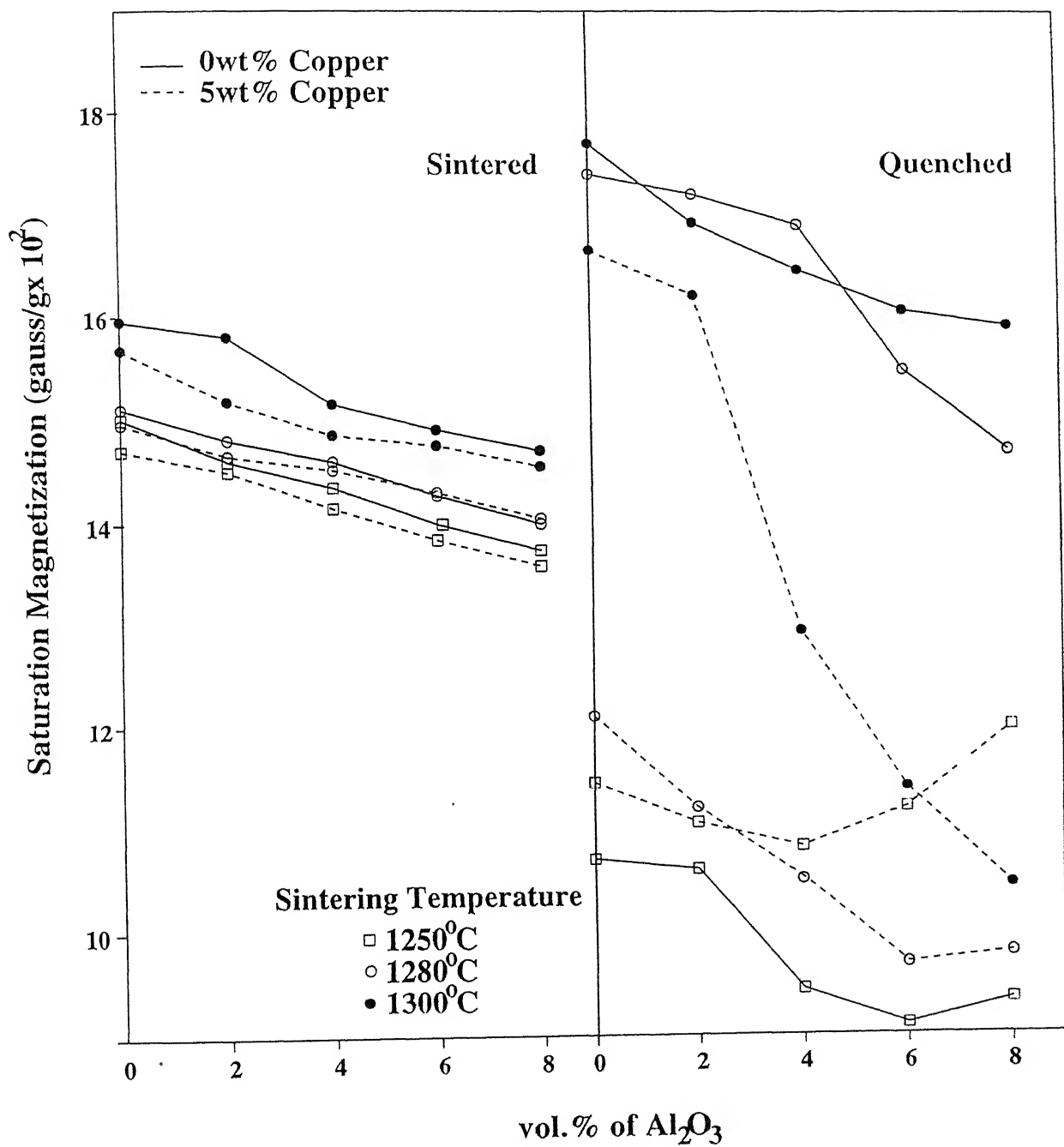
In case of 1300°C sintering, in general, the frictional forces of all composites reached a steady state at either load. With the addition of copper the frictional force increased for each composite at either load. It was interesting that addition of copper to T15 HSS and its 2 vol% Al_2O_3 composite led to a wide fluctuation of values of frictional forces at either load. Although, in case of T15 HSS, it was observed much severe than that of its 2 vol% Al_2O_3 composite. In general, for all situation, the frictional forces of all compositions were higher at higher load and T15 HSS showed minimum frictional force among the all compositions.

3.2.5 Magnetic Properties

Saturation Magnetization (σ_s)

Variation of saturation magnetization with respect to Al_2O_3 content in sintered and heat treated T15 HSS with or without 5 wt% copper is shown in Fig.3.30. Irrespective of sintering temperature, the σ_s decreased with increasing Al_2O_3 content and at any particular composition the higher sintering temperature showed the higher value of σ_s . Addition of copper also followed the similar trend to those of samples without copper.

After quenching, in general, all the quenched samples followed the similar trend to those of sintered ones. The 1250°C sintered samples, after quenching, showed σ_s values



Contd....

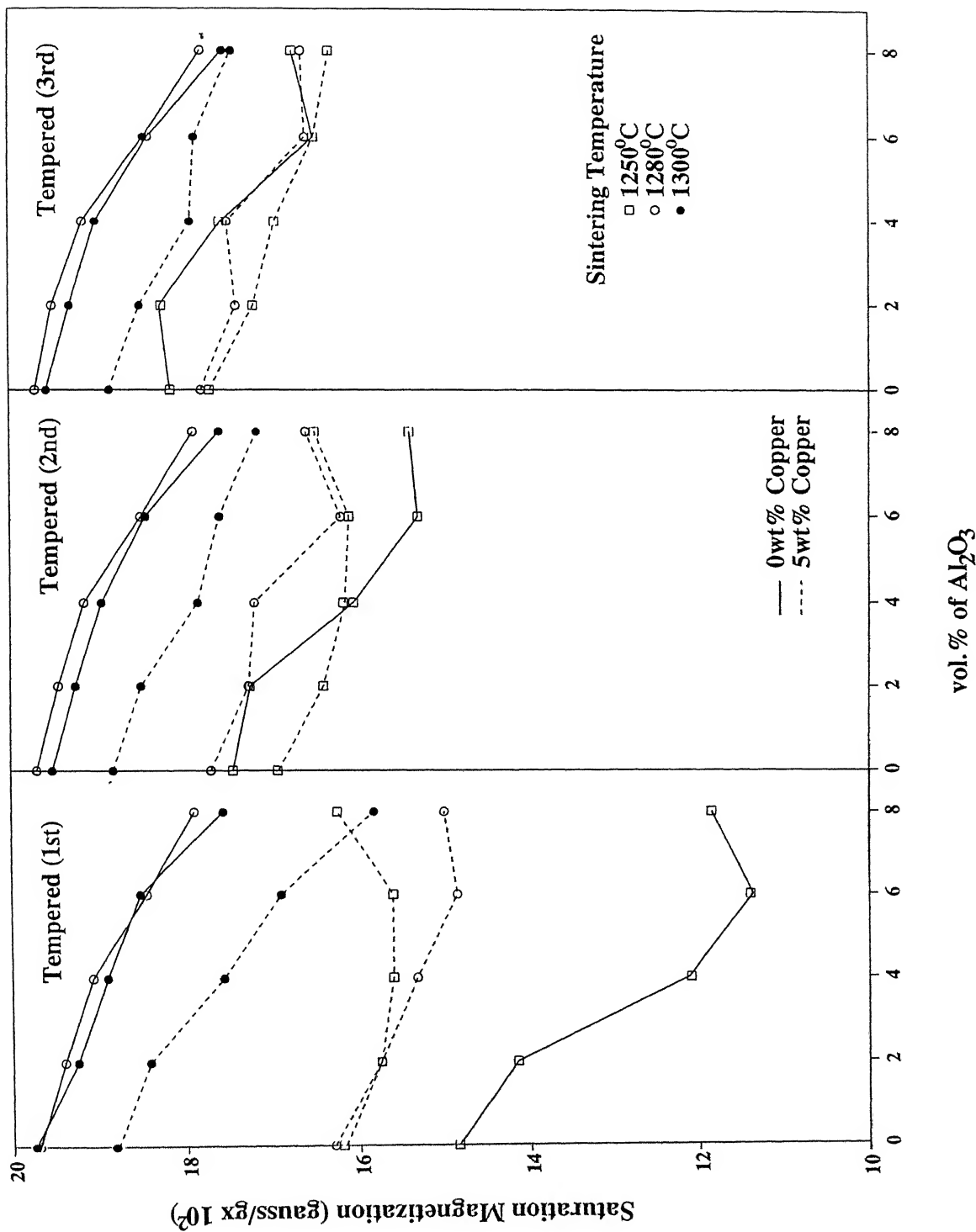


Fig. 3.30 Variation of saturation magnetization with respect to Al₂O₃ content in sintered and heat treated T15 HSS with or without 5 wt% copper addition.

well below to those of as-sintered ones. But for 1280 and 1300°C sintered samples, the σ_s increased after quenching.

The σ_s of 1250°C sintered samples with copper decreased after quenching. The trend was observed similar to that of corresponding as-sintered compositions. However, for 1250°C sintered samples with copper, the σ_s increased at higher volume fraction of Al_2O_3 dispersoid. The 1280°C sintered samples with copper showed a similar trend of σ_s variation but lower in value compared to those of as-sintered ones. The 1300°C sintered samples with copper, after quenching, showed a wide range of variation of σ_s with respect to Al_2O_3 content.

After every tempering, all the samples followed similar trend to those of as-quenched ones. The 1250°C sintered samples showed a gradual increase in σ_s after every tempering. The σ_s of the 1280 and 1300°C sintered samples increased after 1st tempering and further tempering did not change the σ_s .

During tempering, all the compositions containing copper also followed the similar trend to those of as-quenched ones. All the samples with copper, after any tempering, also followed the similar trend to those of compositions without copper. However, it was observed that 1280°C sintered samples with copper showed an increase in σ_s after 2nd tempering.

Magnetic Coercivity

The variation of coercivity with respect to Al_2O_3 content in T15 HSS with or without the addition of 5 wt% copper at various conditions is shown in Fig. 3.31. The coercivity of the as-sintered samples, in general, followed the similar trend to those for sintered porosity. For any particular composition, the higher sintering temperature gave rise to higher coercivity. The samples containing copper, irrespective of sintering temperature, showed higher coercivity compared to those without copper.

After triple tempering, the coercivity of all the samples (with or without copper) decreased and no significant change in the trend of triple tempered samples compared to that of as-sintered samples was observed.

3.2.6 Microstructural Analysis

The optical microstructures of T15 HSS and its containing different vol% of Al_2O_3 with or without the addition of copper sintered at 1300°C temperature are shown in Fig. 3.32. After 1280 or 1300°C sintering, the microstructure was observed well developed and was consisted of grains, carbides and few isolated pores. The primary carbides were observed within grains and at grain boundaries as well. The role of dispersoid in refining

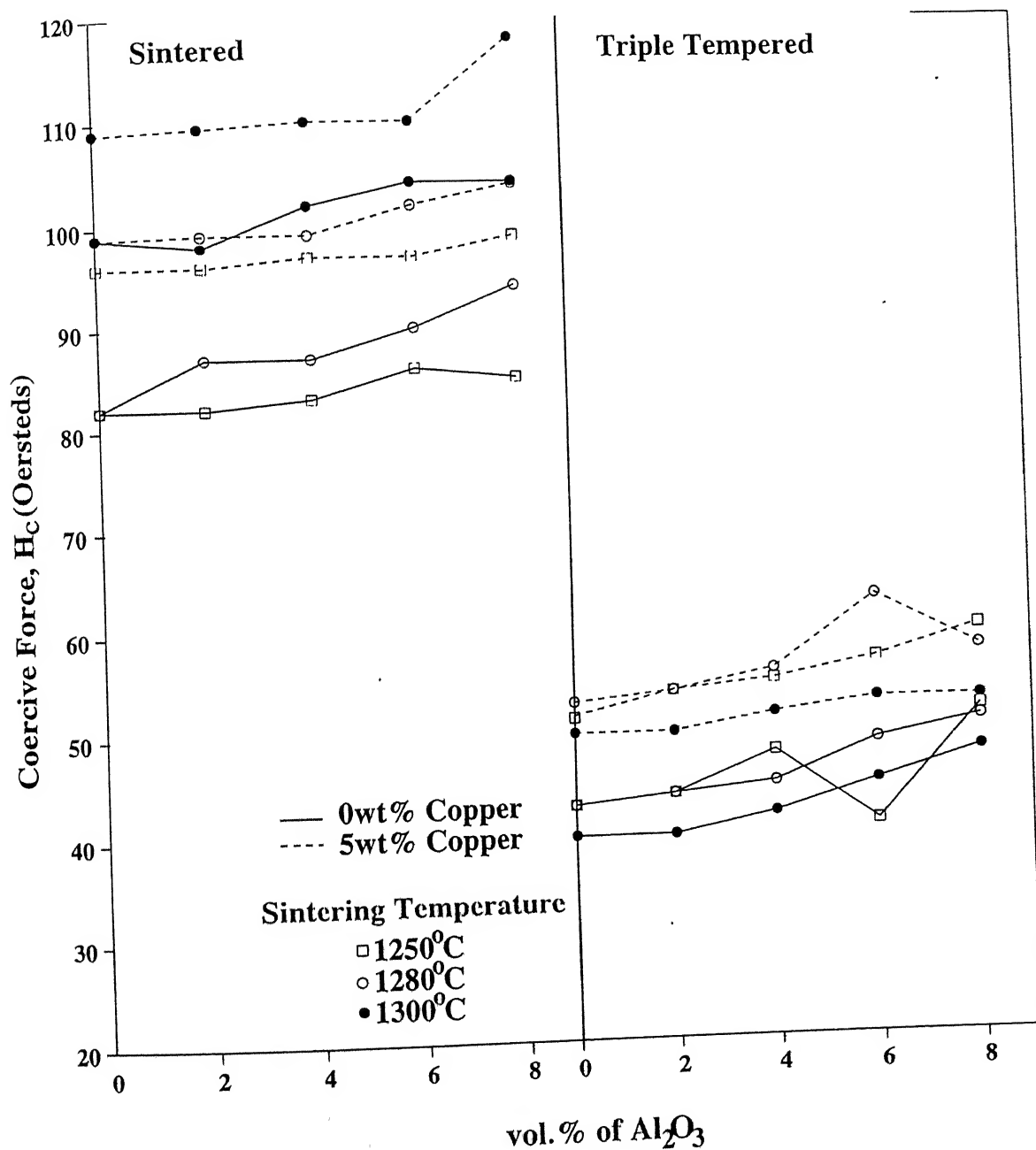
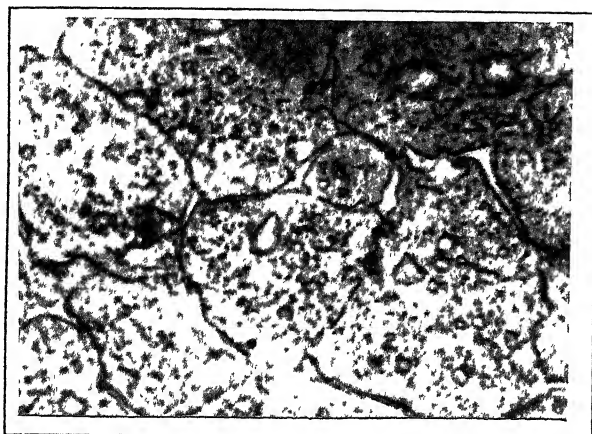
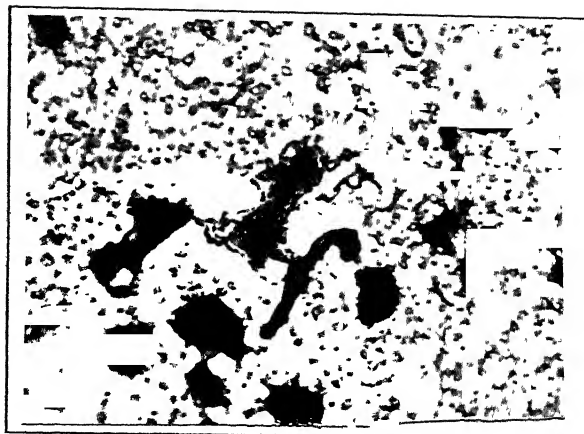


Fig. 3.31 Variation of magnetic coercivity with respect to Al_2O_3 content in sintered and heat treated T15 HSS with or without 5 wt% copper addition



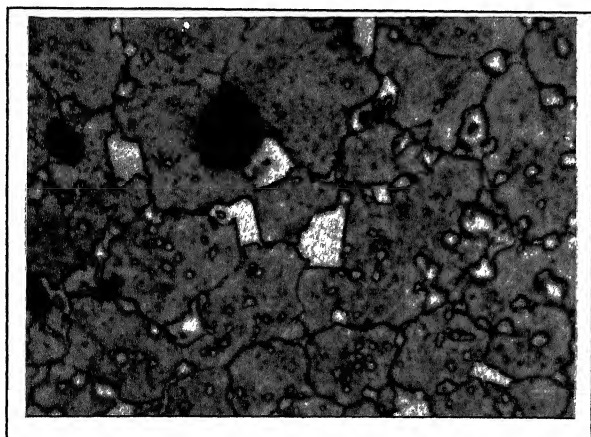
(a)

20 μ m



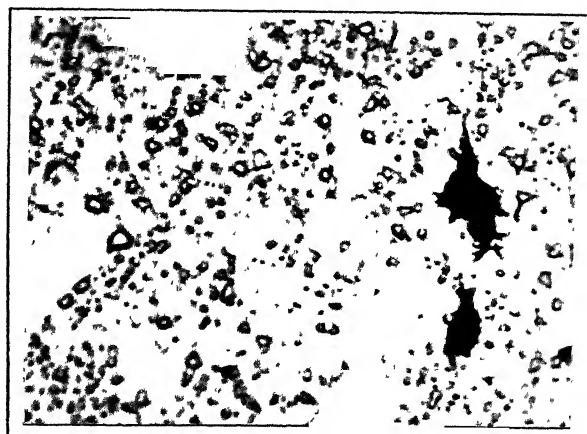
(b)

20 μ m



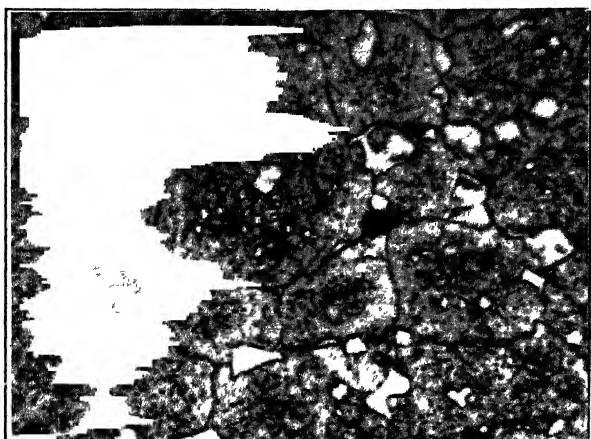
(c)

20 μ m



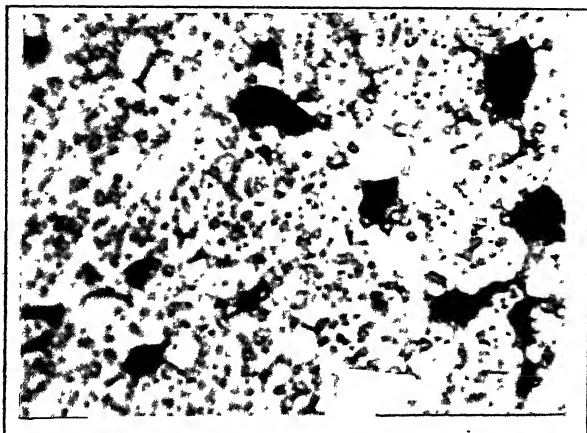
(d)

20 μ m



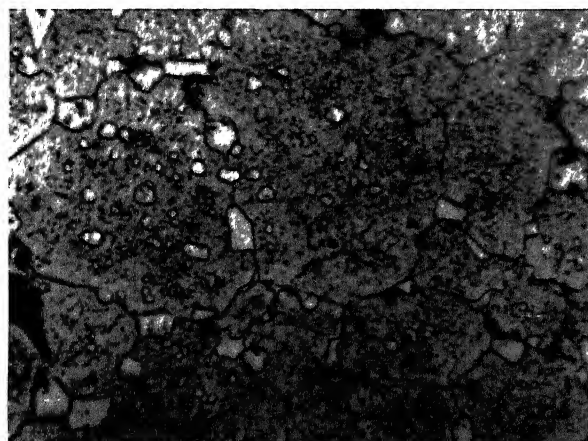
(e)

20 μ m



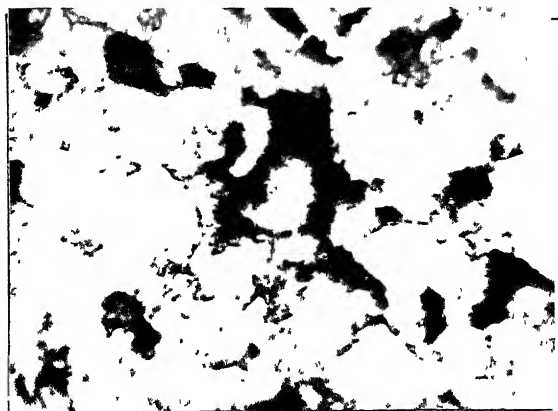
(f)

20 μ m



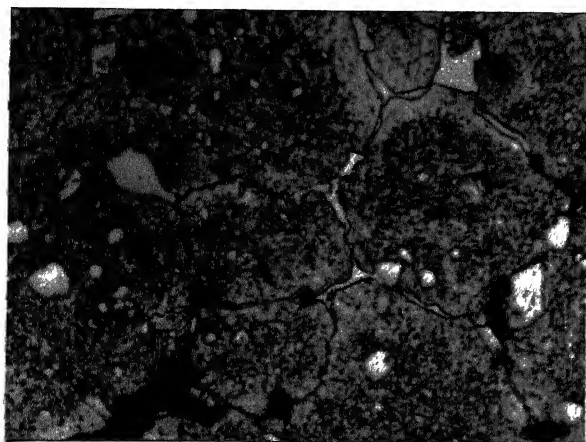
(g)

20 μm



(h)

20 μm



(j)

20 μm



(i)

20 μm

Fig. 3.32 The optical microstructures of T15 HSS and its containing Al_2O_3 composites with or without 5 wt% copper sintered at 1300°C temperature; (a) T15 HSS (b) T15+5 wt% Cu (c) T15+2 vol% Al_2O_3 (d) T15+2 vol% Al_2O_3 +5 wt% Cu (e) T15+4 vol% Al_2O_3 (f) T15+4 vol% Al_2O_3 +5 wt% Cu (g) T15+6 vol% Al_2O_3 (h) T15+6 vol% Al_2O_3 +5 wt% Cu (i) T15+8 vol% Al_2O_3 (j) T15+8 vol% Al_2O_3 +5 wt% Cu

the grain was evident.

With the addition of copper, in case of either 1280 or 1300°C sintering temperature, the sintered density decreased compared to that of compositions without copper. The microstructure consisted of many large pores and fine distribution of primary carbides in the matrix. The grains also got refined.

The average grain size variation with respect to Al_2O_3 content in T15 HSS with or without 5 wt% copper sintered at two temperatures i.e. 1100 and 1300°C is shown in Fig. 3.33. In case of both the sintering temperatures (i.e. 1100 and 1300°C), addition of Al_2O_3 decreased the grain size. However, with increasing Al_2O_3 content the grain size remained almost unchanged. Only in case of 1300°C sintering temperature and at 8 vol% Al_2O_3 content, the grain size increased.

Addition of copper, in case of both the sintering temperatures, decreased the grain size and the role of copper in refining grain size was much more pronounced than that of Al_2O_3 .

The microstructures of T15 IISS and its containing different vol% Al_2O_3 with or without 5 wt% copper (sintered at 1300°C) after quenching and triple tempering are shown in Fig. 3.34 and 3.35, respectively. Irrespective of sintering temperature, the microstructure of all the samples remained almost unchanged in any condition viz. sintering, hardening or tempering. However in all the cases, the as-quenched grains were smaller than those of the sintered samples, indicating a grain refinement during transformation annealing prior to oil quenching. The grain size of all the compositions increased after triple tempering.

SEM micrographs of the worn pin surfaces of the samples sintered at 1300°C and subjected to sliding wear test at higher load (2.5 kg) are shown in Fig. 3.36. No significant difference in the features of the worn out surface between all the compositions without copper was observed. There were two distinct features in the micrographs of worn out surfaces. One was the formation of long and continuous grooves and other the patches of severally damaged regions. The T15 IISS and its 2 vol% Al_2O_3 composite showed less such patches. At higher vol% of Al_2O_3 plowing of the matrix in some regions was also observed.

For the samples with copper, the basic features of the micrographs were almost similar to those of samples without copper. However, compared to compositions without copper, the compositions with copper showed micrographs consisted of much more such patches of damaged regions.

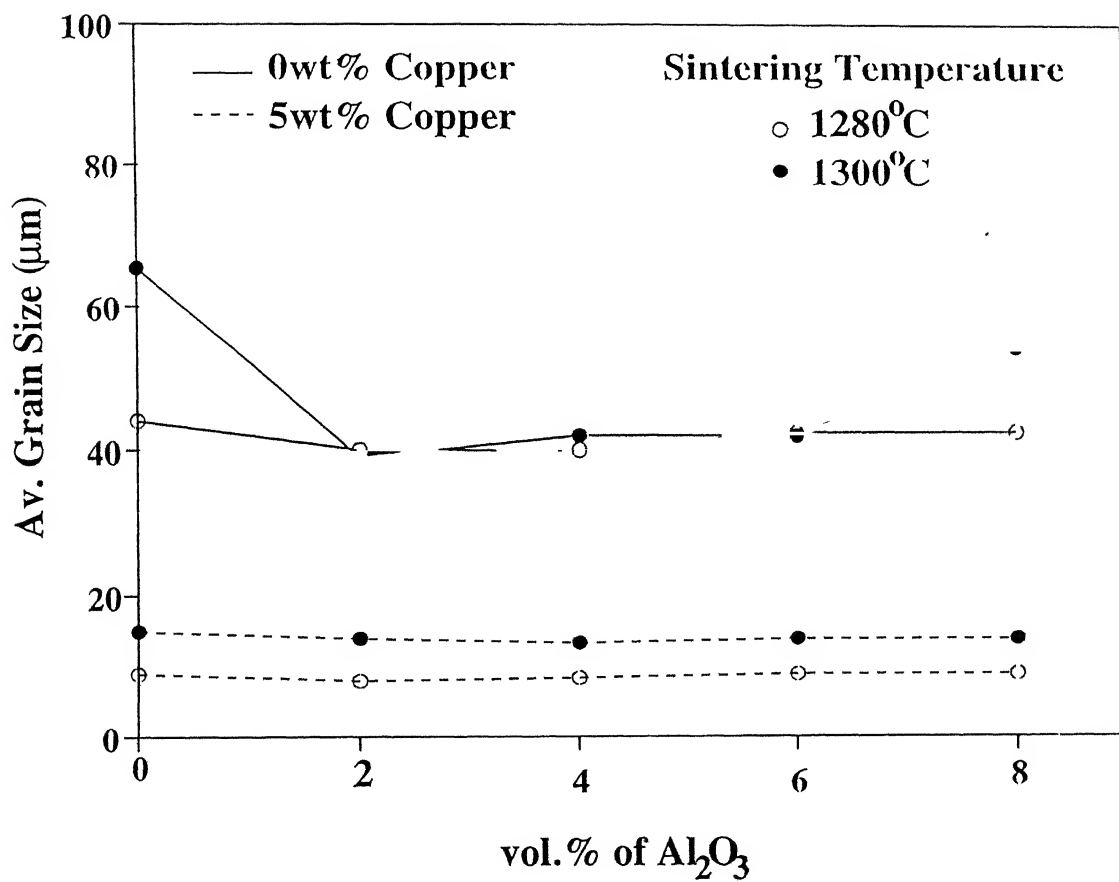
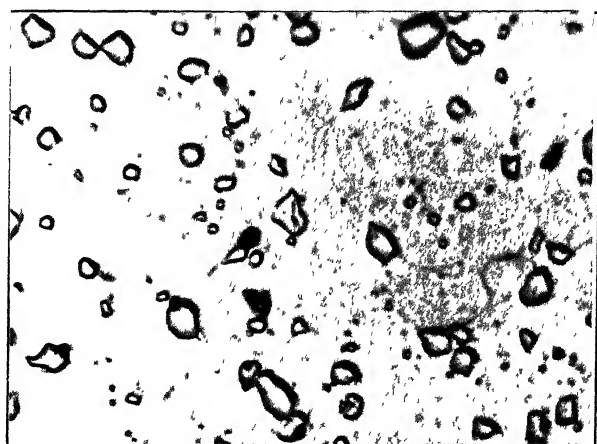
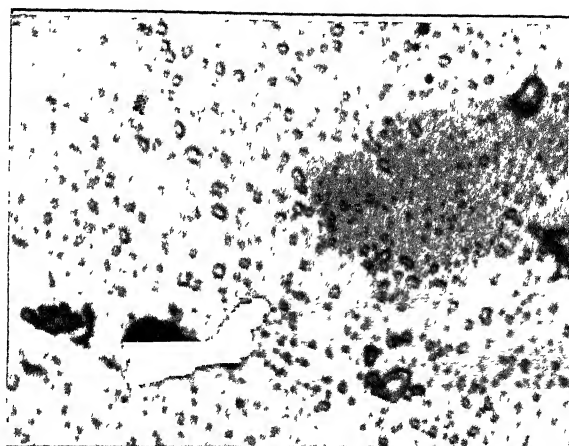


Fig. 3.33 Effect of Al_2O_3 content on average grain size of sintered T15 HSS with and without 5 wt% copper addition.



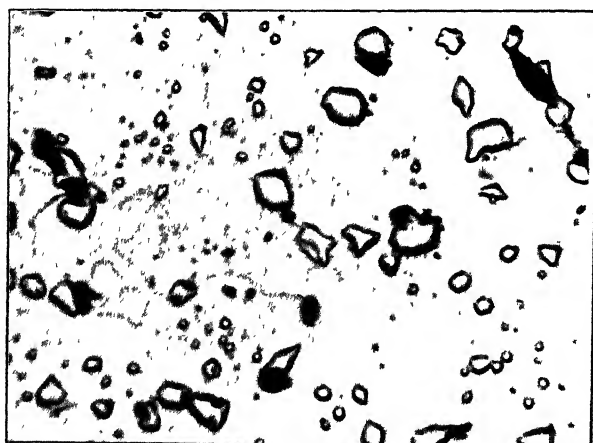
(a)

20 μ m



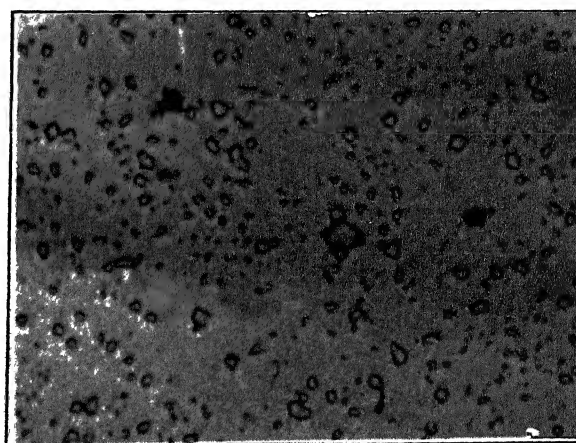
(b)

20 μ m



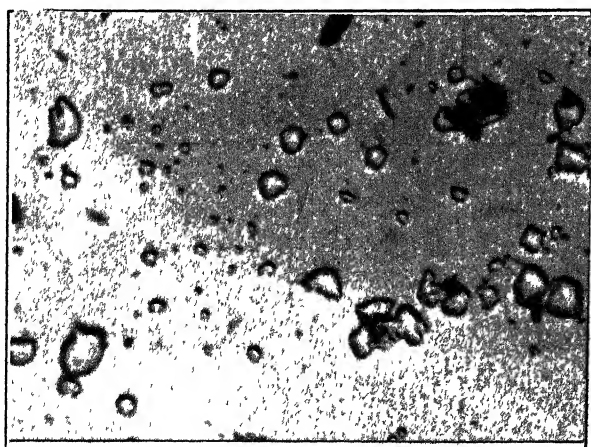
(c)

20 μ m



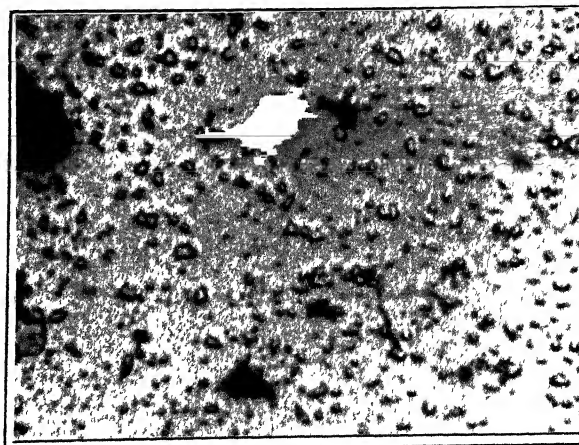
(d)

20 μ m



(e)

20 μ m



(f)

20 μ m

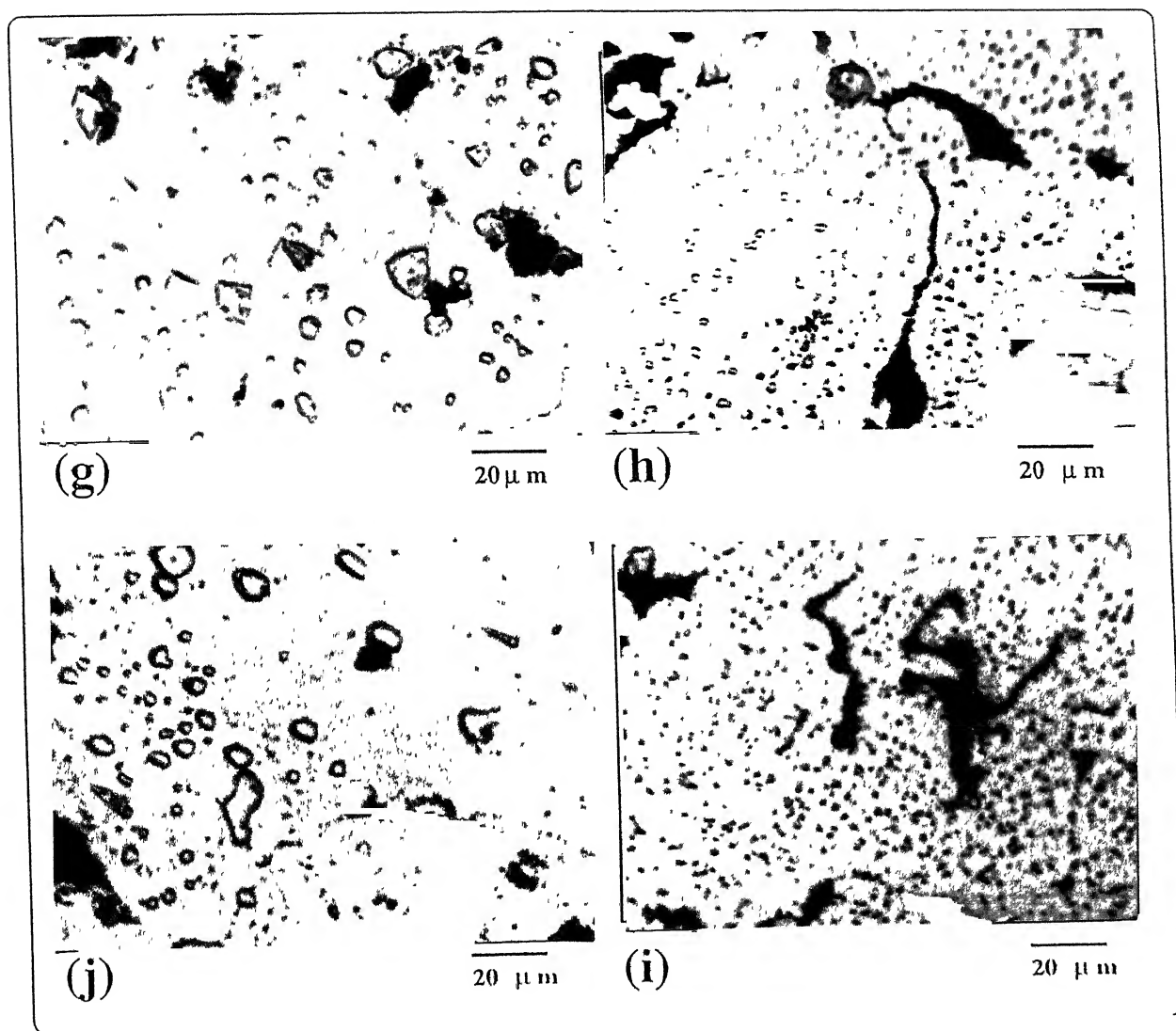
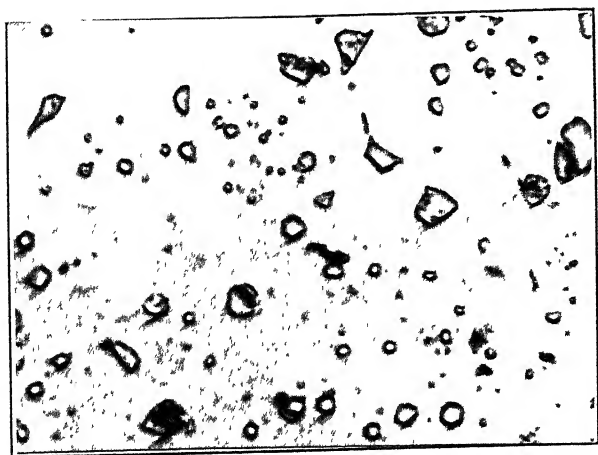
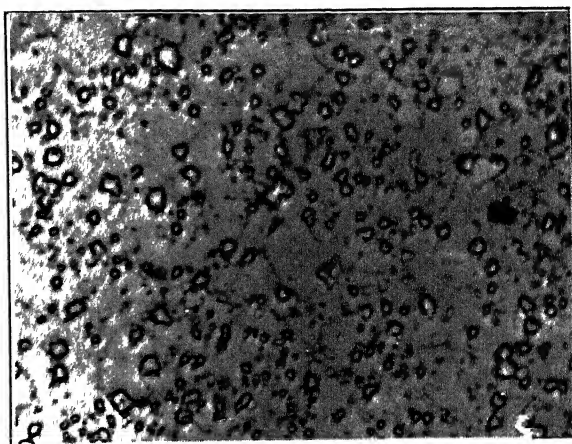


Fig. 3 34 The optical microstructures of T15 HSS and its containing Al_2O_3 composites with or without 5 wt% copper (sintered at 1300°C) after quenching; (a) T15 HSS (b) T15+5 wt% Cu (c) T15+2 vol% Al_2O_3 (d) T15+2 vol% Al_2O_3 +5 wt% Cu (e) T15+4 vol% Al_2O_3 (f) T15+1 vol% Al_2O_3 +5 wt% Cu (g) T15+6 vol% Al_2O_3 (h) T15+6 vol% Al_2O_3 +5 wt% Cu (i) T15+8 vol% Al_2O_3 (j) T15+8 vol% Al_2O_3 +5 wt% Cu.



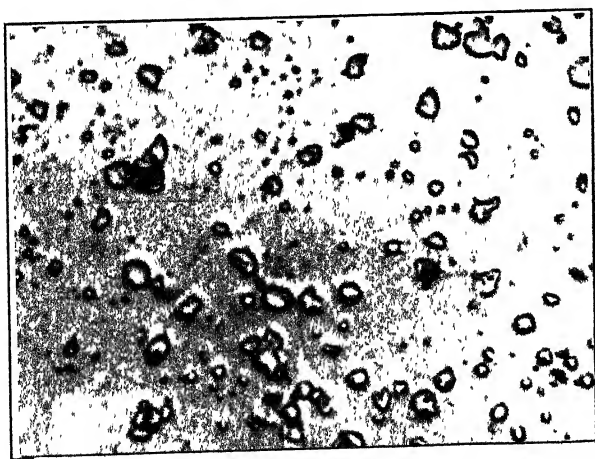
(a)

20 μ m



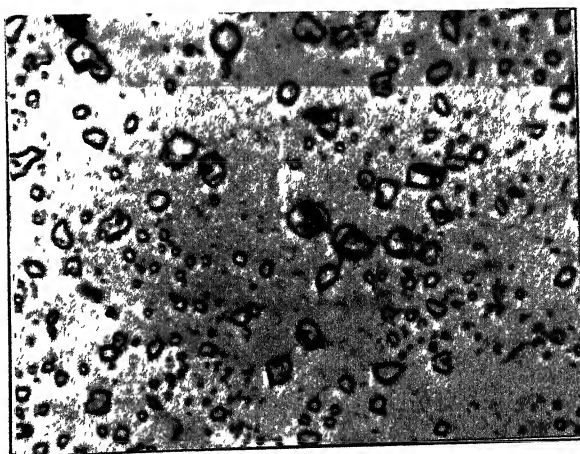
(b)

20 μ m



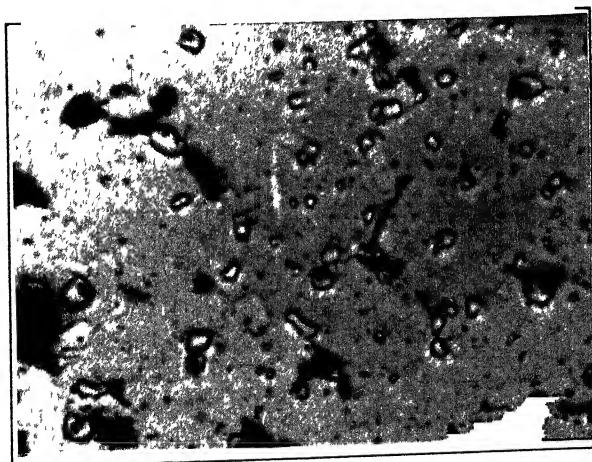
(c)

20 μ m



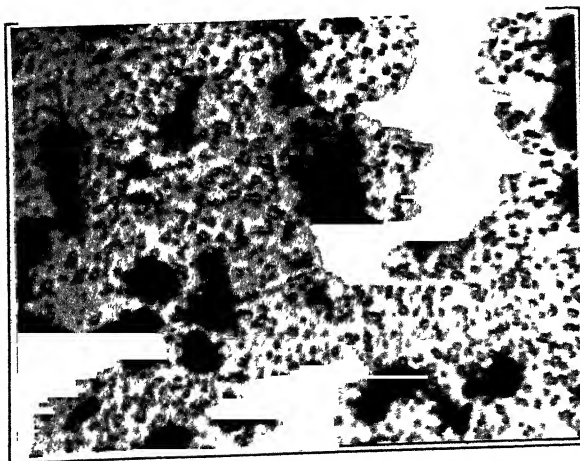
(d)

20 μ m



(e)

20 μ m



(f)

20 μ m

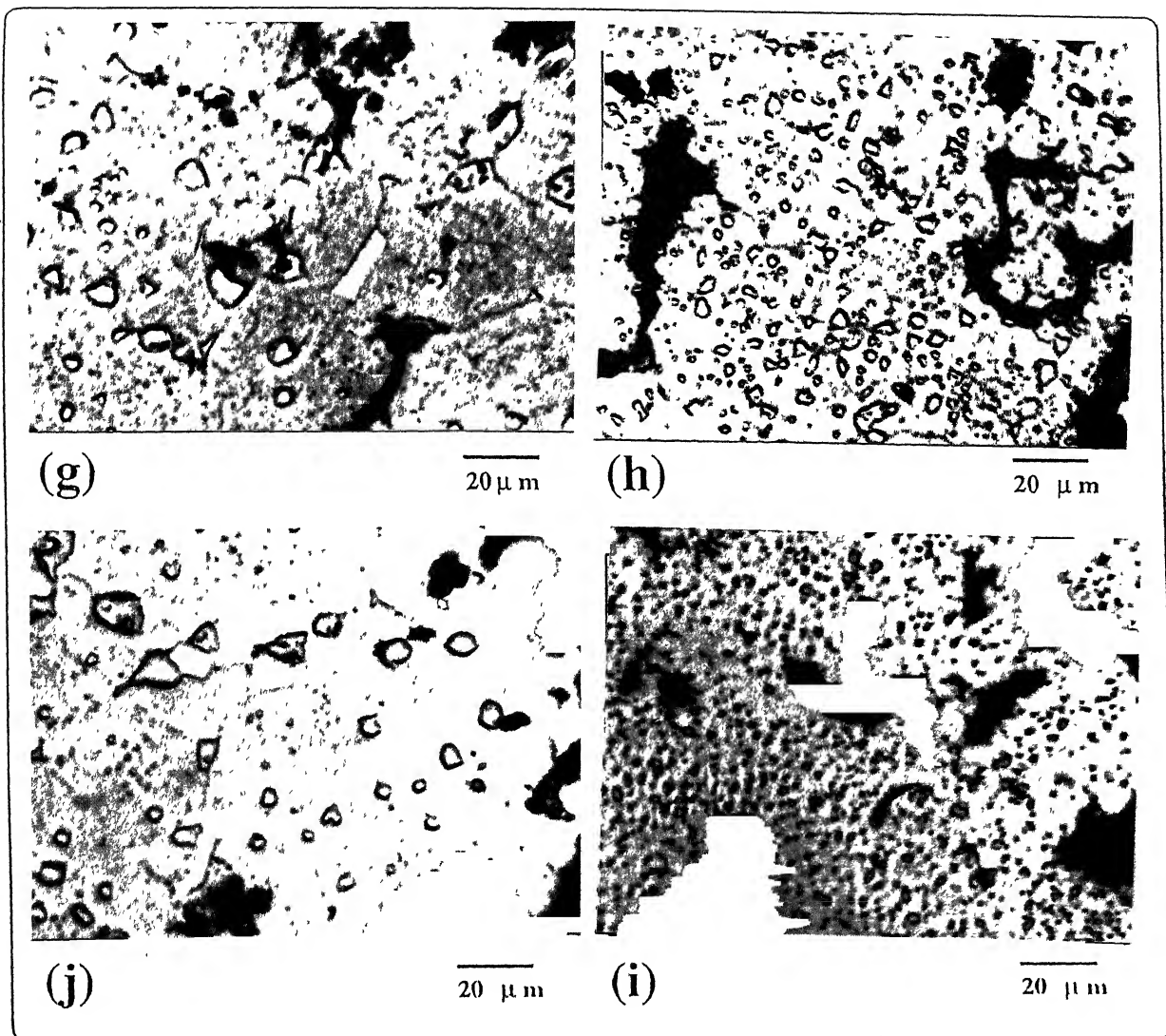
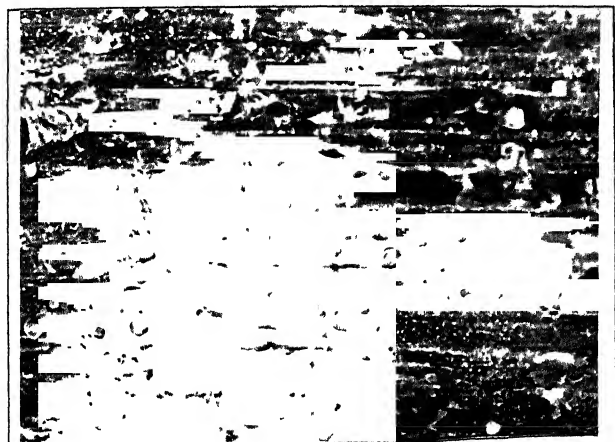
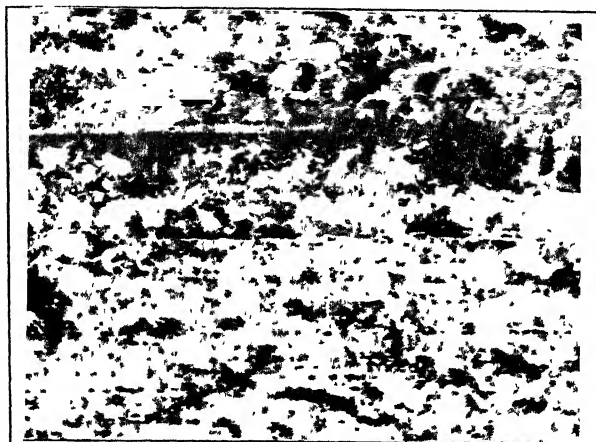


Fig 3.35 The optical microstructures of T15 HSS and its containing Al_2O_3 composites with or without 5 wt% copper (sintered at 1300°C) after triple tempering; (a) T15 HSS (b) T15+5 wt% Cu (c) T15+2 vol% Al_2O_3 (d) T15+2 vol% Al_2O_3 +5 wt% Cu (e) T15+4 vol% Al_2O_3 (f) T15+4 vol% Al_2O_3 +5 wt% Cu (g) T15+6 vol% Al_2O_3 (h) T15+6 vol% Al_2O_3 +5 wt% Cu (i) T15+8 vol% Al_2O_3 (j) T15+8 vol% Al_2O_3 +5 wt% Cu



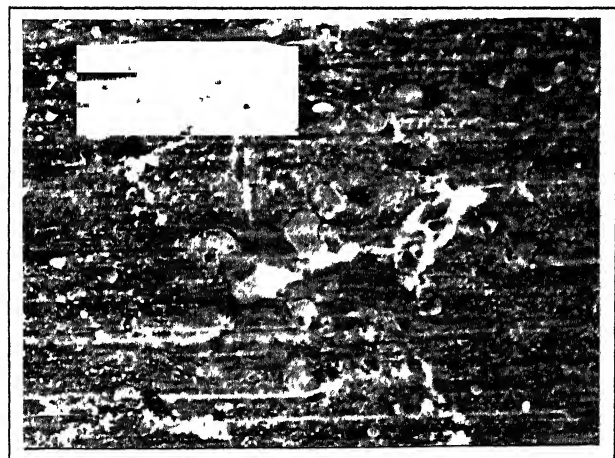
(a)

20 μ m



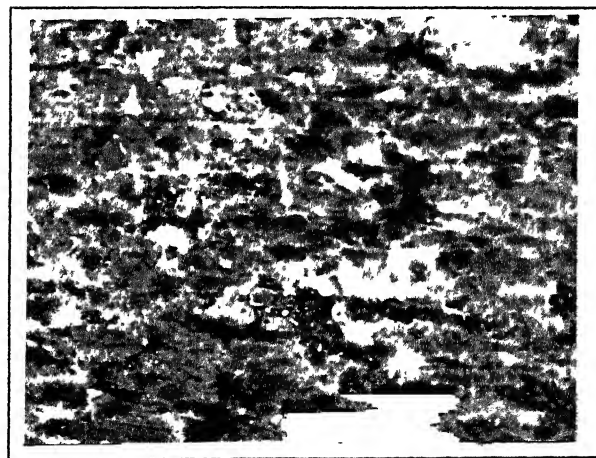
(b)

20 μ m



(c)

20 μ m



(d)

20 μ m



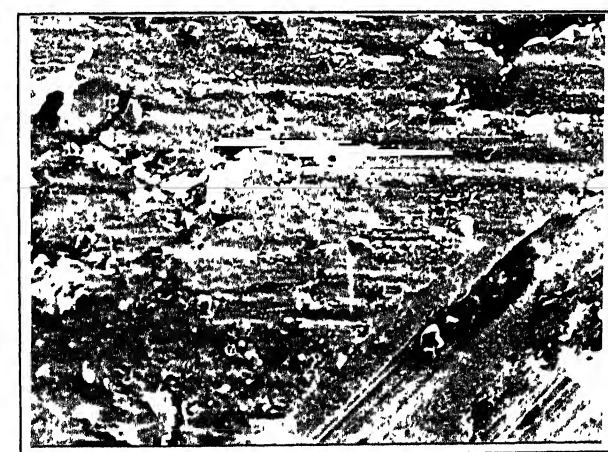
(e)

20 μ m



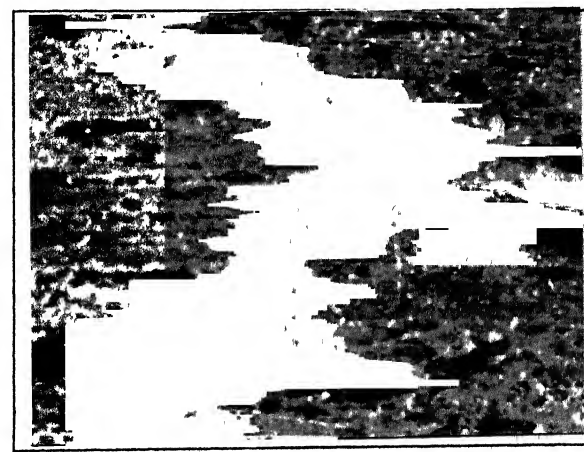
(f)

20 μ m



(g)

20 μ m



(h)

20 μ m

Fig. 3.36 The SEM micrographs of the worn pin surfaces of sintered (at 1300°C) T15 HSS and its containing Al_2O_3 composites with or without 5 wt% copper (sintered at 1300°C) after triple tempering; (a) T15 HSS (b) T15+5 wt% Cu (c) T15+2 vol% Al_2O_3 (d) T15+2 vol% Al_2O_3 +5 wt% Cu (e) T15+4 vol% Al_2O_3 (f) T15+4 vol% Al_2O_3 +5 wt% Cu (g) T15+6 vol% Al_2O_3 (h) T15+6 vol% Al_2O_3 +5 wt% Cu

Chapter 4

Discussion

4.1 T15 HSS (with or without copper/ Al_2O_3 : Model Study)

The liquid phase sintering of HSS pertaining to the supersolidus category, which involves densification by melt formation in a prealloyed powder compact by heating it above the solidus temperature. In this type of sintering the solid and liquid phases have similar composition. Sintering temperature is the most important process variable in supersolidus sintering of HSS. In the present investigation, all the green compacts were pressed to give a porosity in the range of 28-30% of the theoretical density. The densification process, therefore, can be singularly related to the sintering temperature. With increasing the sintering temperature up to the temperature below the solidus, a very limited amount of densification takes place through solid state sintering. The powder particles are sintered in solid state to form a skeleton [15]. In this temperature range proper densification is not achieved and large pores can be seen in the sintered microstructures (Fig. 3.9).

Increase in sintering temperature to optimum gives rise to enhanced densification due to the presence of the higher volume fraction of melt during supersolidus sintering. The liquid phase disintegrates the skeleton into almost individual solid grains. The capillary force provided by the surface tension of the liquid acts to rearrange the solid particles and interparticle voids are eliminated. The solid grains grow by solution-precipitation process. The microstructure corresponding to this sintering temperature consists of fine and uniformly distributed carbide and matrix grains. At higher sintering temperatures, the liquid volume fraction is higher which enhances densification. However, at the same time, this is also associated with grain coarsening and formation of carbide network at grain boundaries (Fig.3.32). The repress/resintering (supersolidus sintering) further enhances densification as during repressing some interconnected pores

as well as closed pores get collapsed which lead to the easily removal of porosity during resintering.

Apparent hardness is a bulk property and it is a complex measure of the combined effect of some factors which include grain size matrix strength, type, volume fraction and size distribution of carbides, the extent of carbide coarsening and porosity [39,41].

The failure during transverse rupture test is associated with the presence of some critical size defects which initiate crack propagation, such as brittle carbides, inclusions and pores [3].

The increase in the as-sintered hardness and TRS value with sintering temperature is associated with the decrease in porosity level. At lower temperatures the low macrohardness is caused by the collapse of pores beneath the hardness indenter. At sintering temperatures higher than the optimum, the macrohardness increases slightly due to slightly higher densification. However, TRS value decreases. This is attributed to the fact that the beneficial effect of decreased porosity level is nullified by the microstructural coarsening associated with higher sintering temperature, which can be verified from the results of microstructural analysis.

During heat treatment, as expected, the hardness increases but the degree of increase is not significantly higher compared to that of reported values of HSS because of low austenitizing temperature. However, due to relatively low value of hardness some toughness is also retained in the matrix which improves the wear resistance property. Triple tempering does not cause any further significant change in hardness and after triple tempering, due to same microstructural coarsening, hardness dropped slightly.

Microhardness of the matrix phase gives a clear picture of how matrix composition changes during sintering at different temperatures [53]. In the solid state sintering region microhardness slightly increases with increasing sintering temperature. But during supersolidus sintering the population of carbides changes, as larger carbides grow at the cost of smaller ones and the microhardness drops.

The wear resistance property is observed better in case of optimum sintering temperature. Below this temperature, the presence of porosity leads to wear of the samples. But at higher than the optimum temperature, though due to better densification porosity decreases but its effect is suppressed by the matrix coarsening. As expected, in case of higher load, the wear loss is observed higher than that for lower load. The ambient oxides (mainly; iron oxides) at the metal surface control the friction.

The magnetic properties of the P/M materials are controlled by the porosity present in the sintered parts [75-77]. HSS come under the category of hard magnetic materials. The coercivity of a ferromagnetic material is a measure of the demagnetizing force necessary to remove all the magnetic lines of force to the value of B_0 in the B-H curve.

It, therefore, represents the resistance to demagnetization. The coercivity is influenced by numerous parameters i.e. mechanical strain, grain size and presence of precipitates and inclusions. Depending on precipitates; the coercivity can be considered to vary with (a) volume fraction of the precipitate (b) size of the precipitate particles (c) precipitate morphology and (d) magnetic property of the precipitate.

In the present investigation, coercivity variation, in general, falls parallel to the hardness variation. Because the same factors which improve mechanical hardness impart better resistance to domain wall motion. After triple tempering, the coercivity drops but it is not clear why it happens so.

The saturation magnetization (σ_s), which represents the maximum magnetic induction, is a structure insensitive property. It is also found to be independent of the sintering conditions being solely a function of density [75]. The main reason for this is obvious that in a porous part less iron is available for a given volume to be magnetized. However, in the present investigation, the σ_s of the unit weight of the sample is reported, which for any particular composition it remains almost unchanged with respect to sintering temperature.

The variation in sintering temperature was purposely done so as to observe the densification behaviour during solid state, transient liquid phase sintering and supersolidus liquid phase sintering stages. From fig. 3.1 it is evident that copper addition enhances densification during all these three stages of sintering. In solid state sintering, the diffusion of copper in ferrous lattice activates sintering which is more pronounced in case of transient liquid phase sintering (1100°C). As the addition of copper (5 wt%) is lower than its solubility limit in iron the onset of second stage of liquid phase sintering i.e. solution and reprecipitation is rather minimal. In case of supersolidus sintering carried out at 1300°C the positive role of copper is still better felt as the intensity of densification is quite appreciable.

However, when inert oxide additive of Al₂O₃ was made, the picture is still interesting. After 1100°C, there is some positive contribution of copper in densification which gets reduced by addition of Al₂O₃ (fig. 3.2). However, in case of supersolidus sintering at 1300°C, the densification is far more pronounced as compared to 1100°C sintering. In this case too, the addition of Al₂O₃ during supersolidus liquid phase sintering decelerates densification similar to the case for transient liquid phase sintering. It is evident from fig. 3.2 that the excellent contribution of supersolidus liquid phase sintering is favourable for straight HSS where as for ceramic dispersoid containing composites other densification methods like HIP'ing etc. must be attempted in order to produce fully dense parts.

During transient liquid phase sintering or supersolidus liquid phase sintering, in presence of copper, the porosity decreases and solid solution strengthening of the matrix

becomes apparent. For the compacts where the addition of copper during supersolidus sintering leads to decrease in densification, the effect of porosity is suppressed by the solid solution strengthening effect and hardness still further increases.

When the sintering temperature is above the melting point of copper, the copper melts and enters into the matrix and strengthens it which result in increase in microhardness. During supersolidus sintering, here also the population of the carbides in the matrix decreases as larger carbides grow at the cost of smaller ones and as a result microhardness decreases slightly.

With addition of copper, the variation of coercivity is parallel to hardness variation is justified. As expected, the addition of copper decreases the σ_s value slightly as less iron is available for a given weight of compact to be magnetized. But in case of 900 and 1100°C sintering temperatures, it is not clear why σ_s values are lower than those of other sintering temperatures.

4.2 T15-Al₂O₃ composites

Hard ceramic particles can easily be incorporated into HSS where advantage can be taken of their excellent P/M characteristics to produce full density metal-matrix composites with compositions and structures that would be difficult to produce by any other means. However the sinterability is reduced by the introduction of finer ceramic particles and by increasing the volume fraction of ceramic addition [52]. Because these lead to increase in the number of interfaces that requires to be wetted by the liquid phase formed during sintering. The liquid phase also flows into cracks and clusters of the ceramic particles. Thus, if the same quantity of liquid phase is always present complete wetting behaviour between the ceramic and liquid phases become more difficult to achieve. Ceramic particles also form an obstruction to particle movement and thereby, hindered particle rearrangement. Again ceramic particles are harder than the metal matrix, the densification of the composite would be further reduced as these hard particles act as diffusion barrier, thus inhibits the densification kinetics. In the present investigation, major part of the densification during liquid phase sintering of the selected steel occurs by the rearrangement of the particles where the amount of the liquid phase at sintering temperatures plays an important role. The liquid formation is associated with the melting of fine particles preferentially along the surfaces of large powder particles and also along the grain boundary within the particles in the optimum sintering temperature range. The absence of sufficient amount of fine particles decreases the densification.

The poor wettability of Al₂O₃ particles with steel melt due to their inertness restricts the particle rearrangement and growth stage required for densification. Such a feature

becomes more prominent with increase in Al_2O_3 content (fig. 3.13). The higher and higher sintering temperature can make the melt less viscous and increase its amount effectively. But it also leads to gross deformation of the compact.

Addition of hard particles do not significantly increase the hardness. The effect of hard dispersoid is nullified by the increase in porosity level. The effect of Al_2O_3 addition on hardness after hardening and tempering is negligible. The increase in microhardness is due to the decrease in grain size of the matrix (fig. 3.10). The addition of ceramic particles restricts grain boundary movement and therefore, yields finer matrix.

Increasing ceramic particles causes a gradual decrease in TRS due to poorer sinterability with steel melt and increased porosity. Moreover, ceramic particles act as crack initiators and thereby, reduce the TRS value.

Contrary to the initial expectation the composites do not show any improvement in wear behaviour. However, in general, the wear resistance of T15-2 vol% Al_2O_3 composite is comparable to that of T15 HSS. It appears that wear properties are influenced more by the sintering parameters rather than by the presence of individual type and volume fraction of dispersoids. Porosity and particle-matrix interface are the decisive factors in governing the wear behaviour of the composites. In case of T15-2 vol% Al_2O_3 composite, the effect of increased porosity is nullified by the higher hardness of the composite. In case of higher volume fraction of dispersoid, presence of higher amount of porosity and weakly bonded interfaces dislodge the Al_2O_3 particles from the matrix which get entrapped between the mating surfaces and cause plowing and cutting action of the matrix resulting in the abrasion of some regions of the matrix. These entrapped Al_2O_3 particles also impede the formation of iron oxide rich protective layer. The film rupture and plowing of the subsurface material raise the friction and also wear loss.

The increase in coercivity with increasing Al_2O_3 content is due to the fact that the large amount of ceramic particles act as inclusions. This is attributed to the restriction of domain wall movement by the ceramic particles and thereby, increasing coercivity.

The saturation magnetization decreases, as expected, with increasing Al_2O_3 content. This is associated with the decreases in the iron content in the steel. The same trend is also followed during heat treatment.

4.3 Role of Copper on T15- Al_2O_3 composites

In case of as-received T15 HSS powder which had a wide range of particle size distribution the densification results (fig. 3.13) are rather opposite than in case where the particle size range was rather narrow (fig. 3.1). For the same vol% of Al_2O_3 addition, the 5 wt% addition of copper is lowering the densification parameter. This suggests that because

of more fine powder fractions in as-received HSS powder, the oxygen content is rather higher as compared to that in the sieved range powder. This will naturally influence the wettability of molten copper over the HSS particle surface. In addition the relatively high fraction of small particles would encourage higher proportion of closed porosity, which during sintering at elevated temperature would give rise to growth in the sintered HSS compacts. This is confirmed by the fact that at lower sintering temperature the intensity of such growth is not that high.

The role of copper in refining the matrix is very much pronounced than that of Al₂O₃. Because copper penetrates along the grain boundaries within the powder particles along with interparticle contacts (fig. 3.32).

Presence of copper strengthens the matrix by solid solution strengthening effect but at the same time increases the porosity. The net effect slightly increases the hardness. After quenching, the hardness increases as expected. However, in case of 1280°C sintered samples, the difference in porosity level between composites containing copper and these without copper is substantial. Here porosity is the decisive factor in variation in hardness the hardness. Thus addition of copper in the composites sintered at 1280°C decreases the hardness compared to compositions without any copper after quenching. During triple tempering, the hardness of copper containing composites decreases.

Fall in TRS of steels, in presence of copper, is due to increased porosity as copper addition which leads to swelling of the compact. The increased porosity along with the ceramic particles which act as crack initiation sites lower the TRS values. However, in case of higher sintering temperature (i.e. 1300°C) the difference in porosity level between compositions with and without copper is minimum. Here the effect of porosity is nullified by the grain refinement and TRS improves.

The microhardness improves due to the strengthening effect of the copper. However, in case of 1300°C sintering, addition of copper decreases the microhardness of the composites. The reason of this is not very clear from the present investigation. The coercivity also follows parallel to the microhardness variation which is justified.

As expected, the saturation magnetization decreases due to addition of copper. Because it decreases the iron content of the compacts. During heat treatment saturation magnetization follows the same trend.

Presence of copper does not change the wear behaviour of the composites significantly, since the solid solution strengthening and grain refinement effects are nullified by the increased porosity. At lower load the ambient oxides on the metal surface control the friction. But at higher load, more frictional heat is generated. Copper diffuses to the contact surface and forms a deposit on it. It also sticks with the disc surface. At the same time the presence of dislodged dispersoid particles ruptures the film and plows the subsurface material and raises the friction and wear loss.

Chapter 5

Conclusion

From the investigation carried out in the present study, following conclusions can be drawn.

1. During solid state sintering of T15 HSS, very little densification occurs. In case of liquid phase sintering, full density ($>98\%$ of theoretical density) can be achieved due to presence of sufficient amount of liquid phase which enhances densification. At still higher temperature microstructural coarsening occurs along with the enhanced densification. The repressing/resintering further imparts densification. Effect of copper in increasing densification is evident during liquid phase sintering. However, presence of sufficient amount of finer particles of T15 HSS appears to give rise to swelling effect.
2. The Vickers macrohardness varies parallel to the densification. Addition of copper strengthens the matrix and thereby, increases hardness. The microhardness of matrix drops during liquid phase sintering. In case of composition containing copper, the degree of decrease is less compared to that of T15 HSS due to grain refinement effect of copper. The best TRS value and wear resistance property can be obtained in case of optimum sintering temperature. Addition of copper decreases TRS but at higher sintering temperatures, it increases TRS. The copper has practically no effect on wear resistance property of T15 HSS.
3. The magnetic coercivity varies parallel to the hardness. Addition of copper also followed the same trend. The saturation magnetization remains almost unchanged with respect to sintering temperature. However, in presence of copper it decreases.
4. The densification of T15- Al_2O_3 composites decreases with increasing Al_2O_3 content. Addition of copper in these composites further decreases densification. Al_2O_3 particles reduce the matrix grain size but the role of copper in grain refinement is much more pronounced than Al_2O_3 particles.

5. The Vickers macrohardness decreases with increasing Al_2O_3 content except 2 vol% Al_2O_3 composite, where the role of Al_2O_3 in increasing the hardness is evident. The addition of copper further increases hardness. TRS value decreases with addition of Al_2O_3 content due to its crack initiating tendency. Addition of copper decreases TRS except at higher sintering temperatures, where the effect of decreased porosity level can be suppressed by grain refinement.
6. The sliding wear resistance of composites shows similar trend like hardness. Presence of copper in composites has practically no effect on wear behaviour.
7. The magnetic coercivity increases with increasing Al_2O_3 content because ceramic particles act as H_c -raising inclusions. Addition of copper, due to its strengthening role in the matrix, further increases it. The saturation magnetization decreases with increasing Al_2O_3 and/or copper content.

CENTRAL LIBRARY
I. I. T., KANPUR
No. M₂ A 125718

Chapter 6

References

1. G.Hoyle, 'High Speed Steels', Butterworth publication, London, 1988.
2. R.Wähling, P.Beiss and W.J.Huppmann, Powder Metallurgy, vol.29, no.1, 1986, 53
3. J.Bolton, Metal Powder Report, vol.51, no.1, 1996, 30.
4. M.T.Podob and L.K.Woods, in 'Modern Developments in Powder Metallurgy', vol.13, Ed. H.H.Hausner, H.W.Antes and G.D.Smith, Metal Powder Industries Federation, Princeton, 1981, p.17.
5. P.Ray and P.K.Pal, 'World Conference on Powder Metallurgy', vol.2, The Institute of Metals, London, 1990, p.159.
6. ASM Speciality Hand Book, 'Tool Materials', Ed. J.R.Davis, ASM International, Materials Park, Ohio, 1995.
7. P.K.Kar, B.P.Saha and G.S.Upadhyaya, International Journal of Powder Metallurgy, vol.29, no.2, 1990, 139.
8. A.S.Fareed, A. Lawley and M.J.Koczak, International Journal of Powder Metallurgy, vol.26, no.4, 1993, 351.
9. B.Sustarsic, F.Vodopivec and L.Kosec, 'Powder Metallurgy World Congress: 1994', vol.2, les éditions de physique, Les Ulis, France, 1994, p.945.
10. K.M.Konoplev and G.E.Titenskaya, Soviet Powder Metallurgy and Metal Ceramics, vol.27, no.10, 1988, 768.
11. G.A.Baglyuk, G.E.Mazharova, S.N.Kaplya, L.A.Poznyak and R.Z.Vlasyuk, Soviet Powder Metallurgy and Metal Ceramics, vol.29, no.7, 1990, 517.

12. L.A.Poznyak, S.Ya.Golub, Yu V.Sorokin and A.S.Fomichev, *Soviet Powder Metallurgy and Metal Ceramics*, vol.31, no.5, 1992, 369.
13. R.Marquart and K.Hummert, 'World Conference on Powder Metallurgy: 1990', vol.2, The Institute of Metals, London, 1990, p.20.
14. K.M Kulkarni, *Metal Powder Report*, vol.45, no.9, 1990, 629.
15. S.Takajo and M.Nitta, 'Sintering'85', Ed. G C Kuczynski, D.P.Uskokovic, Hayne Palmour III and M.M.Ristic, Plenum Press, New York, p.189.
16. P.K.kar and G.S.Upadhyaya, *Tool and Alloy Steels*, vol.29, no.1, 1995, 5.
17. C.S.Wright, J D.Bolton, M.M.Rebbeck and A.S.Wronski, 'First International High Speed Steel Conference Proceedings', Ed. G.Hackl and B.Hribernik, Montanuniversität, Leoben, Austria, 1990, p.93.
18. I.M.Martins, M.Santos, M.M.Oliveira and H.Carvalhinhos, in 'Modern Developments in Powder Metallurgy', vol.19, Compiled by P.V.Gummerson and D.A.Gustafson, Metal Powder Industries Federation, Princeton, 1988, p.319.
19. R.J.Causton and J.Richardson, *Metallurgia*, December, 1979, 775.
20. V.B.Akimenko, A.A.Gadkin, I.Ya.Kondratov, A.A.Lyadskaya, A.K.Petrov, Ye.N.Smirn, V.Z.Spuskanyuk and Yu.F.Chiornyl, *Physics of Sintering*, vol.15, no.1, 1973, 49.
21. H.Nakamura and Y.Mochida, 'First International High Speed Steel Conference Proceedings', Ed. G.Hackl and B.Hribernik, Montanuniversität, Leoben, Austria, 1990, p.99.
22. P.R.Brewin and D.K.Bambury, *Sintered High Speed Steels: Their Applications and Uses*, Brochure from Powdrex Limited, Tonbridge, U.K., 1982.
23. R.M.German, *International Journal of Powder Metallurgy*, vol.26, no.1, 1990, 23.
24. K.M.Kulkarni, in 'Modern Developments in Powder Metallurgy', vol.19, Compiled by P.U.Gummerson and D.A.Gustafson, Metal Powder Industries Federation, Princeton, 1988, p.329.
25. G.A.Baglyuk, S.N.Kaplya, L.A.Poznyak and O.Yu.Kononenko, *Soviet Powder Metallurgy and Metal Ceramics*, vol.31, no.10, 1992, 831.
26. V.I.Lyukevich, Yu.V.Lenvinskii, M.V.Fedorovich and T A.Maryunina, *Soviet Powder Metallurgy and Metal Ceramics*, vol.26, no.12, 1987, 949.

27. A.Okayama, H Ando, K.Someno and M.Tamura, Tetsu-to-Hagane, Journal of Iron Steel Institute, Japan, vol.59, 1973, 253s; Bratcher Translate 9146.
28. L.D.Kulak, A.P.Pikozh and A A Dorogoi, Soviet Powder Metallurgy and Metal Ceramics, vol.26, no.4, 1987, 277.
29. I.H.Moon, J.S.Oh and I.S.Ahn, in 'Modern Developments in Powder Metallurgy', vol.17, Ed. E.N.Aqua and C.I.Whitman, Metal Powder Industries Federation, Princeton, 1985, p.441.
- 30 W.J C.Price, M.M.Rebbeck, A S.Wronski and S.A.Amen, Powder Metallurgy, vol.28, no.1, 1985, 1.
31. E.Dudrová, M.Kabátová, F.Molnár and R.Bureš, Powder Metallurgy, vol.37, no.3, 1994, 206.
32. M.Igharo and J.V.Wood, Powder Metallurgy, vol.31, no.3, 1988, 184
33. K.M.Kulkarni, A.Ashurst and M.Svilar, in 'Modern Developments in Powder Metallurgy', Ed. H.H.Hausner, H.W.Antes and G.D.Smith, Metal Powder Industries Federation, Princeton, 1981, p.93.
34. P.K.Kar and G.S.Upadhyaya, Powder Metallurgy International, vol.22, no.1, 1990, 23.
35. I.Urrutibeaskoa, S.Jauregi, F.Fernandez, S.Talacchia, R.Palma, V.Martinez and J.Urcola, International journal of Powder Metallurgy, vol.29, no.4, 1993, 367.
- 36 P.K.Kar and G S.Upadhyaya, Metal Powder Report, vol.47, no.6, 1992, 34.
37. O.Grinder, L.Berglin and M.Sporrong, in 'Modern Developments in Powder Metallurgy', vol.17, Ed. E.N.Aqua and C.I.Whitman, Metal Powder Industries Federation, Princeton, 1985, p.407.
38. R.A.Andricvskii, N.K.Kasmanytov, Z.Kh.Fuksman, A.S.Gurdzhi and B.U.Asanov, Powder Metallurgy and Metal Ceramics, vol.32, no.9-10, 1993, 821.
39. P.R.Brewin, B.Toloui, P.D.Nurthen, J.A.Fellgett, J.V.Wood, M.Igharo, D.S.Coleman and Q.Shaikh, Powder Metallurgy, vol.32, no.4, 1989, 285.
40. A.S.Fareed, K. S.Kumar, A.Lawley and M.J.Koczak, in 'Modern Developments in Powder Metallurgy', vol.17, Ed. E.N.Aqua and C.I.Whitman, Metal Powder Industries Federation, Princeton, 1985, p.307.

41. L Arnberg and A Karlsson, *International Journal of Powder Metallurgy*, vol 24, no.3, 1988, 203
42. R.A.Andrievskii and N.K.Kasmanyov, *Soviet Powder Metallurgy and Metal Ceramics*, vol 30, no.10, 1991, 818
43. P.Beiss, R.Wähling and D.Duda, in 'Modern Developments in Powder Metallurgy', vol 17, Ed. E.N.Aqua and C.I Whitman, Metal Powder Industries Federation, Princeton, 1985, p.331
44. V.Martinez, R.H.Palma and J.J.Urcola, *Metal Powder Report*, vol.44, no.11, 1989, 751.
45. H.Brandrup-Wognsen, J.Engstrom and O.Grinder, *Powder Metallurgy International*, vol.20, no 1, 1988, 18.
46. H.Berns, J.Lveg, W.Trojahn, R.Wähling and H.Wisell, *Powder Metallurgy International*, vol.19, no 4, 1987, 22.
47. J.A.Whitehead, P.D.Nurthen and P.R.Brewin, *International journal of Powder Metallurgy*, vol.26, no.4, 1990, 345.
48. K.A.Gogaev, L.G.Shtyka, N.P.Korzhova, L.A.Poznyak and V.I.Ul'shin, *Powder Metallurgy and Metal Ceramics*, vol.32, no.9-10, 1993, 763.
49. L.Shtyka and K.Gogayev, 'Powder Metallurgy World Congress. 1994', vol.2, les éditions de physique, Les Ulis, France, 1994, p.977
50. J.D.Bolton, *Metal Powder Report*, Vol 51, no.2, 1996, 33.
51. M.M.Oliveira and J.D.Bolton, *International journal of Powder Metallurgy*, vol.32, no.1, 1996, 37.
52. M.M.Oliveira and J.D.Bolton, *Powder Metallurgy*, vol.38, no.2, 1995, 131.
53. J.D.Bolton and A.J.Gant, *Powder Metallurgy*, vol.39, no.1, 1996, 27.
54. J.D.Bolton and A.J.Gant, 'Powder Metallurgy World Congress: 1994', vol.2, les éditions de physique, Les Ulis, France, 1994, p.983.
55. G.S.Upadhyaya and P.K.Kar, 'Proceedings of 13th Int. Plansee Seminar', Ed. H.Bildstein and R.Eck, *Metall Werk Plansee*, Reutte, vol.2, 1993, p.328.
56. G.S.Upadhyaya and P.K.Kar, 'First International High Speed Steel Conference Proceedings', Ed. G.Hackl and B.Hribernik, Montanuniversitat, Leoben, Austria, 1990, p.477.

57. P.K.Kar, B.P.Saha and G.S.Upadhyaya, International Journal of Powder Metallurgy, vol.29, no.2, 1993, 135.
58. P.K.Kar and G.S.Upadhyaya, Steel Research, vol.62, no 8, 1991, 352.
59. P.K Kar and G.S Upadhyaya, Materials and Design, vol.15, no.2,1994, 99.
60. B.P.Saha and G.S.Upadhyaya, Powder Metallurgy International, vol.24, no.6, 1992, 345.
61. J.D.Bolton and A.J.Gant, Powder Metallurgy, vol 40, no 2, 1997, 143.
62. R.A.Queeney, in 'Advances in Powder Metallurgy and Particulate Materials', vol.8, Compiled by J.M.Capus and R.M.German, Metal Powder Industries Federation, Princeton, 1992, p.89.
63. E.A.Carlson, 'Progress in Powder Metallurgy 1982', vol.38, Ed J.G.Bewley and S.W.McGee, Metal Powder Industries Federation, Princeton, 1983, p.271.
64. R.P.Hervey, SME, Report No. MR78-315, Society of Manufacturing Engineers, Dearborn, U.S.A., 1978.
65. E.A.Dickinson, P.I.Walker and F.L.Jagger, Metal Powder Report, vol.38, no.9, 1983, 491.
66. I Kvasnicka, Powder Metallurgy, vol.26, no.3, 1983, 145.
67. R.Andersson, Metal Powder Report, vol.37, no.11, 1982, 587.
68. A.Nordgren, H.Chandrasekaran and H.Wisell, 'Powder Metallurgy World Congress: 1994', vol.2, les éditions de physique, Les Ulis, France, 1994, p.1027.
69. C.Tronberg and B.O.Bengtsson, 'Powder Metallurgy World Congress: 1994', vol.1, les éditions de physique, Les Ulis, Paris, 1994, p.415.
70. R.J.Henry and P.R.Brewin, Metal Powder Report, vol.44, no.11, 1989, 763.
71. R.Wähling and V.Arnhold, Metal Powder Report, vol.43, no.3, 1988, 188.
72. R.P.Hervey, 'Preformed Powder Metallurgy Tool Steel for Cutting Tools and Other Applications, Brochure, Consolidated Metallurgical Industries, U.S.A.
73. J.Arthur, Journal of Institute of Metals, vol.84, 1956, 327.
74. P.K.Kar, Sintering of Refractory Compound Enriched High Speed Steels and Their Properties, Ph.D. Thesis, I.I.T, Kanpur, India, May, 1991.

- 75. G.Jangs, M Prozda, H.Danninges and R.E.Nad, Powder Metallurgy International, vol.15, no.4, 1983, 173.
- 76. B.A.James and G.Williams, Powder Metallurgy, vol.22, no.2, 1979, 75.
- 77. K.H.Moyer, Powder Metallurgy International, vol.11, no.1, 1979, 29.

A

125718

A

125718

Date Slip

This book is to be returned on the
date last stamped.

IME-1998-M-MAJ-SIN



A125718